



January 2018

# Organic Speciation Of Air Particulate Matter With Thermal Desorption – Pyrolysis – Gas Chromatography – Mass Spectrometry

Brett Thomas Nespor

Follow this and additional works at: <https://commons.und.edu/theses>

---

## Recommended Citation

Nespor, Brett Thomas, "Organic Speciation Of Air Particulate Matter With Thermal Desorption – Pyrolysis – Gas Chromatography – Mass Spectrometry" (2018). *Theses and Dissertations*. 2421.  
<https://commons.und.edu/theses/2421>

This Thesis is brought to you for free and open access by the Theses, Dissertations, and Senior Projects at UND Scholarly Commons. It has been accepted for inclusion in Theses and Dissertations by an authorized administrator of UND Scholarly Commons. For more information, please contact [zeinebyousif@library.und.edu](mailto:zeinebyousif@library.und.edu).

ORGANIC SPECIATION OF AIR PARTICULATE MATTER WITH THERMAL  
DESORPTION – PYROLYSIS – GAS CHROMATOGRAPHY – MASS SPECTROMETRY

by

Brett T. Nesor  
Bachelor of Arts, Minot State University, 2016

A Thesis  
Submitted to the Graduate Faculty

of the

University of North Dakota

in partial fulfillment of the requirements

for the degree of

Master of Science

Grand Forks, North Dakota

December  
2018

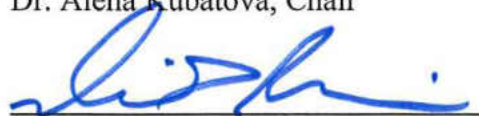
Copyright 2018 Brett Nespor

This thesis, submitted by Brett T. Nespor in partial fulfillment of the requirements for the Degree of Master of Science from the University of North Dakota, has been read by the Faculty Advisory Committee under whom the work has been done and is hereby approved.



---

Dr. Alena Kubátová, Chair



---

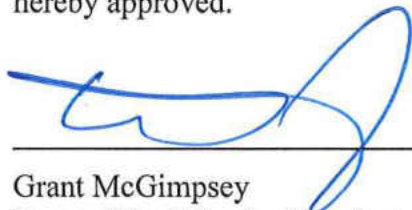
Dr. David Pierce



---

Dr. Evguenii Kozliak

This dissertation is being submitted by the appointed advisory committee as having met all of the requirements of the School of Graduate Studies at the University of North Dakota and is hereby approved.



---

Grant McGimpsey  
Dean of the School of Graduate Studies

November 28, 2018

---

Date

## PERMISSION

Title	Organic speciation of air particulate matter with thermal desorption – pyrolysis – gas chromatography – mass spectrometry
Department	Chemistry
Degree	Master of Science

In presenting this thesis in partial fulfillment of the requirement for a graduate degree from the University of North Dakota, I agree that the library of this University shall make it freely available for inspection. I further agree that permission for extensive copying for scholarly purposes may be granted by the professor who supervised my thesis work or, in her absence, by the chairperson of the department or the dean of the graduate school. It is understood that any copying or publication or other use of this thesis or part thereof for financial gain shall not be allowed without my written permission. It is also understood that due recognition shall be given to me and the University of North Dakota in any scholarly use which may be made of any material in my thesis.

Brett T. Nespor  
November 15th, 2018

## TABLE OF CONTENTS

ABBREVIATIONS .....	viii
LIST OF FIGURES .....	x
LIST OF TABLES .....	xiii
ACKNOWLEDGEMENTS .....	xv
ABSTRACT .....	xxi
CHAPTER I. INTRODUCTION .....	1
I.1. Carbonaceous Atmospheric Particulate Matter .....	1
I.2. Approaches to Quantitative and Qualitative Analysis of Carbonaceous PM.....	7
I.2.1. Thermal Optical Analysis of Carbonaceous PM .....	7
I.2.2. Mass Spectrometric Analysis of Carbonaceous PM.....	9
I.3. Statement of Purpose .....	13
CHAPTER II. EXPERIMENTAL METHODS.....	14
II.1. Materials.....	14
II.2. Sampling .....	14
II.3. Instrumentation .....	15
II.3.1 Thermal Optical Analyzer .....	15
II.3.2 TD-Pyr-GC-MS.....	16
II.3.2.1 Operation of TD-Pyr-GC-MS .....	17

II.4. Optimization of TD-Pyr-GC-MS .....	18
II.5. TD-Pyr-GC-MS of Model Compounds .....	20
II.6. TOA and TD-Pyr-GC-MS of POLCAST Samples.....	21
CHAPTER III. RESULTS AND DISCUSSION.....	22
III.1. Optimization of TD-Pyr-GC-MS.....	22
III.2. TD-Pyr-GC-MS of Model Compounds .....	25
III.2.1 C <sub>21</sub> -C <sub>40</sub> Alkane Mix.....	25
III.2.2 Stearic Acid.....	28
III.2.3 Tristearin .....	33
III.2.4 Oleic Acid .....	35
III.2.5 Triolein.....	38
III.3. Application of TOA and TD-Pyr-GC-MS to POLCAST Samples.....	41
III.3.1 PM <sub>2.5</sub> , OC, and EC Concentrations .....	41
III.3.2. Role of TD-Pyr in Organic Speciation.....	43
III.3.3. Thermal Desorption OC Fraction .....	47
III.3.4 Distribution of Products of Pyrolyzed OC.....	53
CONCLUSIONS.....	59
APPENDICES .....	61
Appendix A.....	62
Appendix B .....	69
Appendix C.....	70

Appendix D.....	71
Appendix E.....	77
Appendix F.....	78
Appendix G.....	83
Appendix H.....	113
REFERENCES .....	116



## ABBREVIATIONS

ACY	Acenaphthylene
AMS	Aerosol mass spectrometry
ANT	Anthracene
BP	Biphenyl
BSTFA	<i>N,O</i> -Bis(trimethylsilyl)trifluoroacetamide
BTEX	Benzene, toluene, ethylbenzene, <i>m</i> -xylene
C <sub>1</sub> NAP	Methylnaphthalene
C <sub>2</sub> NAP	Dimethyl or ethyl naphthalene
C <sub>max</sub>	Maximum number of carbon atoms
CPI	Carbon prefix index
DCM	Dichloromethane
EC	Elemental carbon
EIC	Extracted ion chromatogram
ESI	Electrospray ionization
FA	Fatty acids
FAME	Fatty acid methyl ester
FID	Flame ionization detector
FL	Fluorene
FLA	Fluoranthene
GC	Gas chromatography
HDO	Hydrodeoxygenation
HMW	High molecular weight
HRGC	High resolution gas chromatography
IMPROVE	Interagency monitoring of protected visual environment
k	Retention factor
LC	Liquid chromatography
LMW	Low molecular weight
LPM	Liters per minute
<i>m/z</i>	Mass-to-charge ratio

M <sup>+</sup>	Molecular ion
MMW	Medium molecular weight
MS	Mass spectrometry
MW	Molecular weight
NAP	Naphthalene
NIOSH	National institute for occupational safety and health
OC	Organic carbon
PAH	Polycyclic aromatic hydrocarbons
PHE	Phenanthrene
PM	Particulate matter
POLCAST	Polarimetric cloud analysis and seeding test
PYR	Pyrene
Pyr	Pyrolysis
Pyr-GC	Pyrolysis - gas chromatography
SM1	Standard mixture 1
SM2	Standard mixture 2
SOA	Secondary organic aerosol
TAG	Thermal desorption gas chromatography mass spectrometry
TC	Total carbon
TD	Thermal desorption
TD-Pyr-GC-MS	Thermal desorption pyrolysis gas chromatography mass spectrometry
TG	Triacylglycerides
TIC	Total ion chromatogram
TIC	Total ion current
TMAH	Tetramethylammonium hydroxide
TMCS	Trimethylchlorosilane
TOA	Thermal optical analysis
TOR	Total optical reflectance
TOT	Total optical transmittance
t <sub>r</sub>	Retention time
Wax %	Plant wax percentage

## LIST OF FIGURES

Figure	Page
Figure 1. Schematic of the working principle behind the TOA instrument.....	9
Figure 2. Schematic diagram of the pyroprobe filament found on the CDS pyroprobe 5200 model.....	17
Figure 3. Typical thermal process for pyroprobe during analysis of samples.....	18
Figure 4. TD-Pyr-GC-MS EIC chromatograms of a blank sample corresponding to the occurrence of H <sub>2</sub> O (18 <i>m/z</i> ), N <sub>2</sub> (28 <i>m/z</i> ), O <sub>2</sub> (32 <i>m/z</i> ), and CO <sub>2</sub> (44 <i>m/z</i> ) peaks at a) 300 °C and b) 870 °C.....	19
Figure 5. EIC abundances of characteristic ion for selected compounds to evaluate different filament heating rates and interface times of the pyroprobe with filament desorption temperature of 300 °C.....	23
Figure 6. TD-Pyr-GC-MS EIC abundances for selected compounds to evaluate pyroprobe interface times. Filament heating rate was set at 30 °C/s with a filament desorption temperature of 300 °C.....	24
Figure 7. TD-Pyr-GC-MS EIC of ion 44 <i>m/z</i> to show CO <sub>2</sub> peak at different interface times. .....	25
Figure 8. TD-Pyr GC-MS TIC chromatograms of C <sub>21</sub> -C <sub>40</sub> alkane mix a) 300 °C TD fraction b) sequential 700 °C Pyr fraction.....	26
Figure 9. Pyr-GC-MS TIC chromatogram of alkane mix analyzed following direct pyrolysis at 700 °C.....	28
Figure 10. TD-Pyr-GC-MS chromatograms of stearic acid a) 300 °C TIC b) sequential 700 °C TIC c) EIC of ions 92/91 <i>m/z</i> .....	30

Figure 11. Pyr-GC-MS TIC of stearic acid following the direct pyrolysis at 700 °C. ....	32
Figure 12. Pyr-GC-MS TIC chromatogram of tristearin at a) 300 °C b) sequential pyrolysis at 700 °C and c) direct pyrolysis at 700 °C.....	33
Figure 13. TD-Pyr-GC-MS of oleic acid at a) 300 °C b) sequential pyrolysis at 700 °C and c) directly pyrolysis at 700 °C.....	36
Figure 14. Pyr-GC-MS EIC of <i>m/z</i> ion 91 showing <i>n</i> -alkylbenzene profile following the direct pyrolysis at 700 °C.....	38
Figure 15. TD-Pyr-GC-MS of triolein at a) 300 °C b) sequential pyrolysis at 700 °C and b) directly pyrolysis at 700 °C.....	39
Figure 16. a) Time series plot of the PM <sub>2.5</sub> , OC and EC concentrations as well as filter mass, TEOM, and EPA PM <sub>2.5</sub> measurements collected during POLCAST campaign at Grand Forks, ND, from June 21, 2012 (week 1) - October 19, 2012 (week 17). b) Temperature distribution of OC collected from TOA c) Correlation between TEOM and PM <sub>2.5</sub> filter mass measurements.....	42
Figure 17. Characteristic OC profiles over 6 week sampling period showing TD and Pyr fractions obtained using a) TOA and b-g) TD-Pyr-GC-MS: b) Total TIC (sum) c) <i>n</i> -Alkanes d) Acids & Esters e) <i>n</i> -Alkenes f) Alkylbenzenes & BTEX g) PAHs. TD-Pyr abundances were determined as EIC peak areas for specific ions (Appendix F, Table F1).....	45
Figure 18. Representative TD-Pyr-GC-MS EIC chromatograms from week 12 showing <i>n</i> -alkane profile using target ion 57 <i>m/z</i> .....	48
Figure 19. TD-Pyr-GC-MS EIC profiles showing <i>n</i> -fatty acids (FAs) and FAMES before (a, b) and after derivatization with 1 µL of TMAH (c, d).....	50
Figure 20. Diagnostic ratios for specific PAHs obtained from TD fraction of 6 week TD-Pyr-GC-MS analysis. ....	53
Figure 21. Homological profile of PAHs, alkylbenzenes, alkenes, alkanes, in total Pyr fraction based on EIC peak areas from TD-Pyr-GC-MS a) week 12 b) week 13 c) week 14 d) week 15 e) week 16 f) week 17.....	55
Figure D1. Mass spectra of select peaks of C <sub>21</sub> -C <sub>40</sub> alkane mix after TD-Pyr-GC-MS a) contaminant a b) contaminant b c) contaminant c. ....	71

Figure D2. Mass spectra of 2-tetradecylcyclobutane peak comparison between sample and NIST library.  $M^+$  ion can be seen at 266  $m/z$ , which corresponds to the MW of tetradecylcyclobutane..... 74

Figure D3. Mass spectra of tetradecenylcyclobutane peak comparison between sample and NIST library of 2-tetradecylcyclobutane. Above mass spectra shows loss of 2  $m/z$  from  $M^+$  fragment of tetradecylcyclobutane, verifying double bond within the molecule. The MW of tetradecenylcyclobutane is 264..... 75

Figure D4. Mass spectra of 6,10,14-trimethyl-2-pentadecanone peak comparison between sample and NIST library. .... 76

## LIST OF TABLES

Table	Page
Table 1. Representative list of OC tracers commonly found in PM.....	3
Table 2. Products of pyrolysis of feedstocks including fatty acids, TGs, cellulose, coal.....	11
Table 3. Pyroprobe filament heating rates and interface time optimization conditions .....	20
Table 4. <i>n</i> -Alkane source criteria for 300 °C TD fraction. ....	48
Table A1. Pyroprobe heating profiles for filament and interface showing initial and optimized conditions. ....	68
Table B1. Standard mixture of compounds for optimization of pyroprobe conditions .....	69
Table C1. EIC abundances, STD, and RSD values for SM2 after TD-Pyr-GC-MS analysis. ....	70
Table E1. PM <sub>2.5</sub> and OC and EC concentrations with % of total PM <sub>2.5</sub> collected and measured during POLCAST campaign at Grand Forks, ND, 2012.....	77
Table F1. Compounds identified by TD-Pyr-GC-MS during POLCAST campaign, including retention times ( <i>t<sub>R</sub></i> ) and MS ions.....	78
Table G1. Compounds identified by TD-Pyr-GC-MS during POLCAST campaign week 12.....	83
Table G2. Compounds identified by TD-Pyr-GC-MS during POLCAST campaign week 13.....	88
Table G3. Compounds identified by TD-Pyr-GC-MS during POLCAST campaign week 14.....	93

Table G4. Compounds identified by TD-Pyr-GC-MS during POLCAST campaign week 15.....	98
Table G5. Compounds identified by TD-Pyr-GC-MS during POLCAST campaign week 16.....	103
Table G6. Compounds identified by TD-Pyr-GC-MS during POLCAST campaign week 17.....	108
Table H1. TD-Pyr-GC-MS data normalized to its own week .....	113
Table H2. TD-Pyr-GC-MS data normalized to sample week 15 (most abundant week) .....	114
Table H3. TD-Pyr-GC-MS data normalized to TD and Pyr fractions .....	115

## ACKNOWLEDGEMENTS

I would like to thank my advisor Dr. Alena Kubátová for her guidance, support, and training of how to become a better scientist every day of my studies at the University of North Dakota. I greatly appreciate the contribution of Dr. Evgenii Kozliak for his nonstop commitment to helping me become a better technical writing, continual reviewing of my manuscripts and his non-stop support. I would like to thank Dr. David Pierce for his guidance in being a good teacher's assistant and his help becoming an REU mentor. Finally I would like to thank my former committee members Dr. David Delene and Dr. Julia Zhao.

I am thankful to current and former members of Dr. Kubátová's and Dr. Kozliak's research group (Josh H., Anastasia, Honza, Josh S., Klára, Audrey, Jana, Tyson, Sarah, Rich, and Keith) for their tremendous help, time, and encouragement in any problems I had. I would also like to thank Shane Johnson for his help with computer and instrumentation issues that arose frequently.

I would like to thank the University of North Dakota, UND Chemistry Department Faculty and Staff, and UND Graduate School for accepting me to the program and supporting me financially. I am very grateful for the financial support from the North Dakota EPSCoR Program (Doctoral Dissertation Award), UND Graduate School, and AAAR and ASMS for travel stipends.

Finally, I would like to thank my friends and most of all my family, especially my parents, Ralph and Donna, for their unwavering support and love, and their consistent encouragement to always follow my dreams.



## ABSTRACT

Characterization of particulate matter (PM), more specifically the carbonaceous fraction, is essential for understanding atmospheric processes, source determination, and health impacts. In this thesis, a novel approach to both the quantification and characterization of carbonaceous atmospheric PM was developed and validated on model compounds and collected ambient PM from a local source within Grand Forks, ND.

Thermal optical analysis (TOA) is a commonly used method for the determination of organic (OC) and elemental (EC) carbon within atmospheric PM that yields quantitative results, i.e., total concentrations of OC and EC. However, for speciation of OC, there is no universal method. Typical approaches include solvent extraction followed by gas chromatography-mass spectrometry (GC-MS) or liquid chromatography-mass spectrometry (LC-MS), thermal desorption aerosol GC-MS (TAG), aerosol mass spectrometry (AMS), and pyrolysis GC-MS. In this thesis, thermal desorption (TD) coupled with pyrolysis (Pyr) GC-MS (TD-Pyr-GC-MS) was employed for characterization of carbonaceous PM and determination of specific tracers that were used for source apportionment. This method was developed to be used in combination with quantitative TOA data and qualitative results for both concentrations of OC, and its characterization.

TOA of PM revealed a wide range of OC that makes up the total PM concentration (25 – 75%), showing a wide variability in composition of atmospheric PM. Quantification by TOA

supported the significance of the pyrolytic fraction, in which 73 – 87 % of the OC evolved at temperatures above 400 °C. The comprehensive speciation of OC assessed sequentially with thermal TD (evolving at 300 °C) and Pyr (> 400 °C) coupled to GC-MS enabled the investigation of both low and high molecular weight species' tracers. The TD fraction showed a high abundance of long chain alkanes (waxes) with an odd number of carbon atoms, indicating biogenic origin, along with fatty acids (FAs) and fatty acid methyl esters (FAMEs). Furthermore, the generally ignored Pyr fraction showed a series of homologous compounds, which included *n*-alkenes, *n*-alkylbenzenes, light polycyclic aromatic hydrocarbons (PAHs), *n*-alkanes, and substituted phenols, many of which are thought to be derived from the breakdown of larger molecular weight biogenic sources, e.g., plant waxes and triacylglycerides (TGs). The sequential pyrolytic temperatures steps used in this thesis were essential in understanding the overall composition of PM collected in the Grand Forks area.

Furthermore, the model compounds analyzed in this study with TD-Pyr-GC-MS, i.e., TGs and fatty acids, provided unique insights into the mechanisms of pyrolysis. Moreover, the process of decomposition through hydrodeoxygenation vs. decarboxylation were assessed through analysis of these compounds. In addition, the Pyr of TGs and fatty acids, were shown to form specific homology profiles, mainly *n*-alkylbenzenes and 2-ring PAHs, which further supported their presence in atmospheric PM.

## CHAPTER I. INTRODUCTION

### I.1. Carbonaceous Atmospheric Particulate Matter

Atmospheric particulate matter (PM) generated from anthropogenic and biogenic sources is known to impose a large effect not only on atmospheric processes but on the health of individuals around the world.<sup>1-3</sup> PM consists of liquid or solid particles suspended in air, with diameters in the micrometer range and smaller. PM is generally differentiated into two categories: PM<sub>10</sub> and PM<sub>2.5</sub>, which corresponds to particulate matter smaller than 10 μm (coarse fraction) and those particles that are smaller than 2.5 μm (fine fraction), respectively.<sup>4</sup> The fine fraction, PM<sub>2.5</sub> and smaller, generally causes more harm to humans as these particles can enter deeper along the breathing pathway. PM may be emitted from direct sources (primary PM), or produced from complex chemical reactions in the atmosphere (secondary PM). According to the US EPA, the daily average air quality standard for human exposure of PM<sub>10</sub> is 150 μg/m<sup>3</sup>, while the daily average standard for PM<sub>2.5</sub> is 12 μg/m<sup>3</sup>. The World Health Organization's guidelines are much lower with daily PM<sub>10</sub> levels of 50 μg/m<sup>3</sup> and daily PM<sub>2.5</sub> of 25 μg/m<sup>3</sup>.<sup>4-5</sup> The chemical composition of PM<sub>2.5</sub> varies greatly depending on geographical location, however the main constituents usually consist of ammoniated sulfates and nitrates, crustal materials, carbonaceous species, and water.<sup>6-7</sup> The carbonaceous PM fraction in the atmosphere is a major contributor to total PM levels and accounts for roughly 10 – 65% of the total mass fraction in the United States, of which a large portion (20 – 40%) of the fine particulate mass (PM<sub>2.5</sub> and smaller) is unidentified.<sup>8-9</sup> It is possible for this

carbonaceous PM to contribute to climate change depending on the chemical composition of the compound. It is also known that some species such as polycyclic aromatic hydrocarbons (PAHs) pose serious health risks and have potential mutagenic and carcinogenic effects.<sup>10</sup> Due to the effects that carbonaceous PM have on our everyday lives and on the climate, it is of utmost importance to be able to identify and quantify these carbon compounds in the atmosphere.

The carbonaceous PM can be further divided into two categories: organic carbon (OC) and elemental carbon (EC). OC compounds are represented by a wide range of molecules featuring various functional groups that add to the challenge of chemical characterization. These varying organic compounds can be formed from primary emission sources as well as from complex oxidation reactions in the atmosphere, which are characterized as secondary organic aerosols, i.e., SOA.<sup>8</sup> Many of the primary emission compounds can be used as tracers to determine if PM originates from natural (e.g., dust, forest fires) or anthropogenic processes (e.g., petroleum industry) while secondary compounds can be used as tracers for secondary processes.<sup>11</sup> A list of OC compounds typically found in PM can be seen in Table 1.

Table 1. Representative list of OC tracers commonly found in PM

Compound	MS Ions ( <i>m/z</i> )	Source	Emission Process	Detection Method	Ref
<b><i>n</i>-Alkanes</b>	57, 71, 85 [M <sup>+</sup> ]			GC-MS/FID, GC-MS, TD-GC-MS, HRGC-FID, GC-FID	
C <sub>24</sub> -C <sub>35</sub> (odd/even)		Plant waxes	Direct		12-15
C <sub>12</sub> -C <sub>35</sub>		Vehicles	Combustion		16-17
C <sub>13</sub> -C <sub>32</sub>		Heating oil, meat cooking, asphalt tar, boilers	Combustion, heating		18-21
<b><i>n</i>-Alkenes</b>	55, 69, 83 [M <sup>+</sup> ]			GC-MS, GC-FID	
C <sub>15</sub> -C <sub>37</sub>		Biomass/coal	Combustion		22
C <sub>22</sub> -C <sub>26</sub>		Alkanols	Dehydration		23
C <sub>18</sub> -C <sub>35</sub>		Biomass	Combustion		24
<b><i>n</i>-Alkanoic acids</b>	43, 73, 129 [M <sup>+</sup> ]			GC-MS, HRGC-FID, GC-MS, GC-MS/FID	
C <sub>16</sub> , C <sub>18</sub>		Biomass	Combustion		23
C <sub>20</sub> -C <sub>36</sub>		Plant waxes	Direct, combustion		12, 25
C <sub>10</sub> -C <sub>20</sub>		Microbes	Direct		12
<C <sub>18</sub>		Petroleum	Combustion		26
C <sub>7</sub> -C <sub>18</sub>		Meat cooking, charbroiling	Combustion		19-20
C <sub>7</sub> -C <sub>24</sub>		Asphalt tar, boilers	Heating, burning		21
<b>Dicarboxylic acids</b>	87, 115, 100, 129 [M <sup>+</sup> ]			GC-MS, GC-FID	
C <sub>2</sub> -C <sub>9</sub>		Hydrocarbons/fatty acids, fossil fuels, cooking, wood	Photolysis, combustion		19, 27-28
C <sub>10</sub> -C <sub>26</sub>		Biogenic lipids	Degradation, hydrolysis		29-30

Table 1. cont.

Compound	MS Ions ( <i>m/z</i> )	Source	Emission Process	Detection Method	Ref
<b>Aromatic acids</b> C <sub>6</sub> -C <sub>9</sub>	[M <sup>+</sup> ]	Vehicle exhaust, SOA, asphalt tar, boilers	Combustion, photolysis of toluene, heating	GC-MS, GC-FID	14, 21, 31-32
<b><i>n</i>-Alkanols</b> C <sub>14</sub> -C <sub>30</sub>	69, 83, 97, [M <sup>+</sup> ]	Plant waxes	Direct	GC-FID, GC-MS	25
<b><i>n</i>-Alkylbenzenes</b> C <sub>13</sub> -C <sub>26</sub>	92, 91, [M <sup>+</sup> ]	Fossil fuel, coal, lubricating oil	Combustion/heating	GC-FID, GC-MS	33-34
<b>Hopanes/stearanes</b> C <sub>27</sub> -C <sub>35</sub>	149, 151, 217, 231	Petroleum, diesel, road dust, biomass, asphalt tar, boilers	Combustion, direct, heating	GC-FID, GC-MS, TD-GC-MS	15-16, 18, 24, 26, 35-36
<b>Wax esters</b> C <sub>38</sub> -58 C <sub>40</sub> -C <sub>62</sub> C <sub>21</sub> -C <sub>33</sub>	T <sub>R</sub> match	Plant materials	Combustion	HTGC-MS, GC-FID, GC-MS	37-38 39 40
<b>Triacylglycerides</b> C <sub>53</sub> -C <sub>57</sub>	T <sub>R</sub> match	Biomass	Combustion	GC-FID	37, 41
<b>Sugars</b>  Levoglucosan Mannosan Galactosan	60, 73, 98 147, 204, 217 (TMS <sup>a</sup> )	Biomass	Combustion	GC-MS, GC-FID, GC-MS, HPLC-ED	42-47

<sup>a</sup> MS ions after derivatization with BSTFA. Trimethylsilylated derivatives (TMS)

Table 1. cont.

Compound	MS Ions ( <i>m/z</i> )	Source	Emission Process	Detection Method	Ref
<b>Methoxyphenols</b>		Biomass	Combustion	GC-MS, Py-GC-MS	28, 42, 48-49
Guaiacol	81, 109, 124,				
Syringol	96, 154, 139				
Vanillin	81, 151, 152				
<b>PAHs</b>				GC-MS, Py-GC-MS, GC-FID, TD-GC-MS	
LMW (2-3 ring)	[M <sup>+</sup> ]	Diesel, biomass, wood, coal, charbroiling, asphalt tar, boilers	Combustion		15-16, 18, 20- 21, 50
MMW (4-ring)	[M <sup>+</sup> ]	Diesel, biodiesel, asphalt tar, boilers	Combustion		18, 21, 51
HMW (5-6 ring)	[M <sup>+</sup> ]	Gasoline, biomass, natural gas, meat cooking, asphalt tar	Combustion		19, 50, 52-54
<b>Phthalates</b>	149	Plastic	Combustion	GC-MS, GC-FID	55-57
Bis(2-ethylhexyl) phthalate (DEHP)					
Dibutyl phthalate (DBP)					
Diisobutyl phthalate					
<b>Terpenes &amp; derivatives</b>				GC-MS, HPLC-MS, GC-FID, LC-MS	
$\alpha$ -Pinene	41, 93	Coniferous vegetation	Direct, combustion		58-60
$\beta$ -Pinene	41, 93	Coniferous vegetation	Direct, combustion		
<i>d</i> -Limonene	68, 93, [M <sup>+</sup> ]				
$\Delta^3$ -Carene	93, 121, [M <sup>+</sup> ]				
Pinon aldehyde	[M <sup>+</sup> ]	Pinene	Reaction with O <sub>3</sub> , NO <sub>3</sub> , OH in atmos.		
Pinonic acid	62, 89, 98	Pinene	Reaction with O <sub>3</sub> , NO <sub>3</sub> , OH in atmos.		

Table 1. cont.

Compound	MS Ions ( <i>m/z</i> )	Source	Emission Process	Detection Method	Ref
<b>Organosulfates</b>				GC-MS, LC-MS	
(2,3-Epoxy-2-methyl-1,4-butanediol) sulfate	[M <sup>+</sup> ]	Pinene	SOA formation		61-63
Benzyl sulfate	96, [M <sup>+</sup> ]	Anthropogenic	Emission		61
Glycolic acid sulfate	75, 97 [M <sup>+</sup> ]	Isoprene	Oxidation		61, 64



Elemental carbon, also known as black carbon, consists of fused aromatic rings that are primarily produced from the combustion and pyrolysis of carbonaceous material.<sup>65</sup> Emission sources include: residential heating, transportation services, and power production.<sup>65</sup> EC strongly absorbs light in the visible range and is recognized to have a positive radiative forcing due to the heating of the earth's atmosphere in a similar manner as greenhouse gases.<sup>65-66</sup> Furthermore, it contributes to the warming of the earth as it can deposit layers on surfaces such as ice, leading to reduced reflectivity of solar radiation.<sup>65</sup> EC has also been found to have a negative radiative forcing due to different interactions of EC with clouds. In some cases EC reduces the amount of high level cloud formation, ultimately leading to a negative radiative forcing.<sup>66</sup> Although EC affects the radiation balance of the atmosphere and the earth in both directions, it is considered to have an overall warming effect on the atmosphere.<sup>65</sup>

## I.2. Approaches to Quantitative and Qualitative Analysis of Carbonaceous PM

### *I.2.1. Thermal Optical Analysis of Carbonaceous PM*

To fully understand the effects of carbonaceous PM in the atmosphere, it is necessary to be able to quantify both the OC and EC fraction, as well as the total carbon (TC) content. The most common method to accomplish this task is with a thermal optical analyzer (TOA); also referred to as an OCEC analyzer. Two different methods for analysis are typically used to determine OC, EC, and TC; the National Institute for Occupational Safety and Health (NIOSH) protocol and Interagency Monitoring of Protected Visual Environment (IMPROVE) protocol.<sup>67-68</sup> These protocols both use the thermal evolution method but differ in temperature heating profiles and optical monitoring for determination of OC, EC, and TC.<sup>67</sup> The difference in their heating profiles is that the NIOSH protocol uses a higher temperature for evolving organic carbon than IMPROVE.

The reason for this higher temperature step is to identify interferences caused from inorganic carbon, such as calcium carbonate, which evolves CO<sub>2</sub> at high temperatures (650 - 850 °C).<sup>69</sup> The difference in their optical monitoring process is that the NIOSH protocol mainly uses thermal optical transmittance (TOT) while the IMPROVE protocol uses thermal optical reflectance (TOR) to determine the “split point” between OC and EC, although both instruments are capable of using both TOT and TOR.<sup>68</sup> The need for this laser monitoring process (at 660 nm) is that as much as 30% of OC can be converted to EC through pyrolysis during analysis.<sup>70</sup> When a portion of OC (assumed to be non-light absorbing) is pyrolyzed to EC (light absorbing), a decrease in the overall transmittance or reflectance of the laser occurs, and thus is an indication of pyrolyzed OC. As the analysis continues, the laser transmittance or reflectance will continue to decrease until the point at which the pyrolyzed OC is evolved.<sup>70</sup> At this point, the laser will return to its original value, and thus, any of the EC fraction before this point is assumed to be formed by OC pyrolysis. This continuous laser transmittance/reflectance monitoring prevents an overestimation of the total amount of EC in the sample.

The NIOSH protocol temperature program works on the basis of heating profiles between 100-870 °C in steps that evolve all the OC from the sample.<sup>67</sup> These steps are done in the absence of oxygen, in a helium gas atmosphere.<sup>70</sup> After all OC steps are completed, the instrument is then cooled to around 525 °C and oxygen is added to the helium atmosphere. The instrument is heated back to 870 °C to evolve all of the elemental carbon under the oxygen atmosphere. To determine the amount of carbon present in each analysis, the loaded sample is first transferred to an oxidizing oven and oxidized in the presence of catalyst to CO<sub>2</sub>. The CO<sub>2</sub> is then converted to methane in a methanizer oven, then the CH<sub>4</sub> is analyzed with an FID (Fig. 1)

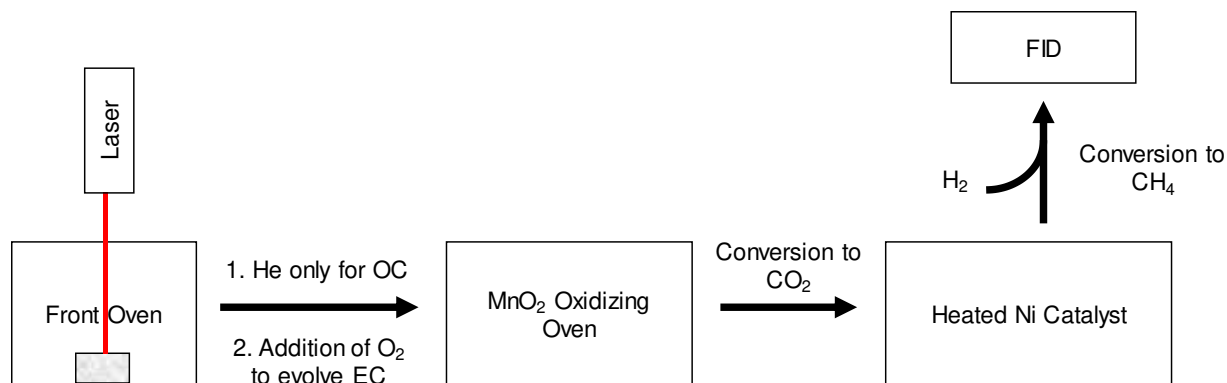


Figure 1. Schematic of the working principle behind the TOA instrument.

### *1.2.2. Mass Spectrometric Analysis of Carbonaceous PM*

Although the concentrations of OC and EC in atmospheric PM can be readily found from TOA instrumentation, this method cannot provide speciation and detailed characterization of the OC (EC cannot be readily speciated through any techniques). Historically, the most common method to speciate the OC fraction of PM is through the use of solvent extraction followed by gas chromatography-mass spectrometry (GC-MS) or liquid chromatography-mass spectrometry (LC-MS) analyses.<sup>71-74</sup> Solvent extraction techniques are typically time consuming, costly, and are mostly limited to analysis of semi-volatile organics.<sup>11, 22</sup>

In recent years, thermal desorption (TD) instruments have been employed that remove the need for solvent extraction methods, with the possibility of online monitoring.<sup>75-80</sup> These instruments generally heat the sample to a maximum of ~ 350 °C in an attempt to thermally desorb volatile species from the sample. However both of these approaches (TD and extraction followed by GC-MS) are limited by targeting only the volatile fraction of the total OC. Thus, development of methods covering a full suite of organic species present in PM and enabling for mass balance closure is essential.

One approach involves the use of online high resolution aerosol mass spectrometers (AMS).<sup>81-84</sup> AMSs are typically coupled with vacuum aerodynamic sampling, followed by pyrolysis (Pyr) at 600 °C and fragmentation by electron ionization.<sup>81, 84</sup> This setup provides the overall composition of organics based on oxygen/carbon/hydrogen ratios and some speciation of thermally stable species based on molecular  $[M^+]$  ions.<sup>81, 85</sup> However, volatile organics present in PM cannot be distinguished from pyrolytic products of higher MW species.<sup>83</sup>

Several previous studies have attempted to address both the volatile and non-volatile PM fraction through a combination of TD and Pyr instruments.<sup>86-89</sup> Streibel et al. evaluated sequential temperature steps of 120, 250, and 340 °C (similar to low TOA temperatures) followed by MS detection and suggested that a vast amount of products evolved at higher temperatures, thus showing need for thorough investigation of Pyr products and mass balance closure.<sup>87</sup> Labban et al. reported the use of separate TD-GC-MS and Pyr-GC-MS setups to investigate soil dust sources showing a significant role of the pyrolytic fraction.<sup>86</sup> More recently, studies have shown that TD and a full range of Pyr steps (400 – 870°C) can be pursued with one instrumental set up, TD-Pyr-GC-MS, thus mimicking the full profile of TOA temperature steps for characterization of OC.<sup>88-89</sup>

Clearly, both the advantages and limitations of methods described above influence data interpretation. As a result, the majority of specific tracers used in source apportionment studies are based on TD and solvent extraction data (Table 1). Furthermore, although the value of Pyr has been shown, less is known of PM related pyrolytic products.<sup>86-88</sup> Still, characteristic markers for specific sources may be investigated on the pyrolytic studies of original feedstocks, i.e., triacylglycerides (TGs), fatty acids, coal, and cellulose (Table 2).

Table 2. Products of pyrolysis of feedstocks including fatty acids, TGs, cellulose, coal

<b>Compound</b>	<b>MS Key Ions (<i>m/z</i>)</b>	<b>Sample</b>	<b>Ref</b>
<b><i>n</i>-Alkanes</b>	57,71,85 [M <sup>+</sup> ]		
C <sub>7</sub> -C <sub>17</sub>		Fatty acids	90-91
C <sub>3</sub> -C <sub>28</sub>		Coal	92-94
C <sub>3</sub> -C <sub>24</sub>		Triacylglycerides	95
Cycloalkanes		Coal, triacylglycerides	94, 96-97
<b><i>n</i>-Alkenes</b>	55, 69, 83 [M <sup>+</sup> ]		
C <sub>7</sub> -C <sub>19</sub>		Fatty acids	90-91
< C <sub>21</sub>		Coal	93
C <sub>7</sub> -C <sub>12</sub>		Coal	96
Cycloalkenes		Triacylglycerides	97
<b><i>n</i>-Alkadienes</b>	39, 54, [M <sup>+</sup> ]		
C <sub>10</sub> -C <sub>17</sub>		Fatty acids	90-91
<b><i>n</i>-Alkylbenzenes</b>	91, 92, [M <sup>+</sup> ]		
C <sub>0</sub> -C <sub>3</sub>		Fatty acid salts, coal	90-94, 96
C <sub>1</sub> -C <sub>18</sub>		Triacylglycerides	97
<b>Ketones/Aldehydes</b>	43, 58, 71, [M <sup>+</sup> ]		
C <sub>3</sub> -C <sub>6</sub>		Cellulose	98-100
C <sub>6</sub> -C <sub>18</sub>		Fatty acids	90-91
<b>Phenols &amp; derivatives</b>	94, [M <sup>+</sup> ]		
C <sub>0</sub> -C <sub>3</sub>		Coal, cellulose, lignin, triacylglycerides	92, 94, 96-97, 99, 101
<b>BTEX</b>	91, 92 [M <sup>+</sup> ]	Lignin	101
<b>PAHs</b>			
LMW (2-3 ring)	[M <sup>+</sup> ]	Coal, cellulose, triacylglycerides, fatty acids	91-96, 99
MMW (4-ring)	[M <sup>+</sup> ]	Coal	92-94, 96
HMW (5-6 ring)	[M <sup>+</sup> ]	Coal	102

Table 2. cont.

Compound	MS Key Ions ( <i>m/z</i> )	Sample	Ref
<b>Anhydrosugars</b>	60, 73, 98, 147, 204, 217 (TMS <sup>a</sup> )	Cellulose	98, 100
Levoglucofan			
Levoglucofanone			
1,4:3,6-Dianhydro- $\alpha$ -d-glucopyranose			
<b>Alkanoic acids</b>	74, 87, 143		
C <sub>2</sub> -C <sub>3</sub>		Cellulose	100
C <sub>2</sub> -C <sub>16</sub>		Triacylglycerides	95, 97
<b>Dicarboxylic acids</b>	87, 115, 100, 129 [M <sup>+</sup> ]	Triacylglycerides	103

<sup>a</sup> MS ions after derivatization with BSTFA. Trimethylsilylated derivatives (TMS)

The combination of TD and Pyr allows for a unique approach to the investigation of OC compounds, their use as tracers, and their TD and Pyr profiles at temperatures of 300, 500, 600, 700 and 870 °C. This characterization can be used in tandem with quantitative TOA data, which uses the same temperature profile, to provide a much broader understanding of PM in the atmosphere, mainly the carbonaceous fraction. Furthermore, we are able to identify compounds that are not always accessible with the previously mentioned methods that target only a specific set of compounds, i.e., volatiles, semi-volatiles, or LMW compounds formed from the pyrolysis of their parent compounds.

### I.3. Statement of Purpose

The aim of this work was to develop an analytical method, namely TD-Pyr-GC-MS, which could be used in tandem with TOA to provide comprehensive characterization of the OC fraction of PM. The advantage of using such a method is that it minimizes sample preparation, which is both time and cost effective, i.e., eliminating the need for solvent extraction. Furthermore, this analytical technique is able to mimic the stepwise temperature profiles of TOA, which no other GC or MS sample introduction method is capable of, providing detailed thermal profiles (TD & Pyr) for a wide range of organic compounds.

TD-Pyr-GC-MS was first applied to model compounds such as TGs and FAs, in an attempt to understand the pyrolytic nature for their decomposition. Specifically, these compounds were chosen as they represent compounds present in the atmospheric PM, but may not be efficiently detected (e.g., TGs) and compounds that are widely abundant (e.g., FAs) from a wide range of sources. The breakdown products after the pyrolysis of these model compounds were analyzed to investigate their proposed mechanism of formation as well as the specific profiles they form after pyrolytic decomposition.

With the aid of the TD-Pyr-GC-MS evolving profiles of model compounds, this method was then applied to atmospheric PM collected in the Grand Forks area. Through detailed analysis of both the TD and Pyr fractions, determination of specific compounds, that is atmospheric tracers with varying volatilities, was enabled, which other methods described in the introduction cannot accomplish. The detection of these tracers, and their abundances through TD-Pyr-GC-MS were used in an attempt to determine the origin of these species, enabling source apportionment, mainly between anthropogenic and biogenic sources.

## CHAPTER II. EXPERIMENTAL METHODS

### II.1. Materials

Organic solvents used in this study included dichloromethane (DCM) and hexane (VWR, Arlington Heights, IL, USA) for dissolving standards for use with TD-Pyr-GC-MS. ACS grade sucrose (Alfa Aesar, Ward Hill, MA, USA) dissolved in deionized water from a Direct-Q 3 UV system purifier (Millipore, Billerica, MA, USA) was used for TOA calibrations. Standards used for pyroprobe optimization included nonane, butylbenzene, 1-tridecene, heptadecane and dotriacontane (standard mixture 1 (SM1), 1000 ppm (w/v) dissolved in DCM) as well as the addition of 1000 ppm (w/v) of benzene, toluene, ethyl benzene, *m*-xylene (BTEX) to SM1, thus creating SM2. For analysis of model compounds, C<sub>21</sub>-C<sub>40</sub> alkane mix, tristearin, triolein, stearic acid, and oleic acid were used. All standard compounds were purchased from Sigma–Aldrich (St. Louis, MO, USA).

### II.2. Sampling

Atmospheric PM<sub>2.5</sub> was collected during a 17 week period as part of the Polarimetric Cloud Analysis and Seeding Test (POLCAST) from June 21, 2012 - October 19, 2012 in rural North Dakota (ND).<sup>104</sup> PM<sub>2.5</sub> was sampled at Clifford Hall (the roof of the 5 story building) located at the University of North Dakota in Grand Forks, near the western outskirts of the city.

PM<sub>2.5</sub> samples were collected weekly on 90 mm (46.56 cm<sup>2</sup> exposed area) tissue quartz filters 2500QAT-UP (Pall Corp, Port Washington, NY, USA) with a semi-volatile organic aerosol



sampler (URG Corp, Chapel Hill, NC, USA) attached to a R224 quad head high-vacuum air pump (Air Dimensions Inc., Deerfield Beach, FL, USA). A 16.7 liters per minute (LPM), 10  $\mu\text{m}$  Teflon coated aluminum cyclone (URG Corp, Chapel Hill, NC, USA) was used to collect  $\text{PM}_{2.5}$  by setting the flow rate to 92 LPM. The quartz filters were heated at 600  $^{\circ}\text{C}$  for 12 hours overnight to remove any trace contaminants before PM collection. A mass flow controller (Alicat Scientific, Tucson, AZ, USA) was set at a rate of 1533  $\text{cm}^3/\text{s}$  (92 LPM) for PM collection. All 90 mm filters were weighed on an analytical balance before and after collection. After collection/analysis, the filters were placed in aluminum foil wrapped on the inside of Petri dishes and stored in a freezer to minimize the loss of semi-volatile compounds until the analysis.

## II.3. Instrumentation

### *II.3.1 Thermal Optical Analyzer*

An OC-EC aerosol TOA analyzer (Sunset Laboratory Inc., Tigard, OR, USA) was used to determine concentrations of OC, EC, and TC of collected PM based on a NIOSH protocol. Quartz filters were cut with a 1.5  $\text{cm}^2$  filter punch and subsequently placed in the instrument. The quartz filters were subject to a temperature profile that began with a 10 s ambient temperature step followed with 5 steps; 300  $^{\circ}\text{C}$  for 75 s, 500  $^{\circ}\text{C}$  for 75 s, 600  $^{\circ}\text{C}$  for 75 s, 700  $^{\circ}\text{C}$  for 75 s, and 870  $^{\circ}\text{C}$  for 120 s, all in a helium atmosphere. This ramp was followed by a cooling step to 525  $^{\circ}\text{C}$  for 45 s. Five more temperature steps were then introduced under a 5% oxygen in helium atmosphere; 550  $^{\circ}\text{C}$ , 625  $^{\circ}\text{C}$ , 700  $^{\circ}\text{C}$ , and 775  $^{\circ}\text{C}$  for 45 s each, followed by 890  $^{\circ}\text{C}$  for 120 s. Lastly, a calibration gas of 5 % methane/helium was added as an internal standard for 110 s. The total analysis time was 885 s.

TOA data was acquired through the OCEC 828 software and was subsequently converted to a text file. This text file was then converted to an Excel template where further data processing took place, including the evaluation of the split point, and concentrations of OC/EC in each temperature fraction.

### *II.3.2 TD-Pyr-GC-MS*

A CDS Pyroprobe model 5000 (CDS Analytical, Oxford, PA, USA) coupled to an Agilent 7890 GC-MS (Agilent, Santa Clara, CA, USA) was used to perform TD-Pyr-GC-MS to identify different organic compounds within air PM and model compounds (detailed programming is described in the following section II.3.2.1). A 38.7 m long HP-5MS column with a 0.25  $\mu\text{m}$  film thickness and 0.25 mm diameter was used (Agilent, Santa Clara, CA, USA). The GC temperature program started at 40 °C for 2 min, followed by a ramp of 40 °C/min to 80 °C, then immediately followed by a ramp to 320 °C at 25 °C/min and held for 4 min. The GC was operated in the split mode (10:1) with helium used as the carrier gas at a constant flow of 1.5 mL/min. MS analysis with electron ionization (70 eV) was done in total ion current mode with a scanning range of 35-550  $m/z$ .

TD-Pyr-GC-MS data was acquired with ChemStation E.02.02.1431 (Agilent, Santa Clara, CA, USA). Individual compounds and their homology patterns were investigated using extracted ion chromatograms (EIC) for each temperature fraction. The retention times and ions used for identification and semi-quantification profile for specific compounds are listed in Appendix F, Table F1. Peak identification was done by comparing with the NIST 05 Mass Spectral library with 80 % match or higher, based on retention profiles of homologous compounds, and/or through confirmation by individual standards.<sup>88, 105</sup>

### II.3.2.1 Operation of TD-Pyr-GC-MS

The CDS pyroprobe 5200 model used in this study was designed to either thermally desorb or pyrolyze samples within the instrument, or to do both by sequentially running multiple sequential temperature steps (the final protocol is shown in Appendix A with pyroprobe temperature programs in Table A1). This process was accomplished by spiking either a liquid or solid sample onto a piece of quartz wool that sits inside a quartz tube, which was held by a platinum filament on the probe (Fig. 2).

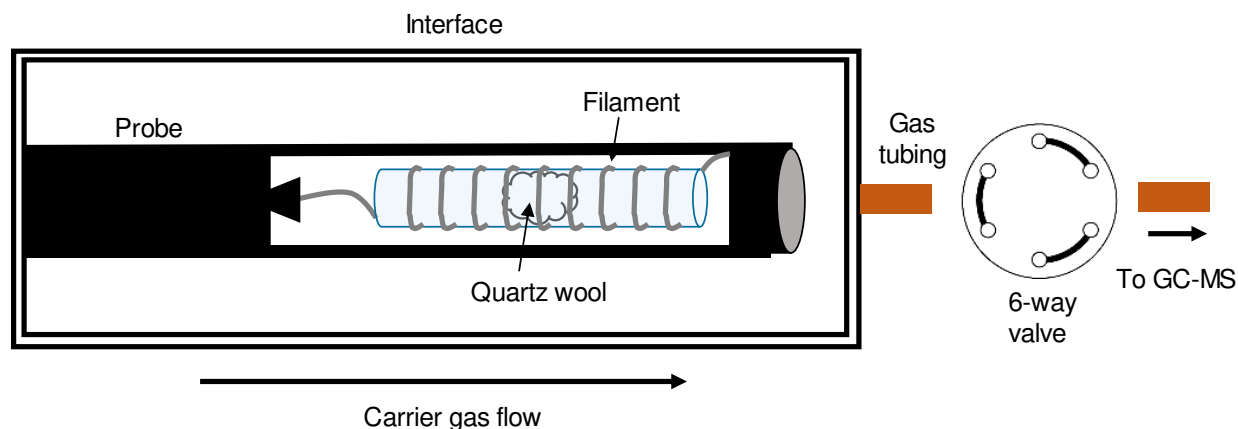


Figure 2. Schematic diagram of the pyroprobe filament found on the CDS pyroprobe 5200 model.

Next, the sample was either dried outside of the instrument (liquid samples) or directly inserted into the main body (solid samples) and sealed from the outside atmosphere. The interface, a housing that is surrounded by heating wrap, was then heated ballistically to a temperature of 300 °C which took approximately 45 seconds (Fig. 3). After the interface reached 300 °C, a 6-way valve that was heated to 320 °C opened, allowing the flow of the carrier gas (He) for transfer to the GC-MS. At the same time the valve opened, the filament began heating to specific temperatures (300, 500, 600, 700, or 870 °C) at a ramp rate of 30 °C/s (for optimization of heating rates and interface times see next section). At this point the sample was either thermally desorbed (< 350

°C) or pyrolyzed (> 400 °C) depending upon the sample temperature. The filament was then held at the set temperature for a duration of 30 seconds, after which it was shut off. Lastly, the 6-way valve closed and the carrier gas was then once again diverted to waste until the GC-MS finished its temperature program. After the GC-MS program was complete, the next pyroprobe temperature step could be analyzed and the complete process repeated itself.

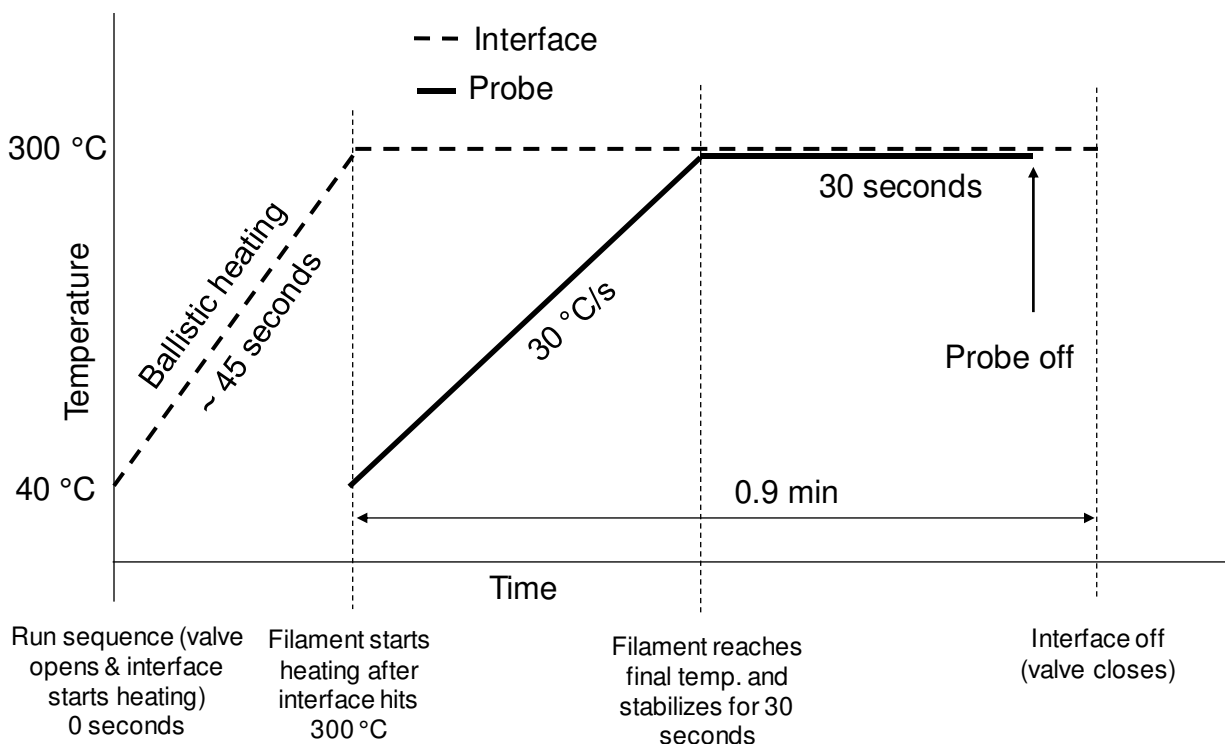


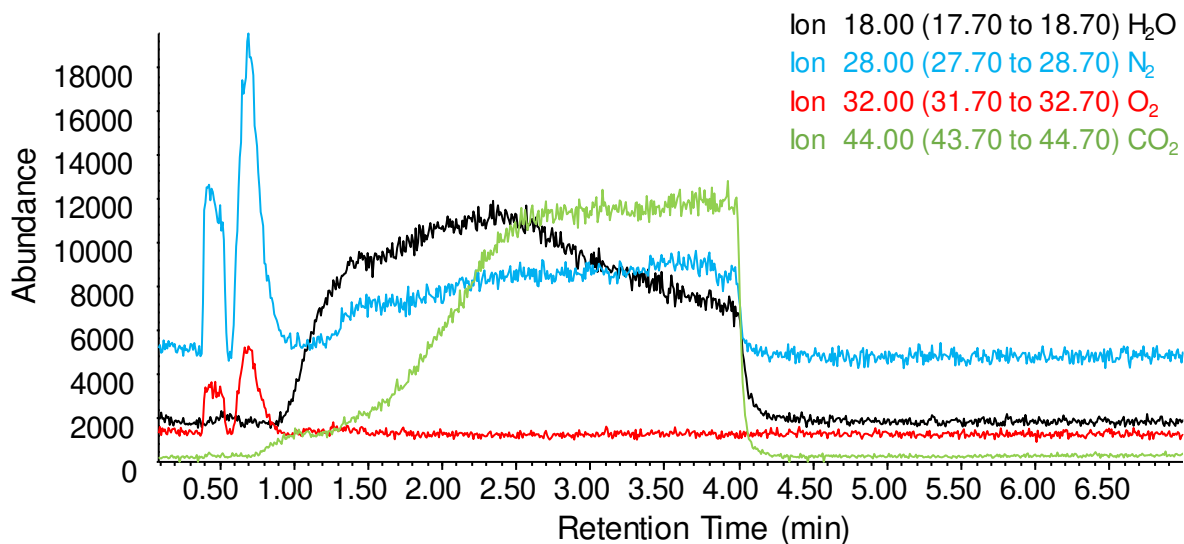
Figure 3. Typical thermal process for pyroprobe during analysis of samples.

#### II.4. Optimization of TD-Pyr-GC-MS

Various parameters for the TD-Pyr instrument affect the performance of the pyroprobe and had to be optimized. The parameters in this study that were optimized were the interface time and filament heating rate which affect the ability of the instrument to volatilize the sample. These parameters were optimized to try to minimize large CO<sub>2</sub>/air peaks that were observed at the beginning of every TD-Pyr GC-MS analysis and can overlap with early eluting compounds as it

extends until ~ 4 min into the GC chromatogram (Fig. 4). The reason for the occurrence of the large CO<sub>2</sub>/air peak at the beginning of each chromatogram was thought to be from the formation of CO<sub>2</sub> within the instrument (if contaminated) as well as possible valve micro leaks.

a)



b)

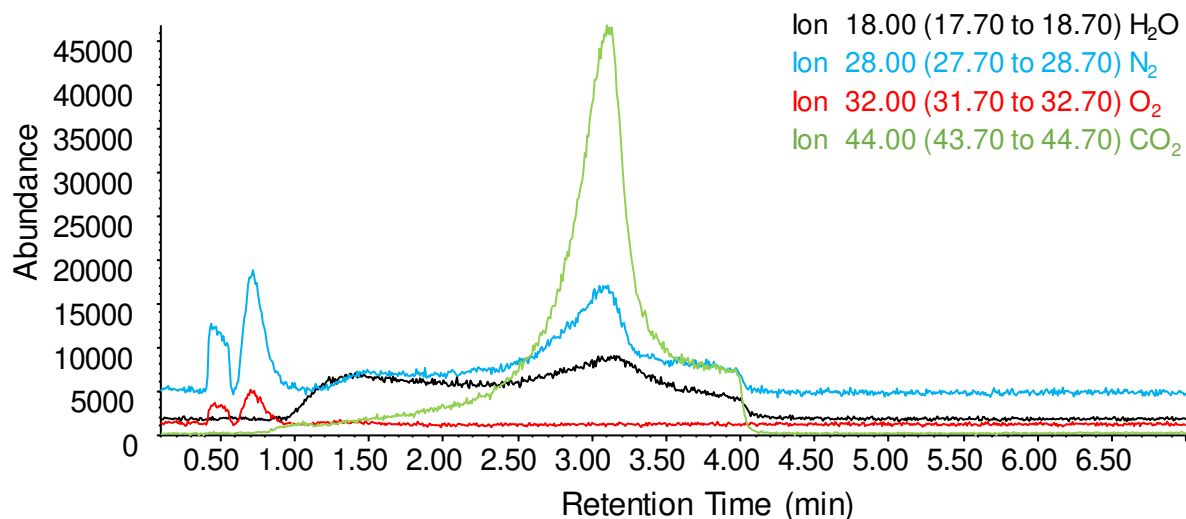


Figure 4. TD-Pyr-GC-MS EIC chromatograms of a blank sample corresponding to the occurrence of H<sub>2</sub>O (18 *m/z*), N<sub>2</sub> (28 *m/z*), O<sub>2</sub> (32 *m/z*), and CO<sub>2</sub> (44 *m/z*) peaks at a) 300 °C and b) 870 °C.

The initial experiments performed to test different filament heating rates and interface times can be seen in Table 3. For each experiment, 5 μL of SM1 was injected, and dried for 60

seconds at 50 °C outside of the instrument. For all experiments the pyroprobe final temperature was 300 °C. EIC *m/z* values were used to determine the optimal filament heating rate and interface times (Appendix B, Table B1)

Table 3. Pyroprobe filament heating rates and interface time optimization conditions

<b>Parameter</b>	<b>Experiment</b>					
	<b>1</b>	<b>2</b>	<b>3</b>	<b>4</b>	<b>5</b>	<b>6</b>
Filament heating rate (°C/s)	10	15	20	30	ballistic <sup>a</sup>	ballistic <sup>a</sup>
Interface time (min)	2.5	1	0.8	0.6	0.6	0.5

<sup>a</sup> The heating rate goes as fast as instrumentally capable

After the first set of experiments, further optimization was done using interface times of 0.9, 1.0 and 1.2 min, respectively, at a filament heating rate of 30 °C/s. This optimization was done with SM2 to understand the behavior of lower MW compounds, namely BTEX compounds. Each sample was run in triplicate and their respective average peak abundances were based on specific EIC *m/z* values to evaluate different interface times (Appendix B, Table B1).

## II.5. TD-Pyr-GC-MS of Model Compounds

To understand the TD-Pyr behavior of certain compounds and their thermal profiles, model compounds were analyzed with the pyroprobe. These model compounds were chosen to represent a wide range of compounds of both biogenic and anthropogenic sources that are thought to exist in atmospheric PM in a relatively biogenic area such as Grand Forks, ND. They included: C<sub>21</sub>-C<sub>40</sub> alkane mix, tristearin, triolein, stearic acid, and oleic acid.

Quartz wool was first placed inside a quartz tube (CDS Analytical, Inc, Oxford, PA, USA), inserted into the filament, and cleaned with a 25 µL DCM spike (x 3). The filament was then heated to 870 °C outside of the probe to remove any trace contaminants+ and DCM. A blank run was then conducted to ensure the system was clean (determined based in a correct baseline), and

repeated if necessary. After achieving clear baseline, the model compounds were analyzed by injecting 10  $\mu\text{L}$  into the quartz tube, followed by drying for 60 seconds at 50  $^{\circ}\text{C}$  outside of the instrument. All model compounds were analyzed with a two-step temperature program, 300  $^{\circ}\text{C}$  (TD) followed by 700  $^{\circ}\text{C}$  (Pyr), as well as at 700  $^{\circ}\text{C}$  directly (one-step), to better understand the pyrolytic nature of the compounds. Compound identification was done with reference to SM1 and SM2 and/or by comparison with the NIST 05 Mass Spectral library.

## II.6. TOA and TD-Pyr-GC-MS of POLCAST Samples

Collected PM filters from the 17 week POLCAST campaign were analyzed by both TOA and TD-Pyr-GC-MS. Quartz filters were cut into 1.5  $\text{cm}^2$  for TOA and into  $\sim 2 \times 15$  mm strips for TD-Pyr-GC-MS analysis, respectively. The quartz filter strips were subjected to the same temperature conditions in both instruments: 300, 500, 600, 700, and 870  $^{\circ}\text{C}$ , under an inert He atmosphere. All weeks (12-17) were analyzed by TOA, while only weeks 12-17 were subject to TD-Pyr-GC-MS, due to instrumental problems.

Derivatization of the PM on quartz filters was carried out with two different methods to assess the occurrence of free acids. First, 100  $\mu\text{L}$  of *N,O*-bis(trimethylsilyl)trifluoroacetamide (BSTFA): trimethylchlorosilane (TMCS) 99:1 (Supelco, Bellefonte, PA, USA) was added to the cut quartz filter in an autosampler vial and heated at 70  $^{\circ}\text{C}$  for 2 hours. The sample on the filter was then dried under  $\text{N}_2$  and analyzed on the TD-Pyr-GC-MS. Second, TMAH (1  $\mu\text{L}$ ) was added to the quartz filter directly on the pyroprobe and analyzed.

## CHAPTER III. RESULTS AND DISCUSSION

### III.1. Optimization of TD-Pyr-GC-MS

The initial TD-Pyr-GC-MS method optimization to determine the ideal filament heating rate and interface time for the pyroprobe can be seen in Fig. 5, which shows the abundance of the quantification ion of each compound obtained from EIC chromatograms (Appendix B, Table B1). The highest abundances, that is the most efficient transfer of analytes from the pyroprobe to GC, were obtained when using a filament heating rate of 20 and 30 °C/s, and an interface time of 0.8 and 0.6 minutes, respectively (white dotted bars) and (black bars) (Fig. 5, the conditions are detailed in Table 3 in Section II.4). The original method, which had a 2.5 min interface time along with a ramp rate of 10 °C/s (white bars), was more favorable to less volatile compounds (i.e., dotriacontane) but losses of volatiles species were found. It is of note that the experiments, which used ballistic heating of the filament, showed losses for almost all compounds and therefore were not suitable. In summary, the results revealed that the 30 °C/s filament heating rate was most appropriate, and was used for the rest of the experiments conducted in this study for two reasons. First, as shown in Fig. 5, we can see that the 30 °C/s ramp rate gave similar abundances of all compounds when compared to lower ramp rates. Furthermore, the use of this faster ramp rate allowed for the reduction of the interface time, which in turn reduced the CO<sub>2</sub> peak at the beginning of the pyroprobe analysis. This reduction of the large CO<sub>2</sub> peak at the beginning of every



chromatogram was drastically minimized, allowing for the easier identification of volatile compounds with TD-Pyr-GC-MS.

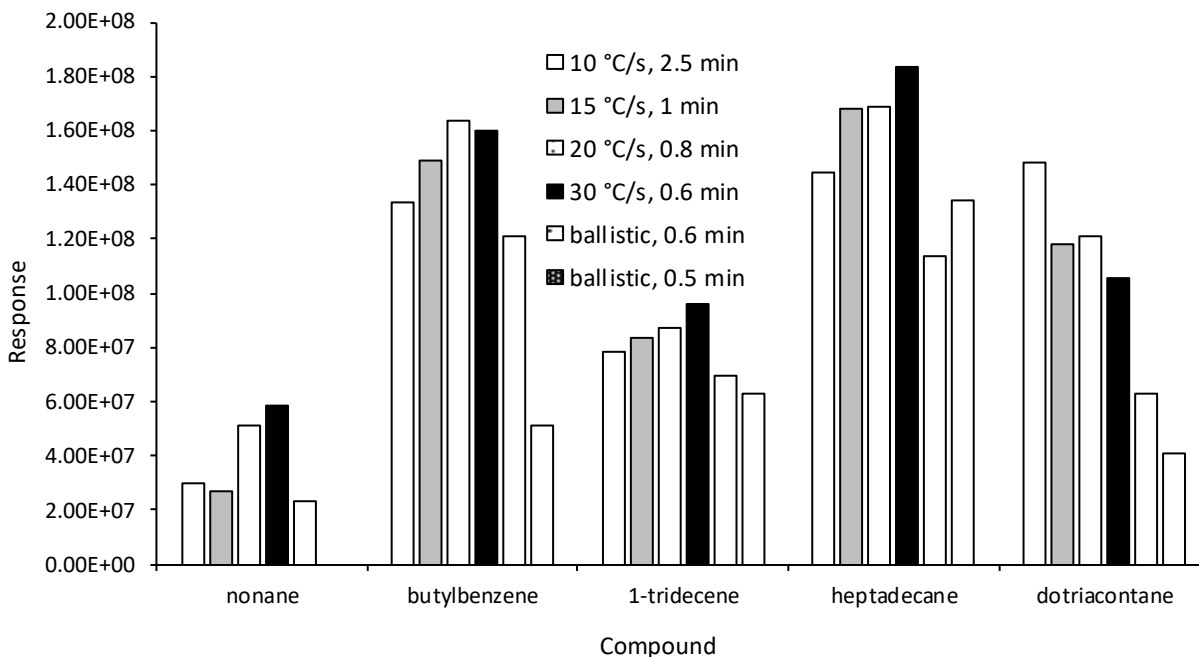


Figure 5. EIC abundances of characteristic ion for selected compounds to evaluate different filament heating rates and interface times of the pyroprobe with filament desorption temperature of 300 °C.

Further optimization of the pyroprobe interface time was done after the initial optimization of the instrument showed that the 30 °C/s filament heating rate produced similar abundances with the 20 °C/s rate (Fig. 5, white dotted bars and black bars). Although, these two filament heating rates were optimized with interface times of 0.6 and 0.8 min, respectively, this was done with a final temperature of the filament set at 300 °C. However, if the filament is set to a high temperature such as 700 °C and held for 30 s, or 870 °C for 10 seconds, this would take longer than 0.6 and 0.8 min; the total time required would be a minimum of 0.9 min. Therefore, a 0.9 min interface time was analyzed against 1.0 min and 1.2 to determine if this had any effect, using SM2. The results revealed that there was no statistical difference between each interface time (Fig. 6). In

general, the 1.0 min interface time showed the highest average abundance for all analytes but dotriacontane. The average RSD values for the standard mixtures were however the lowest during the 0.9 min interface time, with an average of 15.5 % for all the compounds combined, compared to 18.2 and 20.6 % for the 1.0 and 1.2 min interface times, respectively (Appendix C, Table C1). Moreover, this difference was most significant in the average abundances of the volatile compounds, namely BTEX, showing the best repeatability for volatile species. Furthermore, there was no significant difference in the average abundances of each peak for the less volatile compounds showing that they all still elute from the system with shorter interface times. Based on the fact that the average RSD values for all compounds was the lowest in the 0.9 min interface time, along with 0.9 min having the shortest air/CO<sub>2</sub> peak on the GC chromatogram (Fig. 7), this interface time was deemed to be the most efficient. For all subsequent analyses of model compounds and PM samples, these parameters were used.

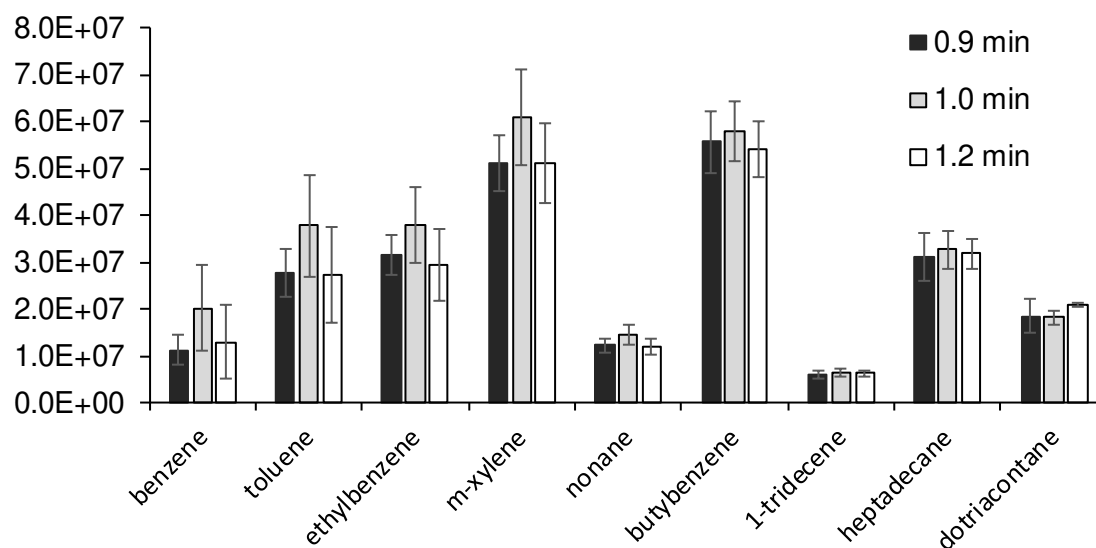


Figure 6. TD-Pyr-GC-MS EIC abundances for selected compounds to evaluate pyroprobe interface times. Filament heating rate was set at 30 °C/s with a filament desorption temperature of 300 °C.

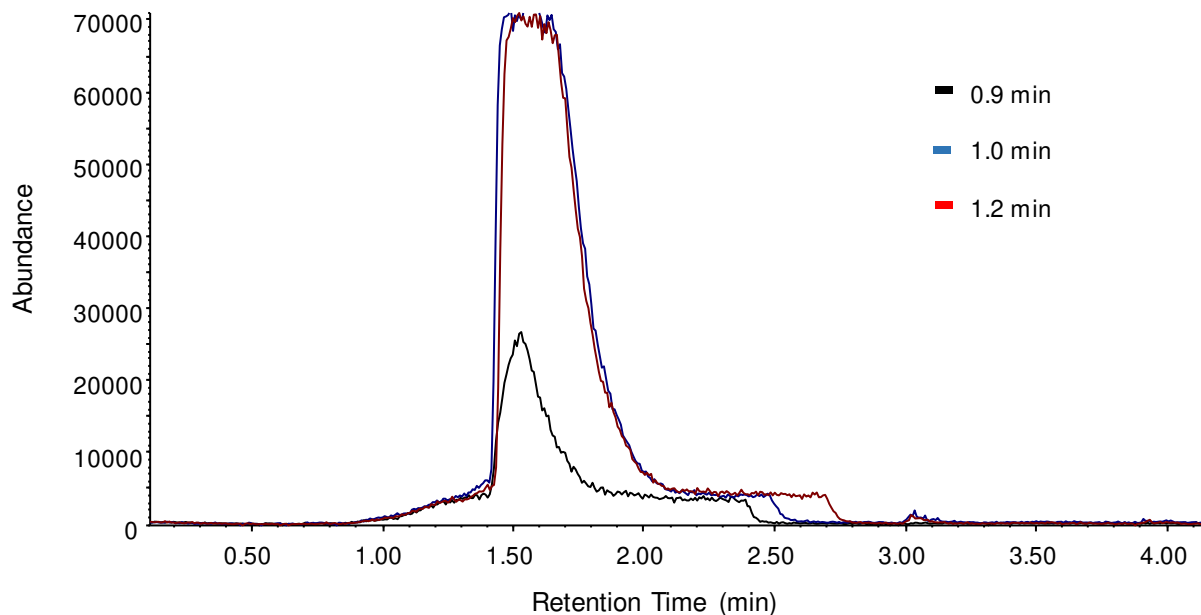


Figure 7. TD-Pyr-GC-MS EIC of ion 44  $m/z$  to show  $\text{CO}_2$  peak at different interface times.

### III.2. TD-Pyr-GC-MS of Model Compounds

The TD (300 °C) and Pyr nature (>400 °C) of model compounds that are of importance to the understanding PM in the atmosphere are discussed in the following sections.

#### III.2.1 $\text{C}_{21}\text{-C}_{40}$ Alkane Mix

As *n*-alkanes are among the most abundant species found in PM from all types of emissions (Table 1), the understanding of their TD and Pyr behavior was of utmost importance. Furthermore, this standard mixture was crucial in evaluating the performance of the pyroprobe and its ability to effectively transfer to GC compounds over a broad range of volatility, i.e., low MW and high MW compounds, and assess possible discrimination (Fig. 8).

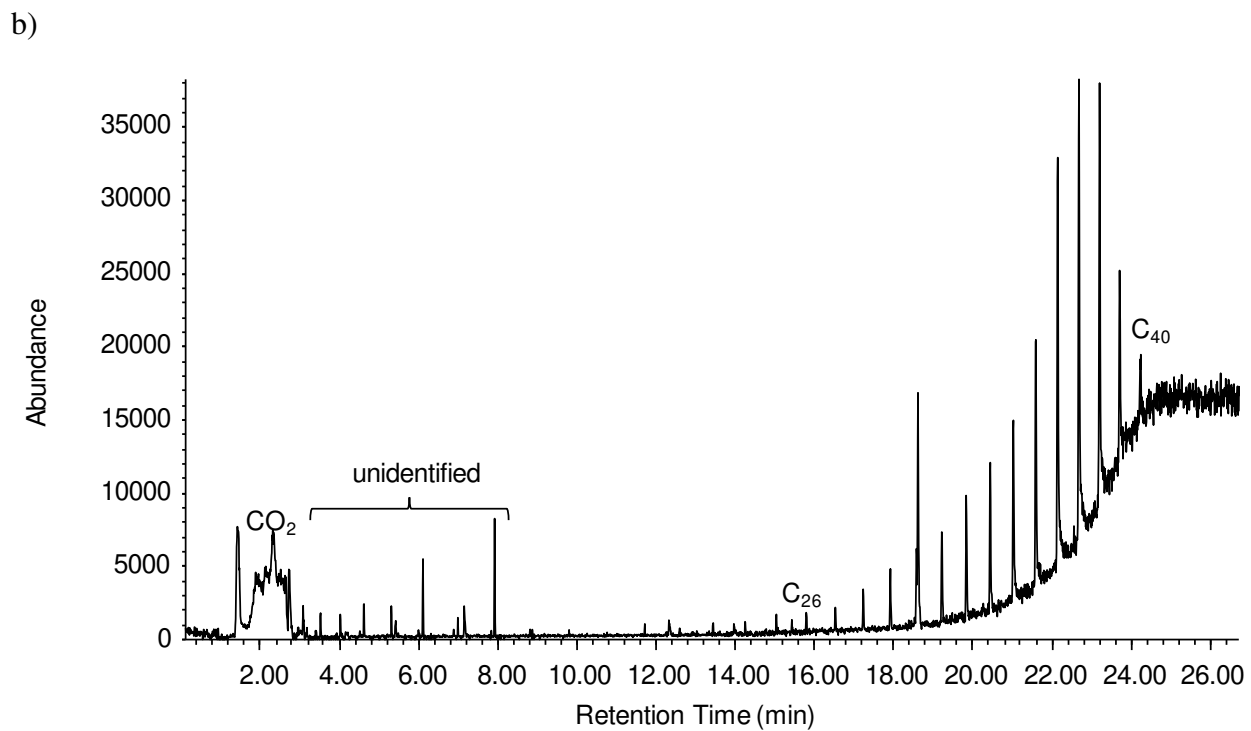
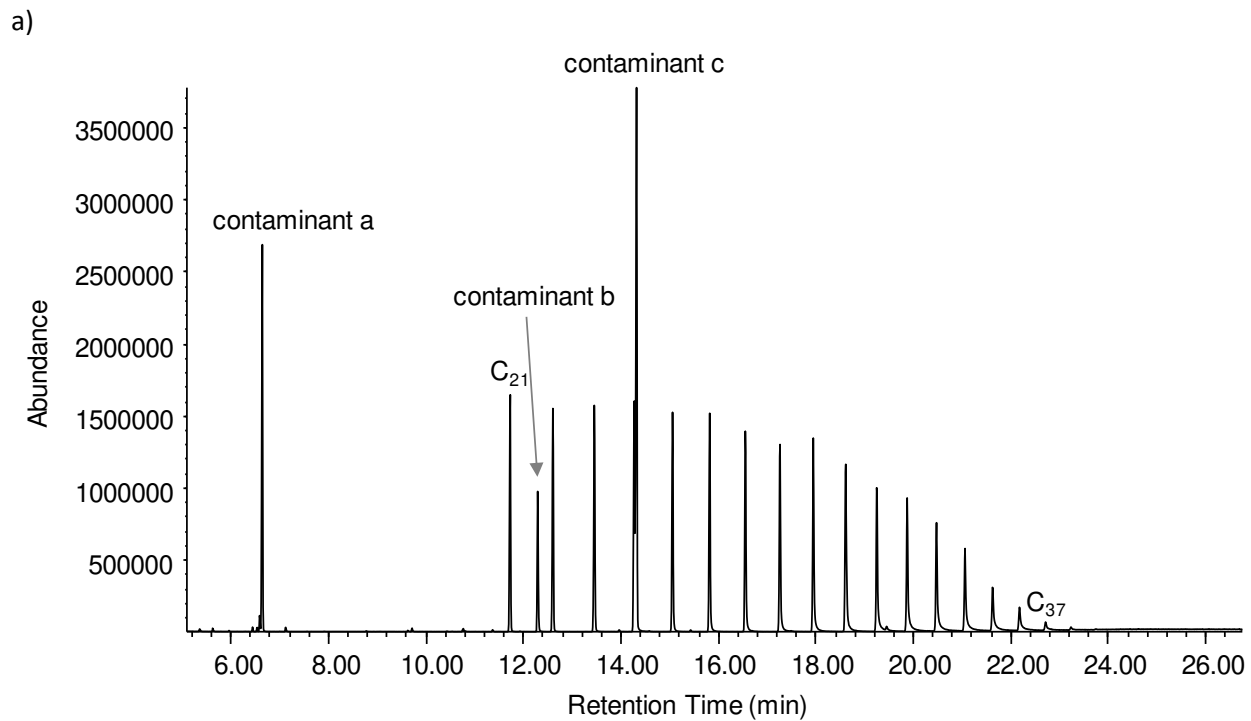


Figure 8. TD-Pyr GC-MS TIC chromatograms of  $C_{21}$ - $C_{40}$  alkane mix a) 300 °C TD fraction b) sequential 700 °C Pyr fraction.

From the above chromatograms, one can see that almost all alkanes except for the last three, C<sub>37</sub> to C<sub>40</sub>, were apparent in the 300 °C fraction. The loss of the last three alkanes within the chromatogram was thought to be from a cold spot within the instrument or some sort of transfer loss from the pyroprobe to the GC-MS (perhaps at the injection port). The TD fraction also contained some impurities of unknown origin (not present within the safety data sheet of the alkane mix) that were tentatively identified as oxacyclotridecan-2-one (90%), dibromodiphenyl sulfide (96 %), and bis(*p*-bromophenyl) disulfide (93 %) from the NIST 05 database (Appendix D, Fig. D1a-c). In the following 700 °C fraction (Pyr fraction of the two-step profile) (Fig. 8b), we observed that some of the long chain alkanes carried over from the TD fraction and appeared there as well, although their abundance was very low. In the beginning of the Pyr fraction, the characteristic CO<sub>2</sub> peak could be seen, along with a few peaks that appeared to be either alkenes or cycloalkanes, but their identification with the NIST library was below 50 % due to very low abundances and significant fragmentation. Altogether, these results confirmed that the pyrolysis of alkanes did not result in many smaller MW products forming, the significance of which is discussed in further detail in Section III.3.2.

The analysis of the alkane mixture using directly one step pyrolysis at 700 °C can be seen in Fig. 9. Under pyrolytic conditions, the chromatogram was identical as when it was run under TD temperatures, there was no breakdown of alkanes into smaller MW compounds. Once again, this finding confirmed that alkanes are very stable, as they tend not to breakdown into smaller MW compounds.

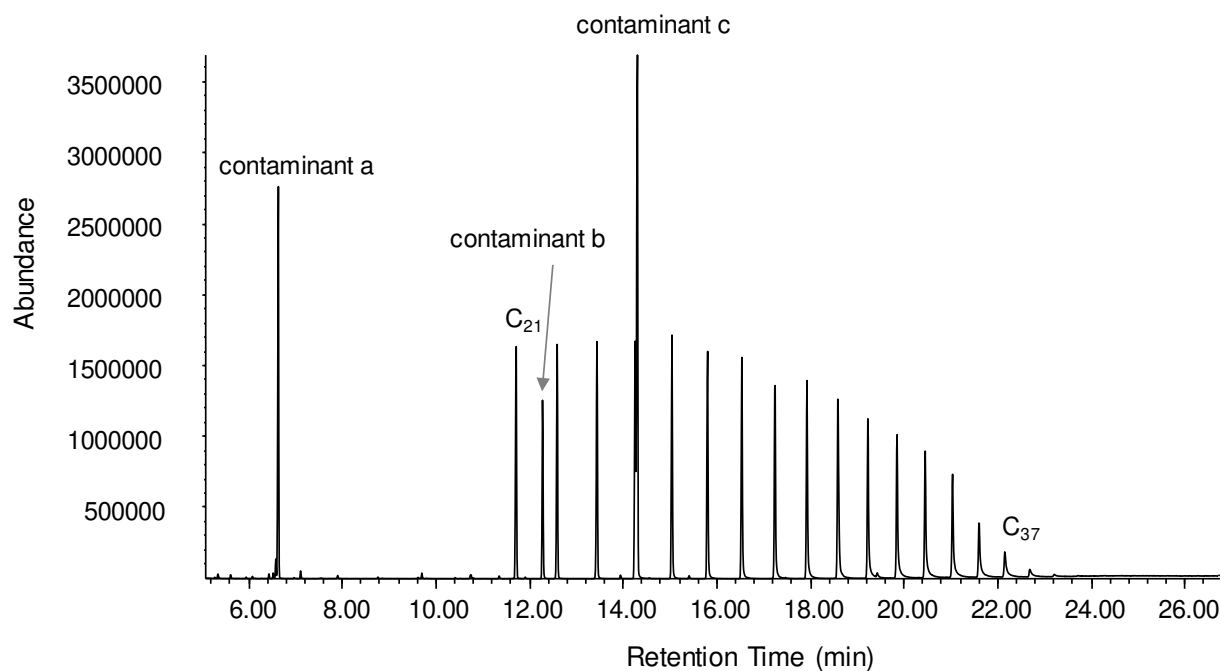


Figure 9. Pyr-GC-MS TIC chromatogram of alkane mix analyzed following direct pyrolysis at 700 °C

### III.2.2 Stearic Acid

As for alkanes under the TD temperature of 300 °C, stearic acid did not break down into smaller compounds; the chromatogram showed an abundant stearic acid peak, along with a contaminant siloxane peak, which is thought to arise from the quartz wool in the pyroprobe tube or from column bleed (Fig. 10a). The sequential temperature step (700 °C of the two-step process) showed that at pyrolytic temperatures, the remaining stearic acid was decomposed, showing as the most abundant peak of 2-tetradecylcyclobutanone (although isomeric position based on MS match is only tentative, Appendix D, Fig. D2), with a series of n-alkenes also present (Fig. 10b). It is of note, 2-tetradecylcyclobutanone was also reported in literature to form from irradiation of stearic acid based triacylglycerides,<sup>106</sup> however no literature shows the formation of this compound directly upon pyrolysis of stearic acid. The mechanism of formation was thought to be from a

stearic acid acyl radical that attacks itself at a C-H bond 4 carbons from the end of the radical, to form the cyclobutyl group, and henceforth the molecule of 2-tetradecylcyclobutanone.

The alkene profile ranged from C<sub>6</sub> to C<sub>17</sub>, while any smaller MW alkenes were either of too small abundance to be detected with the instrumental programming or were not formed readily from pyrolysis. C<sub>17</sub> was the largest size alkene observed in the chromatogram, which may be explained by the decarboxylation of the parent molecule.<sup>107</sup> Alkanes (not shown) were also present in the pyrolytic profile from C<sub>11</sub> to C<sub>17</sub>, accompanying the corresponding alkenes, however at much lower abundances; heptadecane had the highest response, roughly 10 % in height compared to that of heptadecene. The observed formation of alkanes may serve as evidence of significant hydrogen formation, as alkanes appear to be formed by the reaction of the corresponding alkyl radicals with hydrogen (presumably, atomic). The latter appears to be formed *in situ* when alkenes are formed from the same intermediates via hydrogen elimination.

Aromatic hydrocarbons, namely mono-substituted *n*-alkylbenzenes (confirmed by standard and retention time profile), were also formed with similar abundances to the alkane series (10 % of the corresponding alkene peaks) (Fig. 10c). The most abundant *n*-alkylbenzene was dodecylbenzene, which contains 18 carbon atoms. The mechanism in which this compound is formed is theorized to be from hydrodeoxygenation (HDO), as no carbons are lost from the parent stearic acid molecule.<sup>108</sup> Although HDO is typically performed with a catalyst, no catalyst was used in this study, showing a novel way in which HDO occurs. This mechanism appears to compete with decarboxylation followed by cyclization, which would predominantly form undecylbenzene. The driving force of these competing reactions is theorized to be the presence of an abundance of hydrogen in the pyroprobe that leads to hydrodeoxygenation as described above.

Furthermore, a few PAHs were formed that included naphthalene, substituted naphthalenes, phenanthrene, and fluorene. However, all these PAHs were in relatively low abundances other than naphthalene. Both *n*-alkylbenzenes and PAHs have been shown to form as TG cracking products, presumably via alkenyl radical cyclization followed by dehydrogenation.<sup>97</sup> However, the C<sub>17</sub> size was maximal for these breakdown products conducted under high (~400 atm) external pressure,<sup>97</sup> whereas the maximum *n*-alkylbenzene in this thesis was of C<sub>18</sub>. Additionally, C<sub>17</sub> was the maximum number of carbon atoms found for the alkene series. This appears to show that the intermediates of HDO have a greater propensity to cyclization than other cracking products.

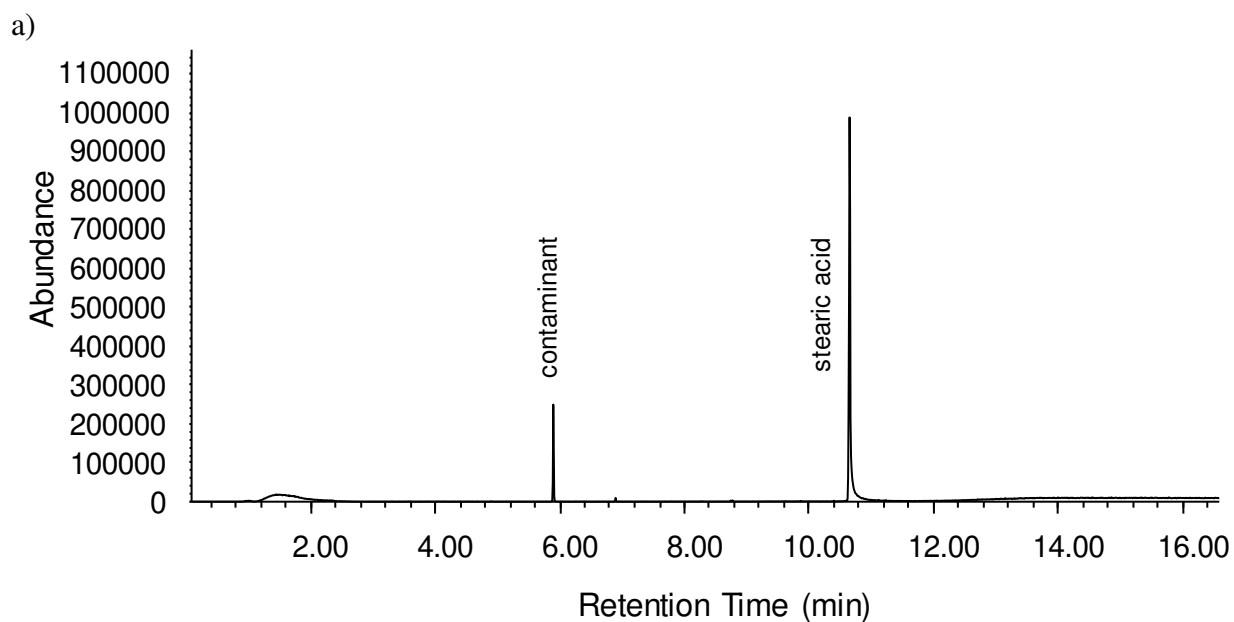


Figure 10. TD-Pyr-GC-MS chromatograms of stearic acid a) 300 °C TIC b) sequential 700 °C TIC c) EIC of ions 92/91 *m/z*



Figure 10 cont.

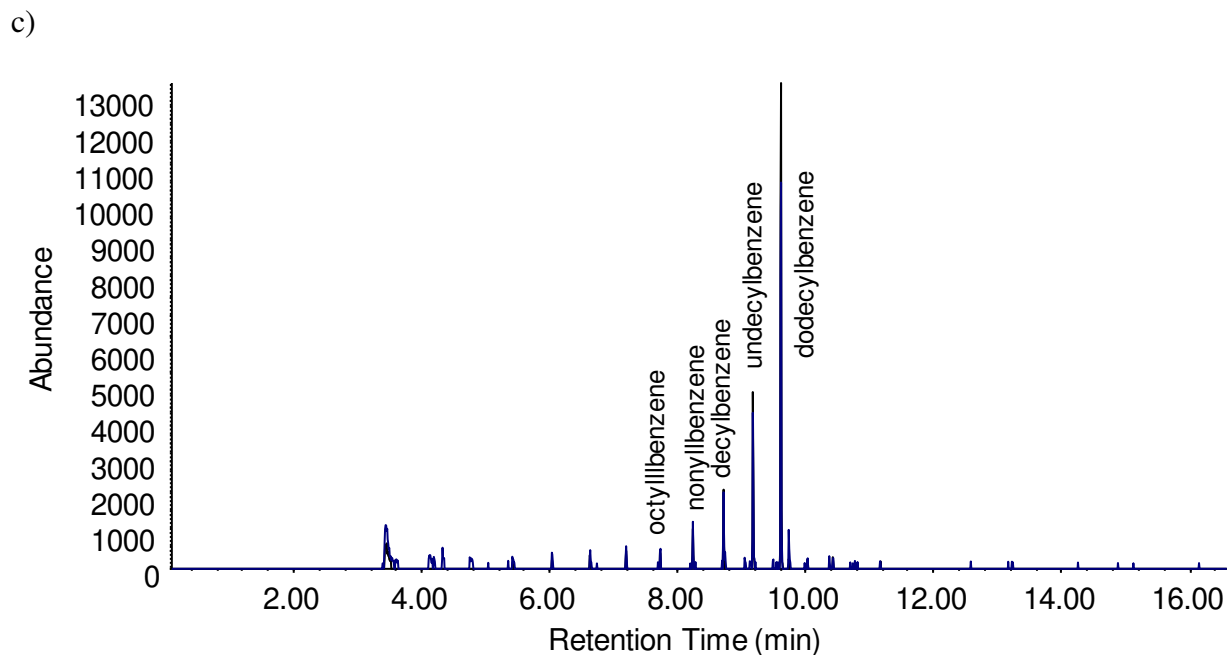
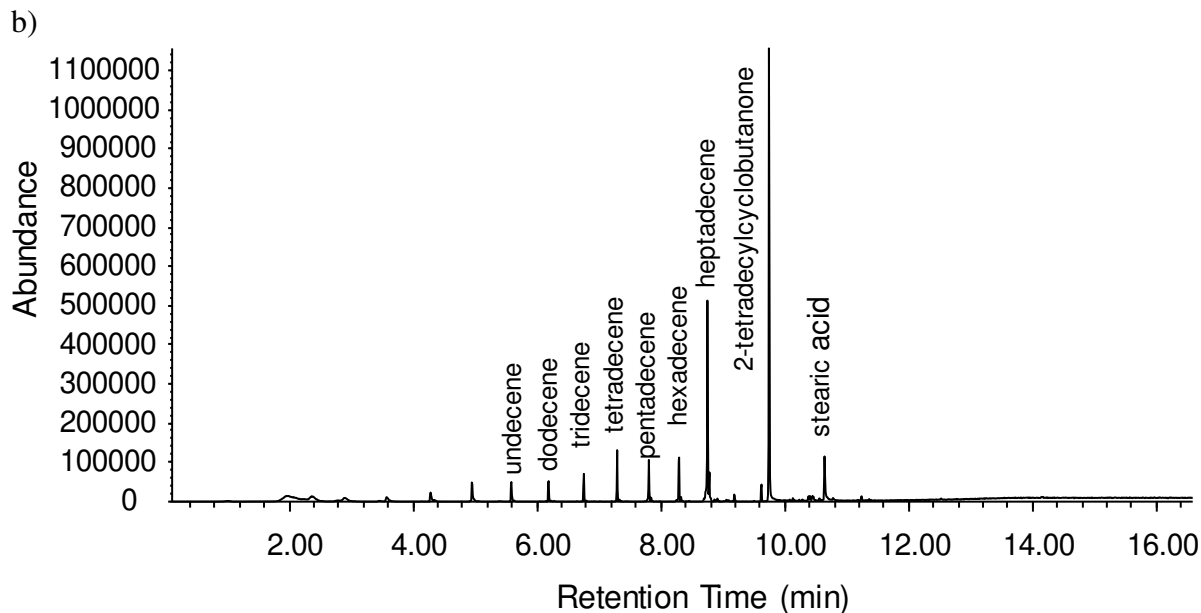


Figure 10. TD-Pyr-GC-MS chromatograms of stearic acid a) 300 °C b) sequential 700 °C c) EIC of ions 92/91  $m/z$

When pyrolyzed at 700 °C directly, the profile was nearly identical to the sequential 700 °C Pyr step, however, 2-tetradecylcyclobutanone was not readily formed and a larger portion of unaltered stearic acid was observed instead (Fig. 11). Furthermore, alkenes, alkanes, *n*-

alkylbenzenes, and PAHs were found to have higher abundances than in the sequential 700 °C fraction. Hence, this difference appears to show that there are two different paths of pyrolysis, dependent on whether the sample is pyrolyzed directly or sequentially. Under direct pyrolysis it appeared that all compounds other than 2-tetradecylcyclobutanone are more readily formed. As for the explanation of this difference, it is suggested that there is some process of carryover from the 300 °C fraction that leads to the formation of 2-tetradecylcyclobutanone in the sequential pyrolytic step by breaking down the adsorbed stearic acid instead of its release into the gas phase. When, by contrast, heating to 700 °C was immediate, as opposed to sequential, abundant hydrogen formation may “quench” the radical intermediates of 2-tetradecylcyclobutanone formation.

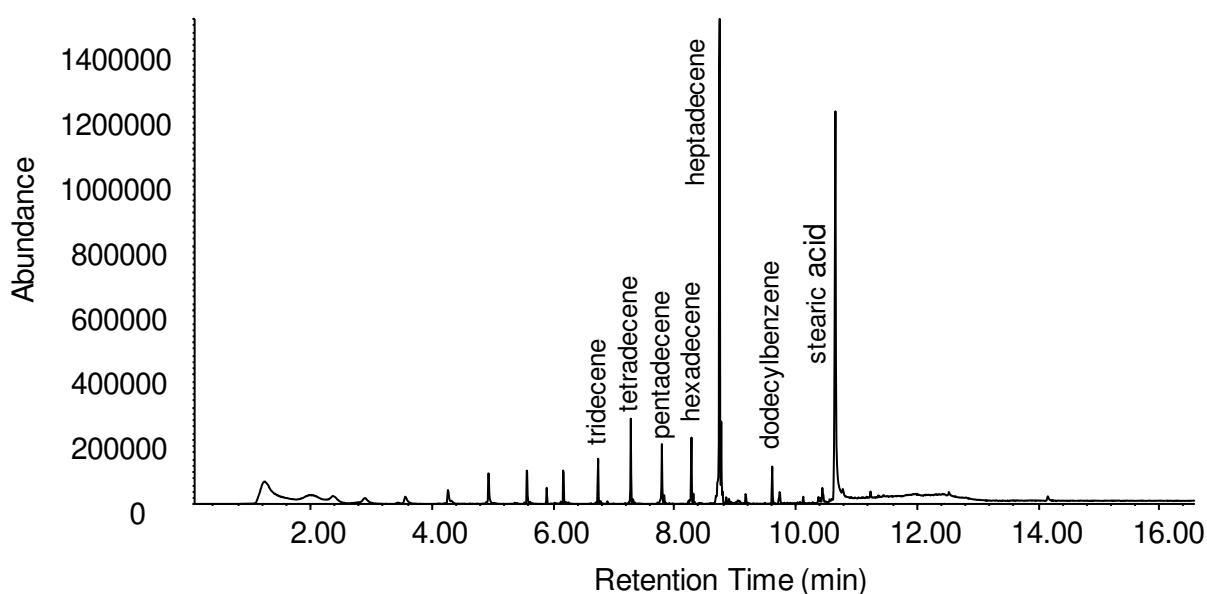


Figure 11. Pyr-GC-MS TIC of stearic acid following the direct pyrolysis at 700 °C.

### III.2.3 Tristearin

As expected, the TD and Pyr behavior of tristearin was similar to that of stearic acid. At 300 °C, tristearin decomposed slightly, forming stearic acid at a low abundance (Fig. 12a). The subsequent pyrolytic step showed abundances of alkenes and the 2-tetradecylcyclobutanone peak, in the same way as observed with stearic acid (Fig. 12a). Heptadecene and dodecylbenzene, were the most abundant alkenes and alkylbenzenes, respectively. The major difference between tristearin and stearic acid decomposition product profiles was the formation of an ester, allyl stearate, from the suspected cleavage of the glycerol backbone of the triacylglyceride (Fig. 12b). Between retention times of 10 to 12 min, there were a slew of new minor peaks compared to that of stearic acid (Fig. 12 vs. Fig. 11), but their identification was not easily feasible based on the NIST library.

a)

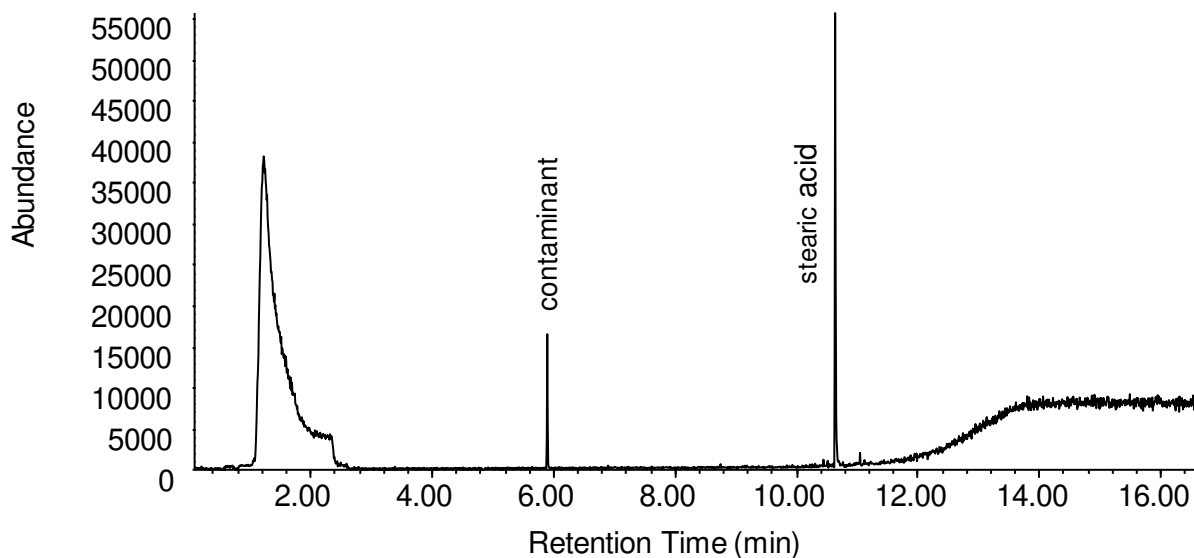
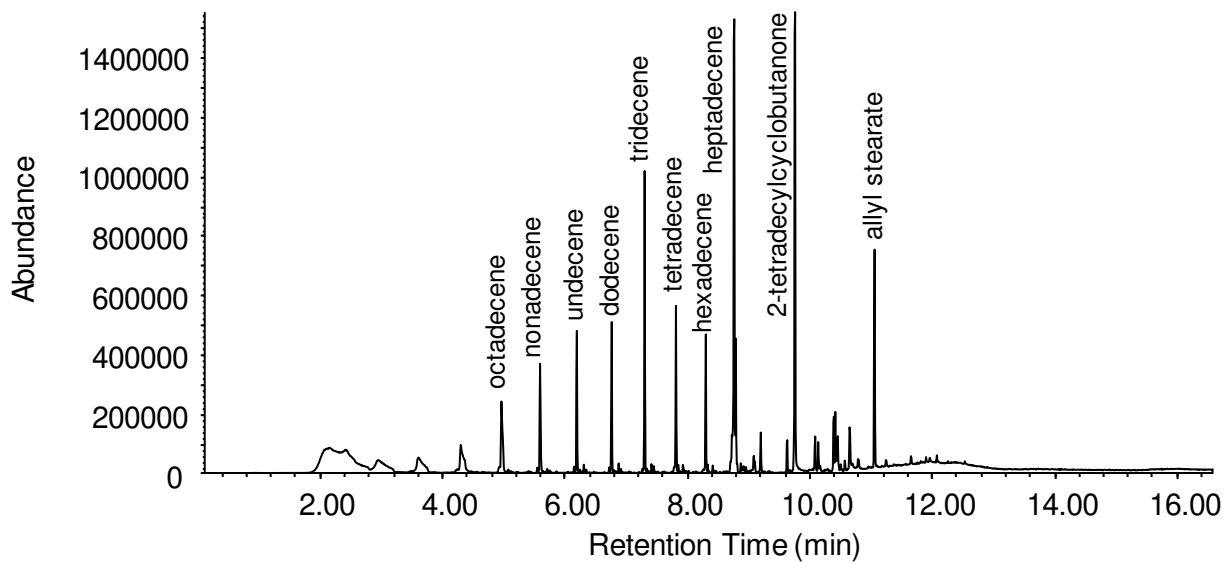


Figure 12. Pyr-GC-MS TIC chromatogram of tristearin at a) 300 °C b) sequential pyrolysis at 700 °C and c) direct pyrolysis at 700 °C.

Figure 12 cont.

b)



c)

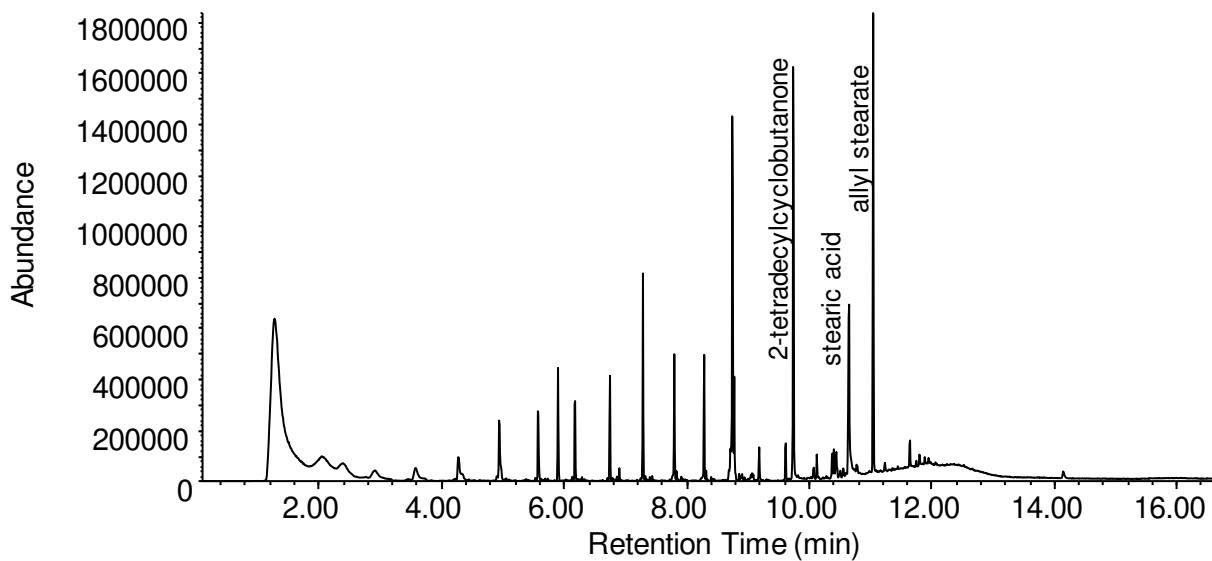


Figure 12. Pyr-GC-MS TIC chromatogram of tristearin at a) 300 °C b) sequential pyrolysis at 700 °C and c) direct pyrolysis at 700 °C.

In a slight contrast to stearic acid decomposition, direct pyrolysis and sequential (following 300 °C) pyrolysis of tristearin at 700 °C, resulted in nearly identical TIC chromatograms (Fig. 12b-c); the alkene/alkane profile showed no significant differences between the one and two step Pyr profiles. The one difference observed was that there was a significant amount of stearic acid in the chromatogram following the direct pyrolysis, while the sequential step did not show this feature, as this would have been removed during the 300 °C desorption step. Notably, the abundance of allyl stearate was higher in the direct 700 °C step. This observation suggests that during direct pyrolysis, more of tristearin is broken down at the glycerol backbone, while with the sequential Pyr step, the FA chain is cleaved in the presence of hydrogen to form stearic acid.

#### *III.2.4 Oleic Acid*

Following the TD temperature of 300 °C, the profile of oleic acid was similar to that of stearic acid as the only compound that observed was unaltered oleic acid (Fig 13a). However, the Pyr profile of oleic acid is rather different to that of stearic acid, presumably due to the double bond within the molecule. One would expect to see a profile that included alkadienes and alkenes, which would match the abundant alkene/alkane profile seen in the TD-Pyr of stearic acid. Yet, only two alkadienes were apparent, i.e., isomers of heptadecadiene, observed at a retention time of 8.65 mins (Fig. 13b). Furthermore, alkenes were not observed either, which suggests that there is less hydrogen generation during the pyrolysis of oleic acid, or perhaps decompositions reactions occur more readily and do not require or involve hydrogen formation. Tetradecenylcyclobutanone, the unsaturated analog of the 2-alkylcyclobutanone observed with stearic acid decomposition was also found, but in very low amounts (Fig. 13b, Appendix D, Fig. D3). Thus, minimal HDO appears

to occur for oleic acid decomposition as opposed to its saturated counterparts. This corroborates the assumption that more hydrogen formation happens in the case of saturated feedstocks.

Between the sequential 700 °C step and the direct pyrolysis, there were no significant differences except that oleic acid appeared under direct pyrolysis, but did not following the sequential step (Fig. 13c). This was reasoned to be that all the intact oleic acid thermal desorbs from the filter at 300 °C and there is none left over for the sequential run. The tetradecenylcyclobutanone peak appeared in both Pyr analyses, and had very similar abundances.

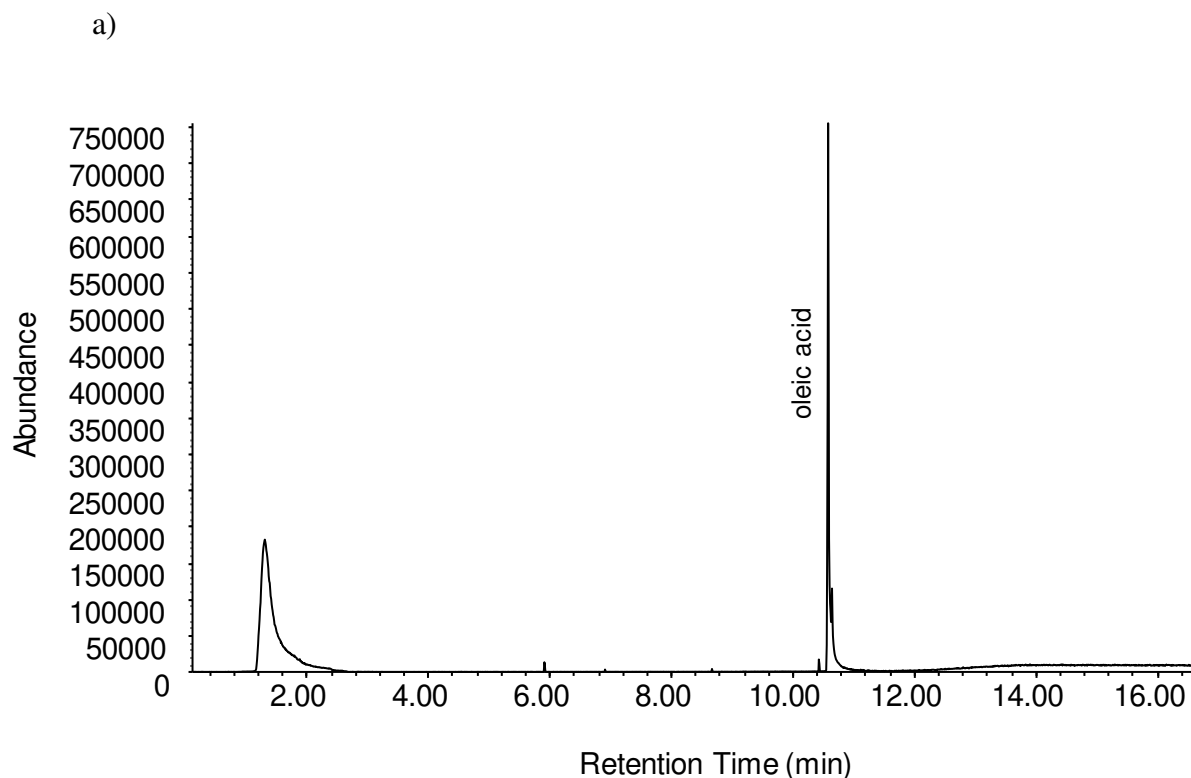
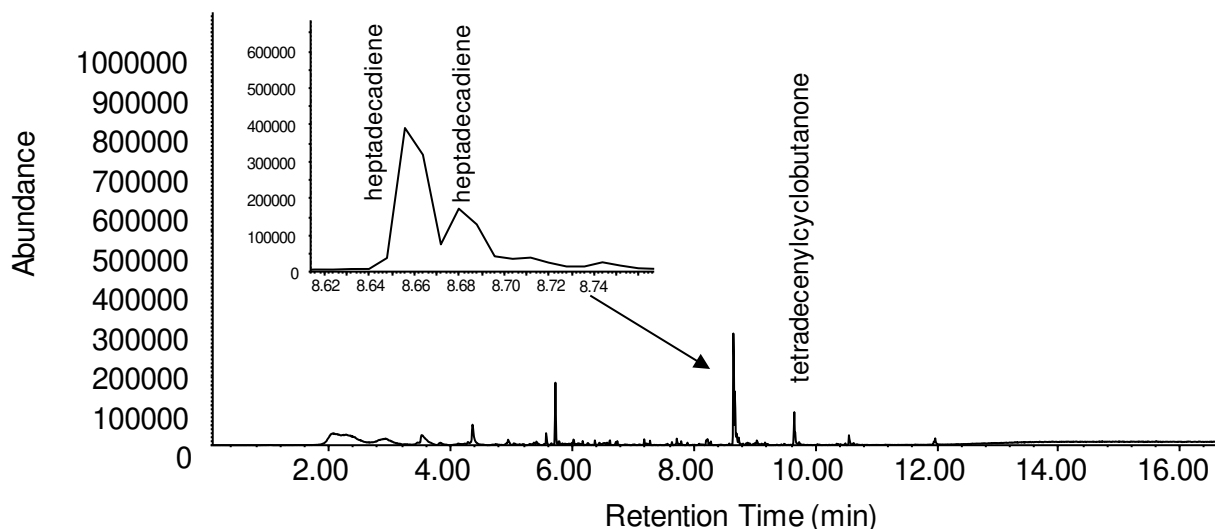


Figure 13. TD-Pyr-GC-MS of oleic acid at a) 300 °C b) sequential pyrolysis at 700 °C and c) directly pyrolysis at 700 °C.

Figure 13 cont.

b)



c)

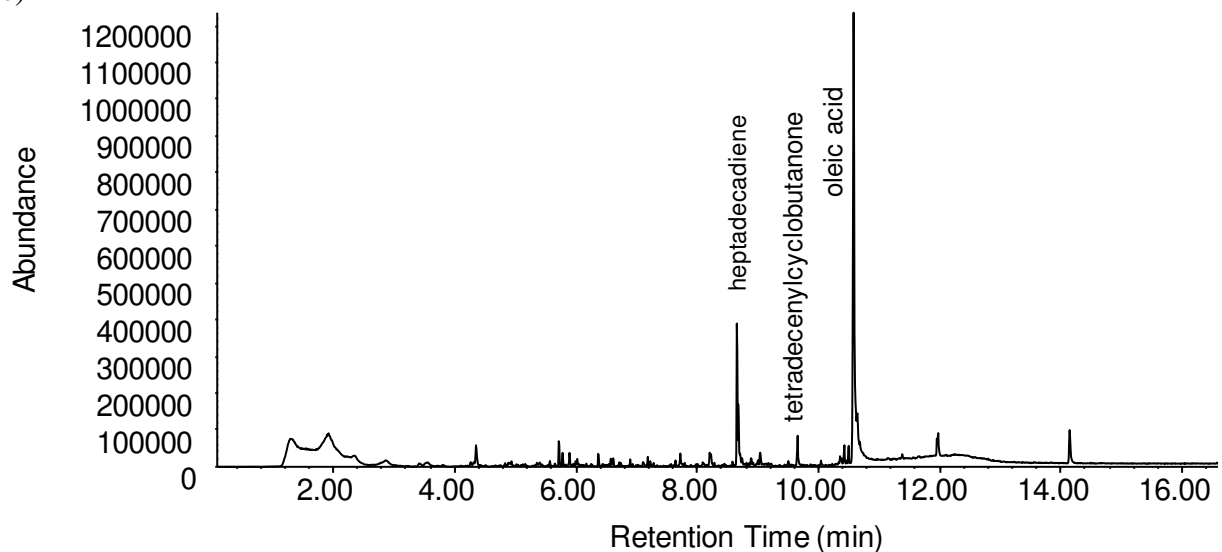


Figure 13. TD-Pyr-GC-MS of oleic acid at a) 300 °C b) sequential pyrolysis at 700 °C and c) directly pyrolysis at 700 °C.

Similarly to stearic acid, a homologous series of mono-substituted *n*-alkylbenzenes was observed, however the most abundant peak shifted from dodecylbenzene to heptylbenzene for oleic acid (Fig. 14). We propose that *n*-heptylbenzene, which has a carbon number of 13, is formed more readily due to the double bond in oleic acid, although the exact reason for this preference

remains unknown. Lastly, just as for stearic acid, pyrolysis of oleic acid, yielded several PAHs. The most abundant PAH was naphthalene (C<sub>10</sub>), while other PAHs including substituted C<sub>1</sub>-naphthalene (C<sub>11</sub>) and phenanthrene (C<sub>14</sub>) were also found but in small amounts.

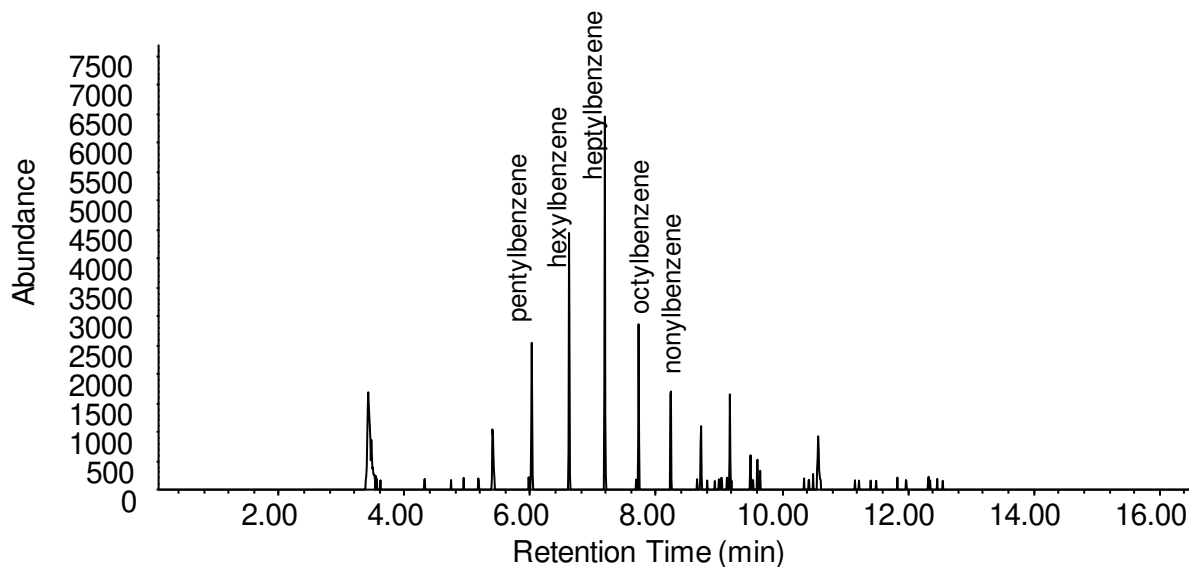


Figure 14. Pyr-GC-MS EIC of  $m/z$  ion 91 showing  $n$ -alkylbenzene profile following the direct pyrolysis at 700 °C.

### III.2.5 Triolein

As with the previously mentioned acid/triacylglycerides pair, the only product formed under TD of triolein was oleic acid (Fig. 15a). Moreover, the pyrolytic profile of triolein is in good agreement with that of tristearin as the cleavage of one of the triacylglyceride FAs forms oleic acid or allyl oleate. This is thought to be dependent on which ester bond is broken within the glycerol backbone. The sequential Pyr and direct Pyr showed no significant differences, other than slight changes in abundances of compounds observed (Fig. 15b-c). Under pyrolysis, the 2 isomers of heptadecadiene are still formed along with the alkylbenzene profile, with a maximum abundance at heptylbenzene. This maximum of the alkylbenzene profile is different than that of



tristearin which showed a maximum at dodecylbenzene. Tetradecenylcyclobutanone was also found in the pyrolytic fractions, with much higher abundances than observed for oleic acid. This suggests that the formation of the alkenylcyclobutanone is similar to what was observed with tristearin, with the minor exception of the double bond inside the alkyl chain. Cyclooctene was also observed in the chromatograms, although the mechanism of formation is not well understood.

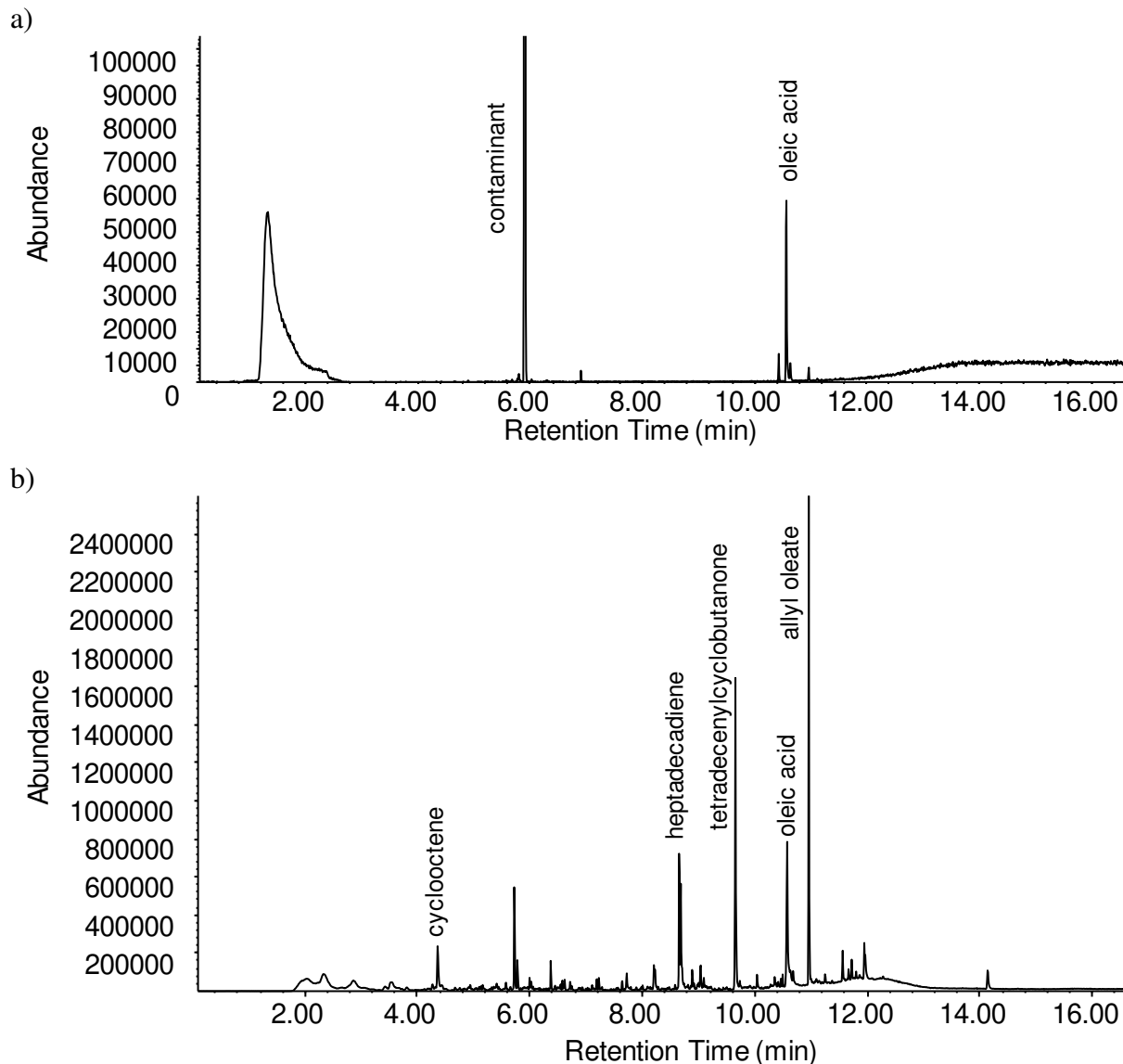


Figure 15. TD-Pyr-GC-MS of triolein at a) 300 °C b) sequential pyrolysis at 700 °C and b) directly pyrolysis at 700 °C

Figure 15 cont.

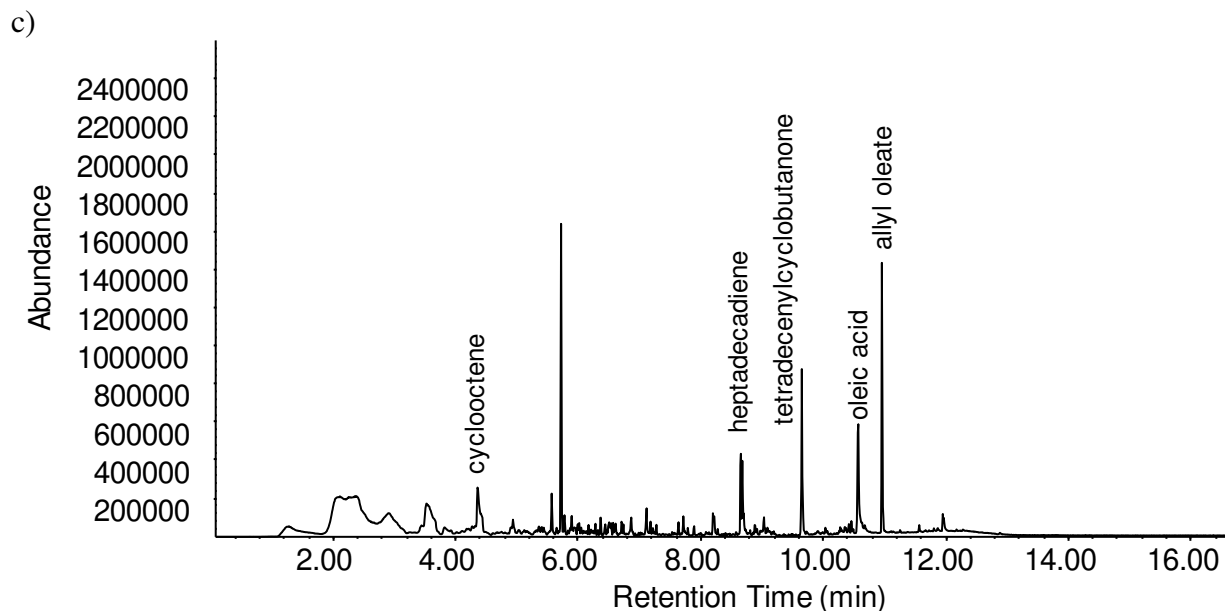


Figure 15. TD-Pyr-GC-MS of oleic acid at a) 300 °C b) sequential pyrolysis at 700 °C and b) directly pyrolysis at 700 °C

In conclusion, the pyrolytic profiles of the FA and TG model compounds shown above give unique profiles that if present in PM greatly aid in understanding the source of the PM. More specifically, the formation of alkenes, alkadienes, alkanes, mono-substituted alkylbenzenes, light PAHs, and esters, are expected to be observed in the TD-Pyr-GC-MS chromatograms if these model compounds are present in the atmosphere. Furthermore, it is possible to distinguish between saturated and unsaturated feedstocks, using markers such as the shift of the most abundant alkylbenzene observed. This observation depends on the amount of saturation of the original compound, which greatly helps with source apportionment.

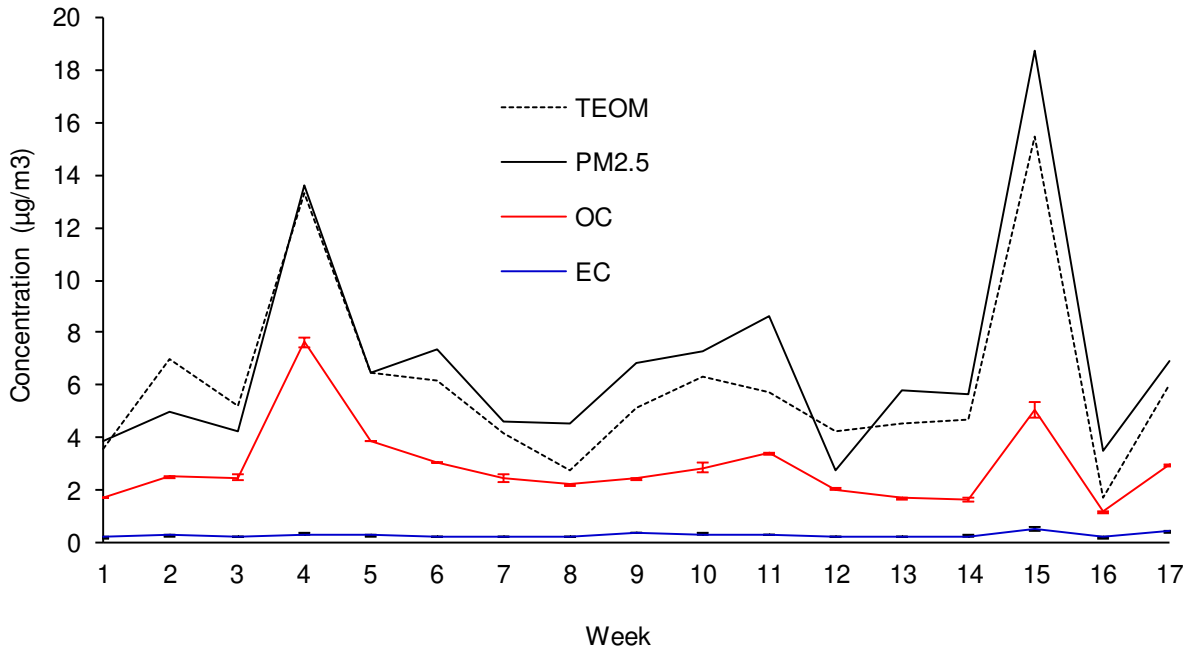
### III.3. Application of TOA and TD-Pyr-GC-MS to POLCAST Samples

#### *III.3.1 PM<sub>2.5</sub>, OC, and EC Concentrations*

TOA of the POLCAST filter samples showed that OC contributes a significant amount to the overall composition of PM<sub>2.5</sub> in Grand Forks, ND (Fig. 16a, Appendix E, Table E1) during the 17 week POLCAST campaign. The average concentration of OC varied between 1.17 and 7.70  $\mu\text{g}/\text{m}^3$ , while the average concentration of EC ranged between 0.17 and 0.55  $\mu\text{g}/\text{m}^3$  (Fig. 16a); levels of EC during the campaign contributed very little to the overall composition of the PM<sub>2.5</sub> and are therefore not discussed further. PM<sub>2.5</sub> concentrations determined by filter mass were confirmed by on site TEOM measurements (Fig. 16c).<sup>109</sup> The peak OC concentration was observed in week 4 with a value of 7.7  $\mu\text{g}/\text{m}^3$ . Week 12 showed the highest contribution of OC to the total PM fraction of 74 %.

The OC portion of PM<sub>2.5</sub> was further broken down into temperature fractions to show the volatility of compounds collected during the campaign (Fig. 16b). Between 20-40 % of all OC evolved at 300 °C, corresponding to TD volatile and semi-volatile organic species. The majority of OC evolved only at pyrolytic temperatures of 500 °C (25 %) and 870 °C (33 %), indicating that a large OC portion is represented by non-volatiles. Although TOA provided concentrations of OC during the entire 17 week campaign, TD-Pyr-GC-MS analysis to determine OC speciation began on week 12 due to the development of the method and instrumental difficulties. Thus, the following sections discuss the TD-Pyr-GC-MS analysis in weeks 12 – 17.

a)



b)

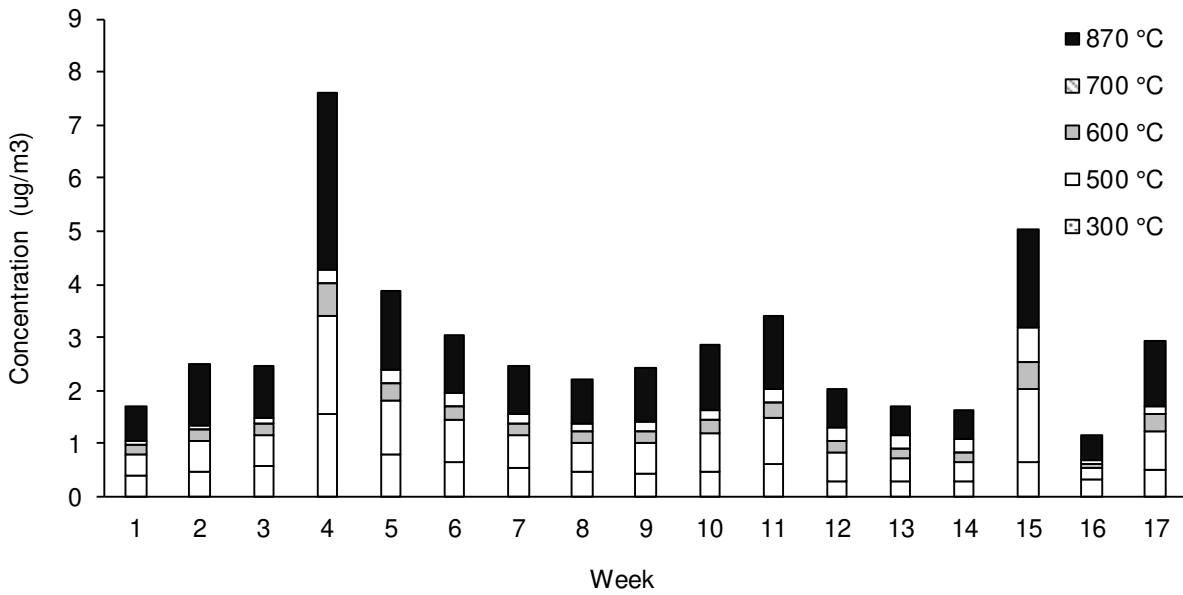


Figure 16. a) Time series plot of the PM<sub>2.5</sub>, OC and EC concentrations as well as filter mass, TEOM, and EPA PM<sub>2.5</sub> measurements collected during POLCAST campaign at Grand Forks, ND, from June 21, 2012 (week 1) - October 19, 2012 (week 17). b) Temperature distribution of OC collected from TOA c) Correlation between TEOM and PM<sub>2.5</sub> filter mass measurements.

Figure 16 cont.

c)

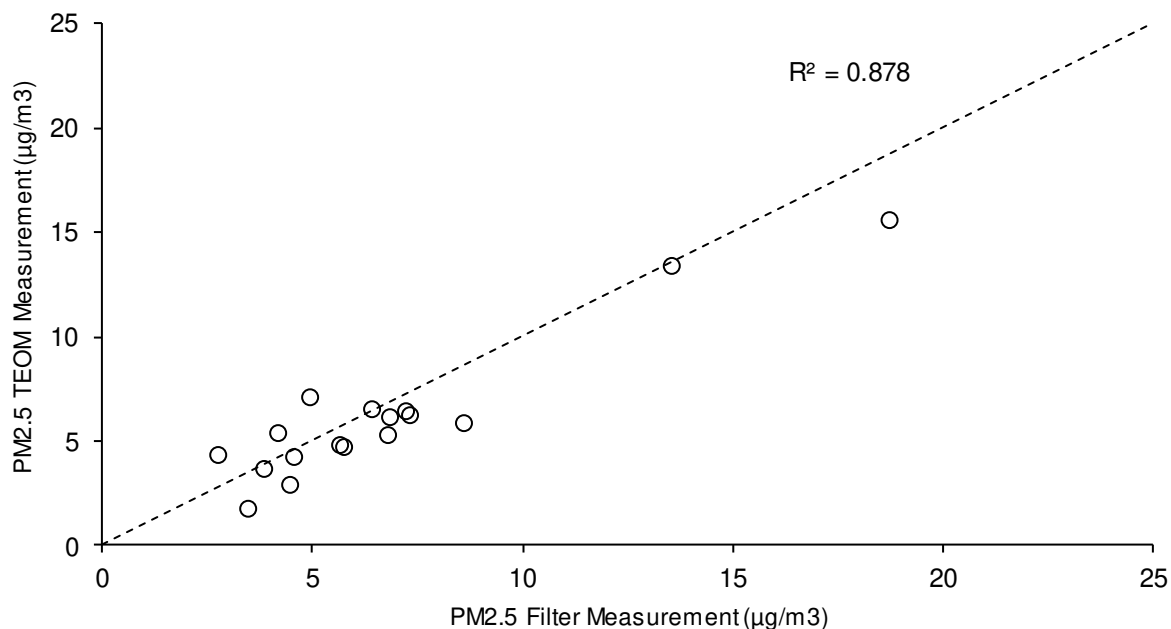


Figure 16. a) Time series plot of the PM<sub>2.5</sub>, OC and EC concentrations as well as filter mass, TEOM, and EPA PM<sub>2.5</sub> measurements collected during POLCAST campaign at Grand Forks, ND, 2012. b) Temperature distribution of OC collected from TOA c) Correlation between TEOM and PM<sub>2.5</sub> filter mass measurements.

### III.3.2. Role of TD-Pyr in Organic Speciation

The total abundance of all compounds determined by TD-Pyr-GC-MS corresponds with the TOA profile for weeks 12 – 17 (Fig. 17a-b). This is apparent from both week 15, which had the highest total abundance and week 16, the lowest. The abundance of the TD fraction based on TD-Pyr-GC-MS analysis was consistently higher (33-68 %) than for TD-TOA (13-27 %). This is likely due to the semi-quantitative character of GC-MS analysis as a result of variation in ionization efficiency of EI MS for different compounds (compared to TOA, which converts all compounds to methane and thus provides unambiguous quantification). Furthermore, the abundance of the Pyr fraction in TD-Pyr-GC-MS may be underestimated as a result of possible

conversion of some species during pyrolysis to CO<sub>2</sub> (which may be under quantified).<sup>110-111</sup> The significant percentage of compounds observed in the pyrolytic fraction (32-68 %) with TD-Pyr-GC-MS confirms that the semi-volatile OC fraction, which is usually characterized by either TD or solvent extraction GC-MS methods, may not be representative of the overall OC composition (Fig. 17b).<sup>78</sup> This observation suggests that the Pyr fraction enables a broader characterization of the total PM composition.

Specific profiles for OC compounds and tracers obtained within the TD-Pyr fractions show the preference of some analytes (*n*-alkanes and acids) to show up primarily in the TD fraction, whereas other analytes are mostly pyrolytic of origin (*n*-alkenes, alkylbenzenes, and PAHs) (Fig. 17 c-g). The following sections discuss these OC compounds, their distribution across the TD - Pyr temperature fractions, and their relations to both anthropogenic and biogenic sources.

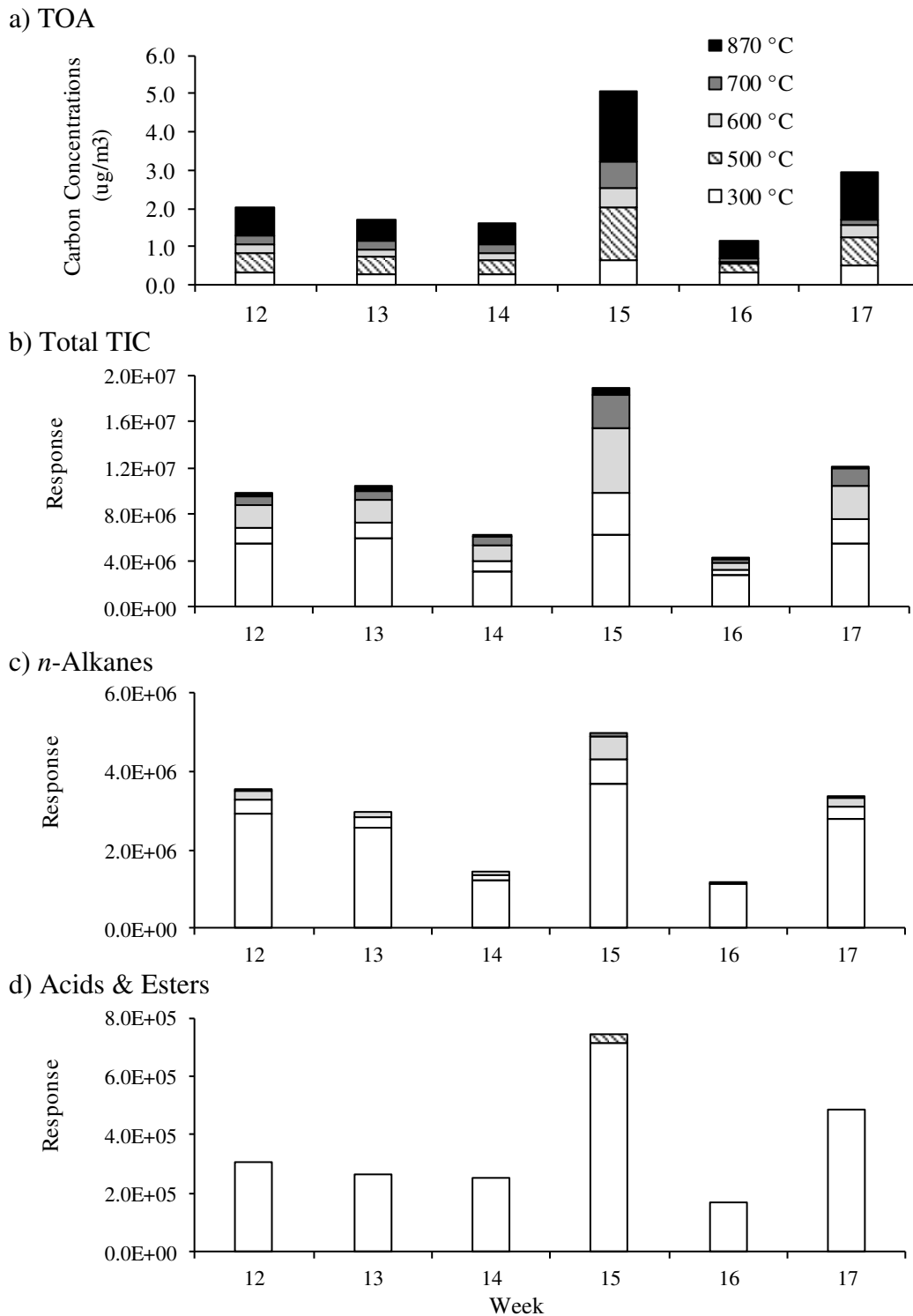
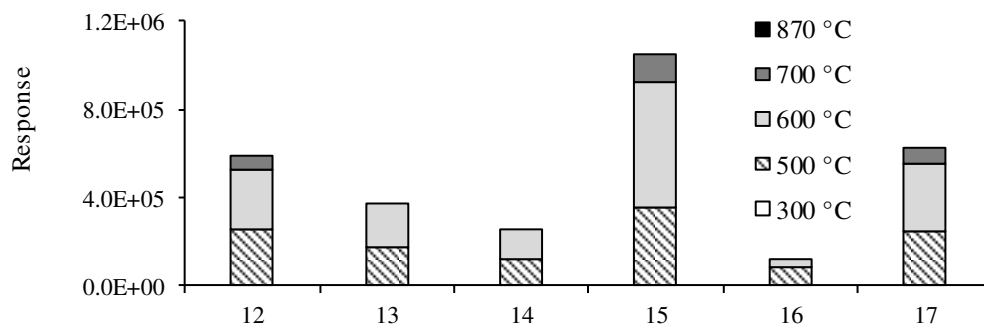


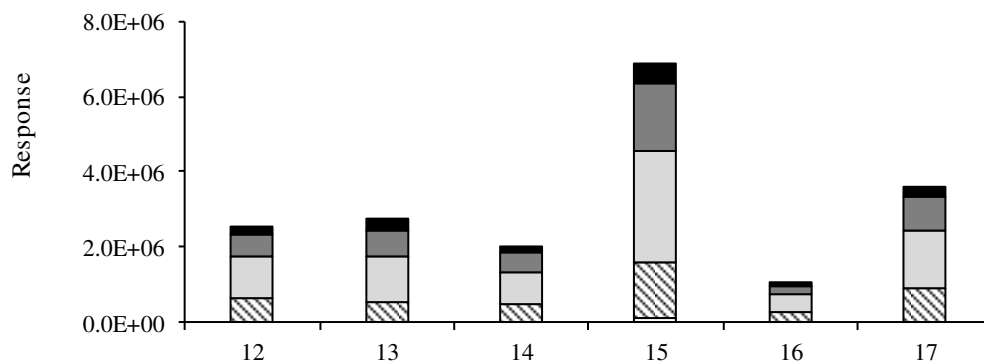
Figure 17. Characteristic OC profiles over 6 week sampling period showing TD and Pyr fractions obtained using a) TOA and b-g) TD-Pyr-GC-MS: b) Total TIC (sum) c) *n*-Alkanes d) Acids & Esters e) *n*-Alkenes f) Alkylbenzenes & BTEX g) PAHs. TD-Pyr abundances were determined as EIC peak areas for specific ions (Appendix F, Table F1).

Figure 17 cont.

e) *n*-Alkenes



f) *n*-Alkylbenzenes & BTEX



g) PAHs

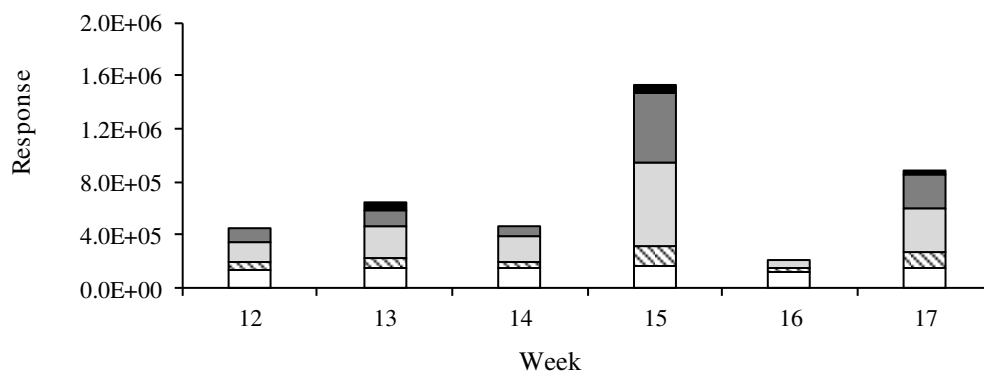


Figure 17. Characteristic OC profiles over 6 week sampling period showing TD and Pyr fractions obtained using a) TOA and b-g) TD-Pyr-GC-MS: b) Total TIC (sum) c) *n*-Alkanes d) Acids & Esters e) *n*-Alkenes f) Alkylbenzenes & BTEX g) PAHs. TD-Pyr abundances were determined as EIC peak areas for specific ions (Appendix F, Table F1).



### III.3.3. Thermal Desorption OC Fraction

The most abundant class of compounds found in the TD fraction was a homological series of *n*-alkanes, representing 23-36% of the total TD-Pyr profile and accounting for 40-59 % of the TD fraction over the last 6 weeks of sampling (Fig. 17c, Appendix H, Table H3). This class of compounds was most abundant in week 15 (59 % of TD) and had a minimum in week 14 (40 % of TD). The *n*-alkanes detected ranged from C<sub>21</sub> to C<sub>34</sub> and consisted primarily of long chain, odd numbered alkanes (C<sub>27</sub>, C<sub>29</sub>, C<sub>31</sub>) (Fig. 18). Their abundance in PM<sub>2.5</sub> is known to come from biogenic sources, mainly, plant waxes, along with anthropogenic sources such as fossil fuel combustion, unburnt heating oil, and biomass/wood burning.<sup>12, 16, 18, 28, 42</sup>

To evaluate the source of *n*-alkanes in the TD fraction, we employed several proven indicators, carbon prefix index (CPI), maximum number of carbon atoms (C<sub>max</sub>), and plant wax percentages (Wax %) (Table 1).<sup>25, 112-113</sup> CPI values between 1 and 2 are generally indicative of anthropogenic sources, while CPI values above 2 are indicative of biogenic sources, mainly plant waxes.<sup>22, 25, 112, 114</sup> In this sampling period, CPI values ranged between 1.51 (week 16) and 7.08 (week 12) indicating weeks of both biogenic and anthropogenic sources (Table 4). C<sub>max</sub> values occurred at C<sub>29</sub> for all weeks other than week 16, which had a C<sub>max</sub> of C<sub>25</sub>. C<sub>max</sub> values of C<sub>27</sub>, C<sub>29</sub>, and C<sub>31</sub> are indicative of plant wax origin while C<sub>25</sub> maximum has been reported from unburned lubricating oil emission in cars.<sup>12, 22, 115</sup> Wax % were above 50 % in all weeks except week 16 (23 %), with a maximum of 75 % in week 12. From the CPI, C<sub>max</sub>, and Wax % values it is apparent that week 16 *n*-alkanes had anthropogenic sources, while the other 5 weeks all showed strong evidence of *n*-alkanes from biogenic sources, mainly plant waxes.

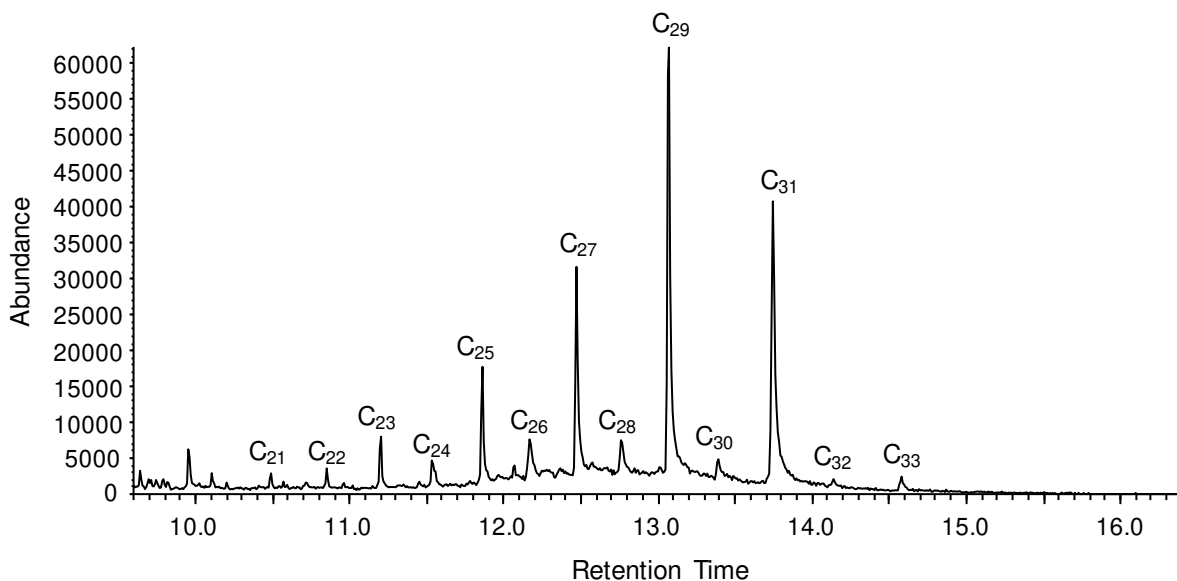


Figure 18. Representative TD-Pyr-GC-MS EIC chromatograms from week 12 showing *n*-alkane profile using target ion 57 *m/z*.

Table 4. *n*-Alkane source criteria for 300 °C TD fraction.

Criteria	Weeks					
	12	13	14	15	16	17
CPI	7.08	4.47	3.43	3.51	1.51	3.41
C <sub>max</sub>	C <sub>29</sub>	C <sub>29</sub>	C <sub>29</sub>	C <sub>29</sub>	C <sub>25</sub>	C <sub>29</sub>
Wax %	75	63	56	57	23	55

$$\text{CPI} = \frac{[\sum(C_{13}\text{-}C_{35})_{\text{odd}}]}{[\sum(C_{12}\text{-}C_{34})_{\text{even}}]}$$

$$\text{Wax \%} = \frac{[\sum(C_n - 0.5(C_{n-1} + C_{n+1}))]}{[\sum C_n]} \times 100 \%$$

Along with *n*-alkanes, *n*-fatty acids (FAs) and fatty acid methyl esters (FAMES) were found predominantly in the TD fraction. These two groups of compounds were detected without the use of a derivatization agent and accounted for 4-11 % of the TD fraction (Fig. 19a-b and Appendix H, Table H3). C<sub>6</sub>, C<sub>7</sub>, C<sub>8</sub>, C<sub>9</sub> and more abundant C<sub>16</sub> and C<sub>18</sub> acids were observed (characteristic *m/z* =60) along with a series of FAMES ranging from C<sub>16</sub> to C<sub>28</sub>. *n*-Fatty acids are known to be

large contributors to the overall OC fraction of PM as they come from a variety of sources including plant waxes, cooking and grilling, petroleum and diesel exhaust, and biomass/wood burning.<sup>12, 16, 19, 28</sup> FAMES, on the other hand, are not generally known to be abundant in the atmosphere although they have been linked previously to the combustion of wood, coal, or biodiesel.<sup>25, 34, 116-117</sup> To further investigate the source of these compounds, derivatization agents, BSTFA and TMAH, were used. Under BSTFA derivatization (data not shown), all underivatized acids including C<sub>16</sub> and C<sub>18</sub> were trimethylsilylated, while FAMES were still observed, confirming the presence of FAMES in the original samples. The observed prevalence of C<sub>16</sub> and C<sub>18</sub> FAMES may indicate that some of them may be biodiesel components.

Following the TMAH derivatization, no acids were present (Fig. 19c), while the FAMES abundance increased 10-20 times dependent upon the sampling week (Fig. 19d). This suggests that along with the FAMES profile, there is a sizable fraction of *n*-fatty acids, which are either underestimated or not detected without derivatization. Long chain fatty acids, > C<sub>22</sub>, are indicative of plant wax origin and further show that many of the TD fraction contributors are of biogenic origin.<sup>12</sup> The observed prevalence of those acids that are even carbon numbered (Fig. 3b,d) corroborates this assumption.

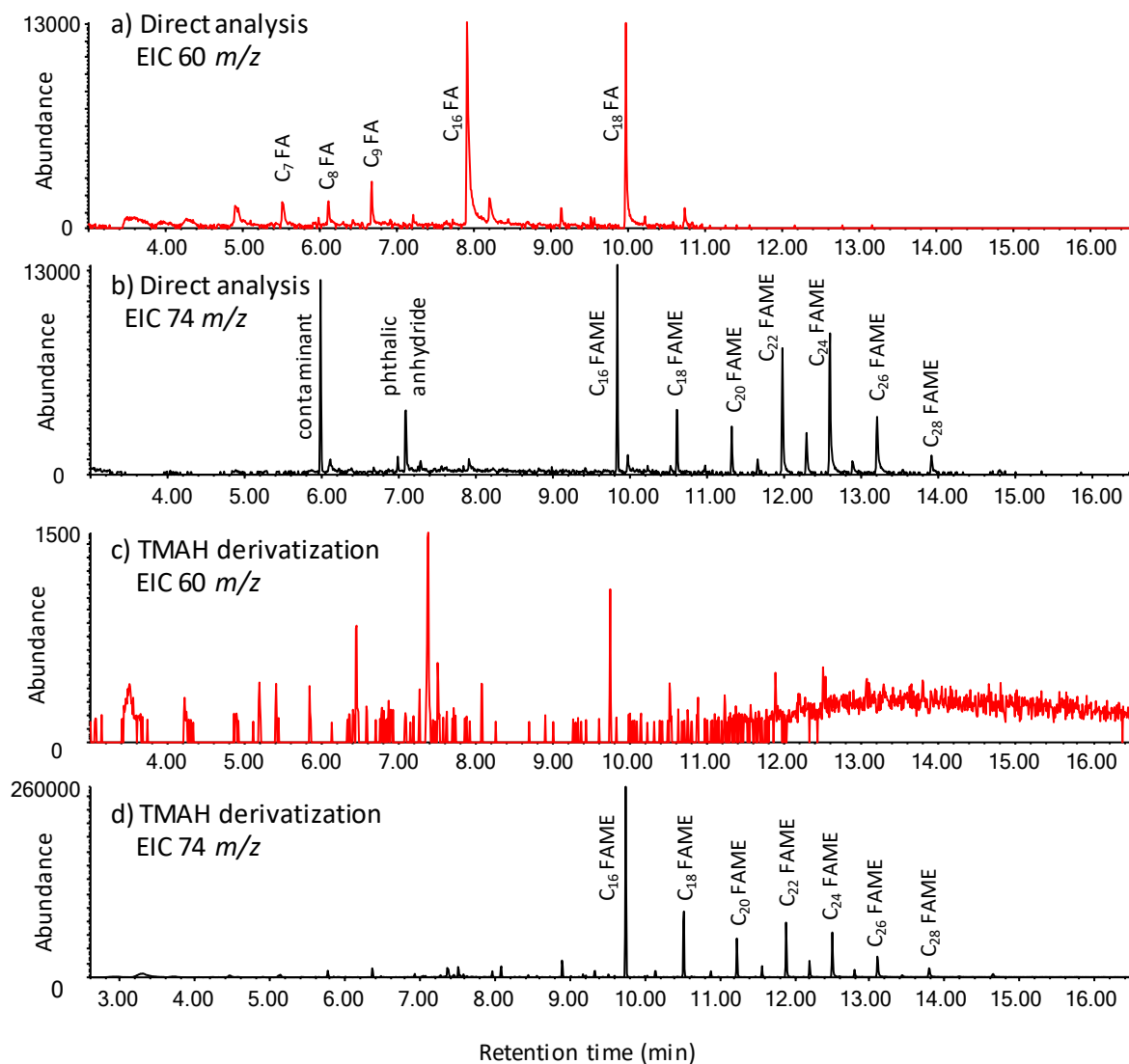


Figure 19. TD-Pyr-GC-MS EIC profiles showing *n*-fatty acids (FAs) and FAMES before (a, b) and after derivatization with 1  $\mu$ L of TMAH (c, d).

Besides *n*-alkanes, acids, and FAMES, a wide variety of organic compounds were present within the TD fraction that did not exhibit a specific homology profile. Two carbonyl compounds, nonanal and 6,10,14-trimethyl-2-pentadecanone (isomeric position tentative and based on NIST match, Appendix D, Fig. D4), were detected in all weeks and may be linked to sources of biogenic origin. The latter, also known as phytone, was the most abundant compound found in the TD

fraction other than alkanes and accounted for a maximum of 21 % of the TD fraction in week 13 and a minimum of 1 % in week 17 (Appendix H, Table H3).<sup>118</sup> Phytone, a biogenic secondary organic aerosol component formed from the oxidation and heating of phytol, is known to be emitted from plants.<sup>22</sup> Nonanal, a possible product of atmospheric oxidation of alkanes also being emitted from a variety of plant species, was detected but accounted for a very small share of the TD fraction.<sup>28, 119</sup>

Levoglucosan, one of the most commonly used tracers for the burning of biomass, was detected in three of the 6 weeks with a very strong abundance in week 17.<sup>120-123</sup> A similar compound, levoglucosenone, a product of the dehydration of levoglucosan in acidic conditions, occurred in all weeks.<sup>124</sup> The process of formation of levoglucosenone is thought to occur within the pyroprobe, as levoglucosenone is not readily formed in the atmosphere or without the aid of a catalyst.<sup>125</sup> In week 16, these two compounds accounted for 17 % of the TD fraction (Appendix H, Table H3), suggesting a heavy influence of biomass burning during that sampling period.

A group of plasticizers, more specifically three phthalate esters, and a plasticizer precursor, phthalic anhydride, were also observed. (Appendix G, Table G1-G6). Although it is possible that these compounds are from sampling artifacts, we theorize that they may be produced by either leaching or thermal decomposition of plastics; their abundance changed from week to week, with the highest abundance in week 13. Furthermore, a series of OC compounds that may possibly be from contamination or other processes were recovered, but their abundances were very low, making them only tentatively identified and their source unknown (Appendix G, Table G1-G6).

In addition to the mentioned compounds, a series of PAHs were detected in the TD fraction, which included naphthalene (NAP), methyl substituted naphthalenes (C<sub>1</sub> NPA), biphenyl (BP), fluorene (FL), phenanthrene (PHE), anthracene (ANT), fluoranthene (FLA), and pyrene (PYR).

These PAHs were not abundant in the TD fraction and only made up between 2 % (week 13) to 5 % (week 14) of the overall TD profile. Although typically reported as a gas-phase PAH,<sup>51, 126</sup> the most abundant PAH recovered in this study was naphthalene. Similarly, a study by Ellickson et al., showed that gas plus particle phase NAP was the most abundant PAH found in both rural and urban areas of Minnesota.<sup>127</sup> Moreover, a study by Zhang et al. (2011) showed that gas phase naphthalene is readily produced from the burning of crops including rice, wheat, and corn.<sup>52</sup> Although these studies were based upon solvent extraction, the profile of NAP correlates well with this study.

Criteria similar to those applied to *n*-alkanes were previously developed and can be used to distinguish between sourcing of PAHs by using diagnostic ratios of certain PAHs compared to others.<sup>50, 128-129</sup> FL/(FL+PYR) ratios of < 0.5 are telling of petrol emissions, while > 0.5 is thought to be from diesel emissions.<sup>128-129</sup> FLA/(FLA+PYR), ratios are generally separated into 3 categories: < 0.4 for petrogenic emission (incomplete combustion), 0.4 – 0.5 for fossil fuel combustion, and > 0.5 for grass, wood, and coal combustion.<sup>129</sup> Furthermore, values above 0.1 for ANT/(ANT+PHE) indicate pyrogenic origin, compared to those below 0.1 which are thought to be from petrogenic sources.<sup>50, 129</sup> In this study, the ratio of ANT/(ANT+PHE) varied between 0.23 and 0.35, while the FLA/(FLA + PYR) ratio ranged from 0.35 to 0.54. Both of the observed ratios tend to indicate combustion, e.g., of fossil fuels or grass, wood, and coal (Fig. 20). Fluorene was not observed in the TD fractions, and therefore diagnostic ratios were not considered for this molecule.

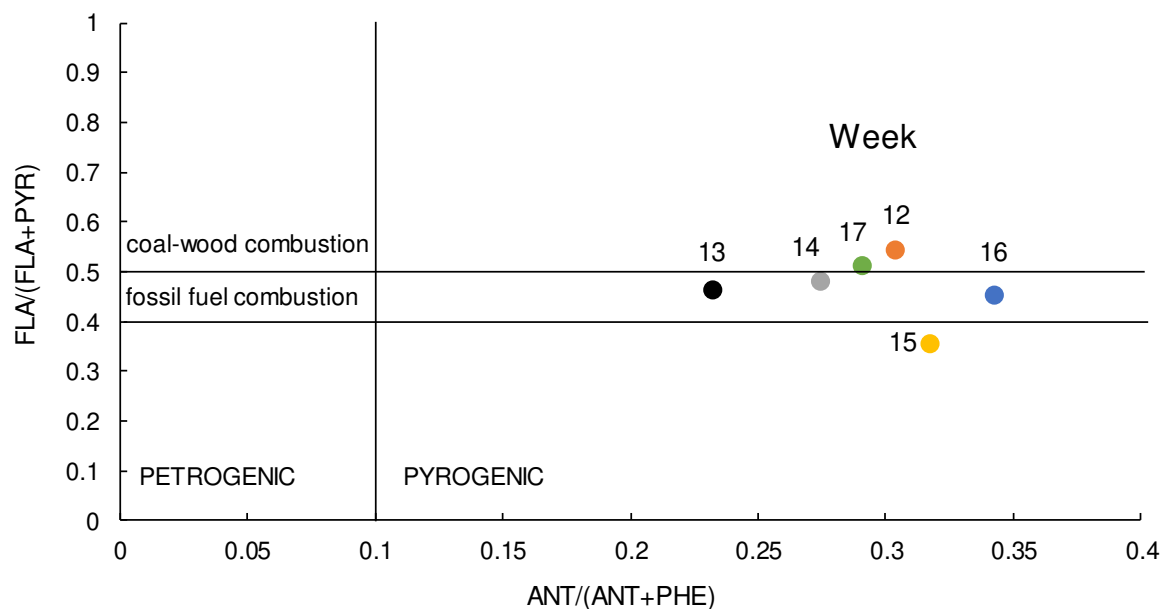


Figure 20. Diagnostic ratios for specific PAHs obtained from TD fraction of 6 week TD-Pyr-GC-MS analysis.

Overall, the profiles of the compounds and tracers found in the thermal desorption fraction, mainly *n*-alkanes, point to primarily biogenic origin with higher abundances in week 15, possibly related to harvesting activities. Other possible sources were noted as well, with week 16 possibly related to the combustion of wood, plastic materials, etc. Nevertheless, from the perspective of overall OC PM composition, the TD fraction determined by TD-Pyr-GC-MS was less abundant than the Pyr fraction and thus, possible sources of Pyr fraction are assessed below.

#### III.3.4 Distribution of Products of Pyrolyzed OC

The Pyr fraction of TD-Pyr-GC-MS showed complimentary homological profiles of *n*-alkenes, *n*-alkylbenzenes, and PAHs, which corresponded to the profiles of the breakdown products of the PM model compounds (FAs and TGs) (Fig. 21a-f). The *n*-alkenes homology series observed ranged between C<sub>9</sub> to C<sub>23</sub> in all sampling weeks, with the lower carbon numbers (C<sub>11</sub>-

C<sub>17</sub>) being more abundant. *n*-Alkylbenzenes featured a similar but narrower molecular size profile, with a C<sub>9</sub> to C<sub>18</sub> distribution in most weeks. Similar to these monoaromatic hydrocarbons, the PAH profile in the Pyr fraction contained compounds with a carbon number of 17 or lower. Our previous research along with studies by Lappi et al. have shown that both *n*-alkylbenzenes and PAHs are by-products of the thermal cracking or pyrolysis of TGs and fatty acids.<sup>90-91, 95, 97, 130</sup> The apparent reason for the observed size limit of these compounds (C<sub>17-18</sub> or less) is the breakdown of C<sub>18</sub> acids or triacylglycerides. *n*-Alkenes may also be formed in this process, although they may also result from long-chain alkane cracking, which is evidenced by their broader homology profile (Fig. 21). Presumably, alkyl radicals formed upon stearic acid decarboxylation/hydrodeoxygenation followed by potential further fragmentation (as well as alkane/wax cracking), end up as alkanes and alkenes whereas unsaturated alkenyl radicals formed from oleic and linoleic acids may undergo one or two steps of cyclization, to form alkyl benzenes (along with cyclic alkanes/alkenes as intermediates) and PAHs (mainly NAP or alkyl substituted NAPs), respectively.<sup>130</sup>

Although detected in the Pyr fractions and included in Fig. 21, *n*-alkanes did not show any prevalence of odd-numbered homologs, and thus cannot unequivocally be assigned to a specific origin. Furthermore, the *n*-alkanes observed in the Pyr fraction may be remnants carried over from the TD fraction that did not completely desorb from the filter, due to the low volatility of these HMW compounds. If this is true, the total abundance of hydrocarbons in PM may be underreported if TD is carried out as a stand-alone technique, due to the possibility of strong hydrocarbon or HMW compound adsorption. Hence, this may show yet again the importance of using Pyr in addition to TD temperature steps, when performing PM speciation.



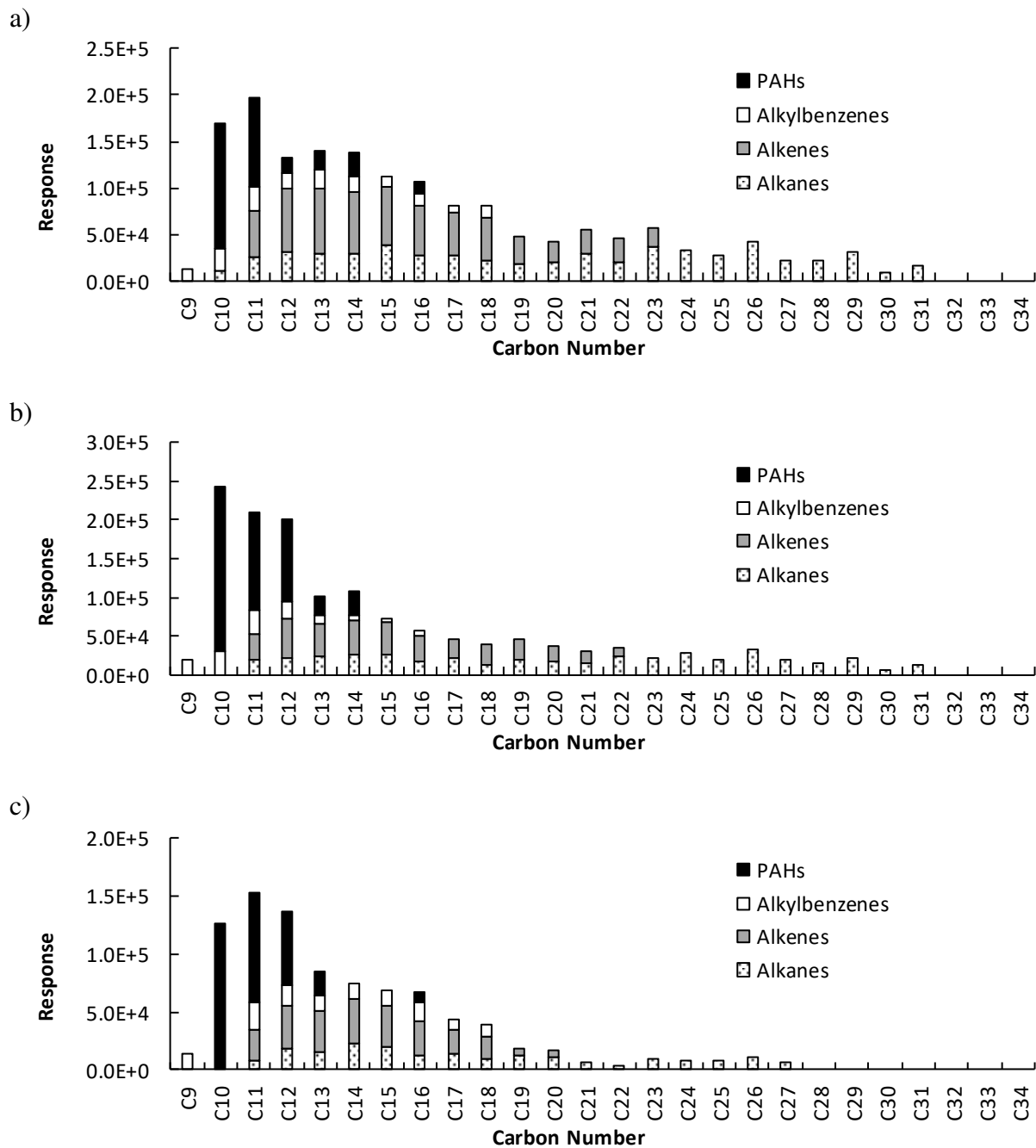


Figure 21. Homological profile of PAHs, alkylbenzenes, alkenes, alkanes, in total Pyr fraction based on EIC peak areas from TD-Pyr-GC-MS a) week 12 b) week 13 c) week 14 d) week 15 e) week 16 f) week 17.

Figure 21 cont.

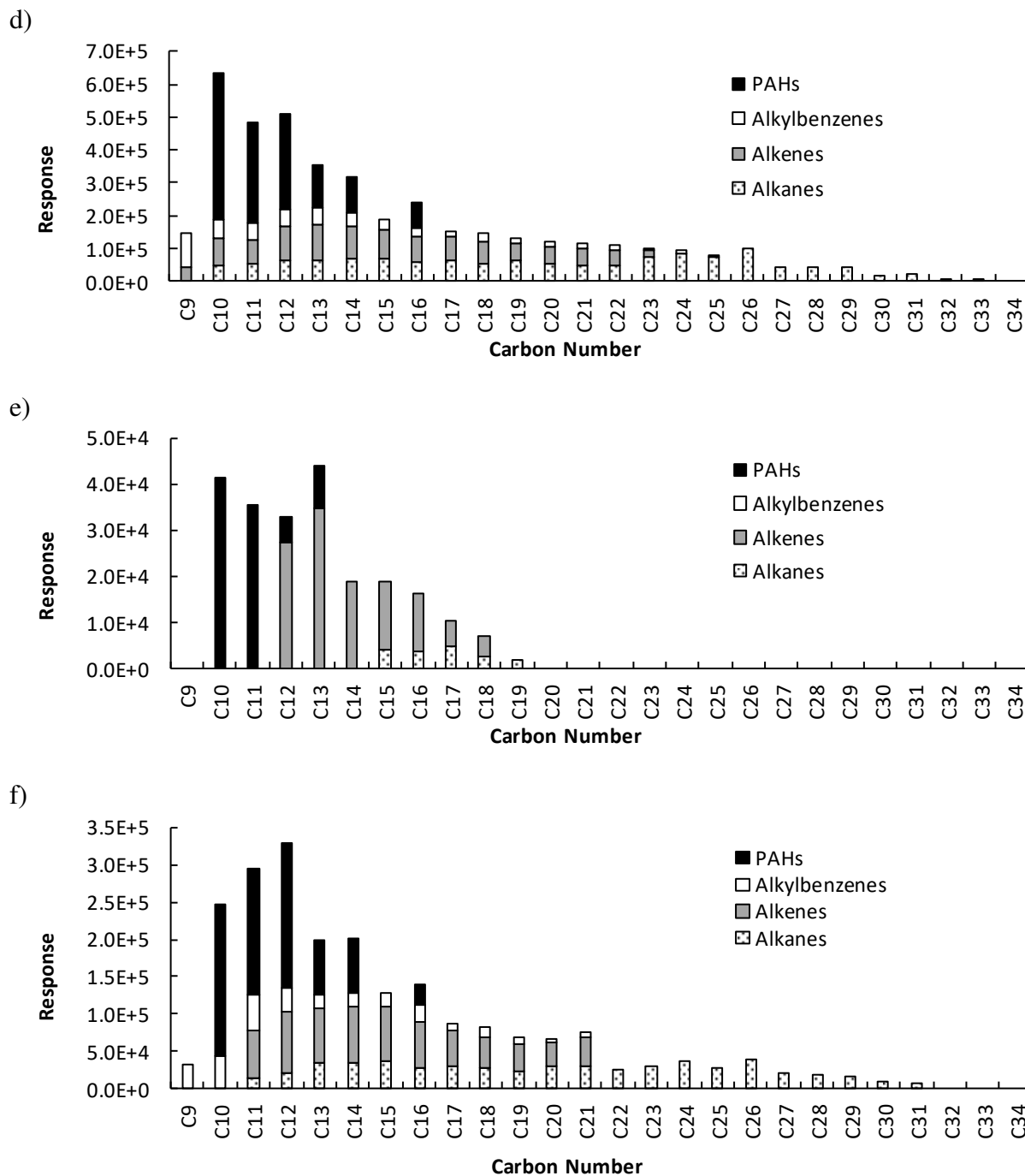


Figure 21. Homologous profile of PAHs, *n*-alkylbenzenes, alkenes, alkanes, in total Pyr fraction based on EIC peak areas from TD-Pyr-GC-MS a) week 12 b) week 13 c) week 14 d) week 15 e) week 16 f) week 17.

In addition to the PAHs found in the TD fraction (all of which were observed in the Pyr fraction), a series of new PAHs were detected, including dimethylated or ethylated NAPs (C<sub>2</sub> NAPs), acenaphthylene (ACY), and also fluorene (FL) (Fig. 22). Furthermore, the PAH profile was dominated by 2 ring PAHs, primarily, NAP and C<sub>1</sub> NAP. Previous research has shown that the combustion of crop residues leads to the formation of LMW PAHs, with NAP being the dominant PAH.<sup>52, 131</sup> Crop residues are more than likely present within the atmosphere in Grand Forks due to agricultural processes, and subsequently would be collected on the quartz filters. After TD-Pyr-GC-MS it is likely that these residues would form LMW PAHs.

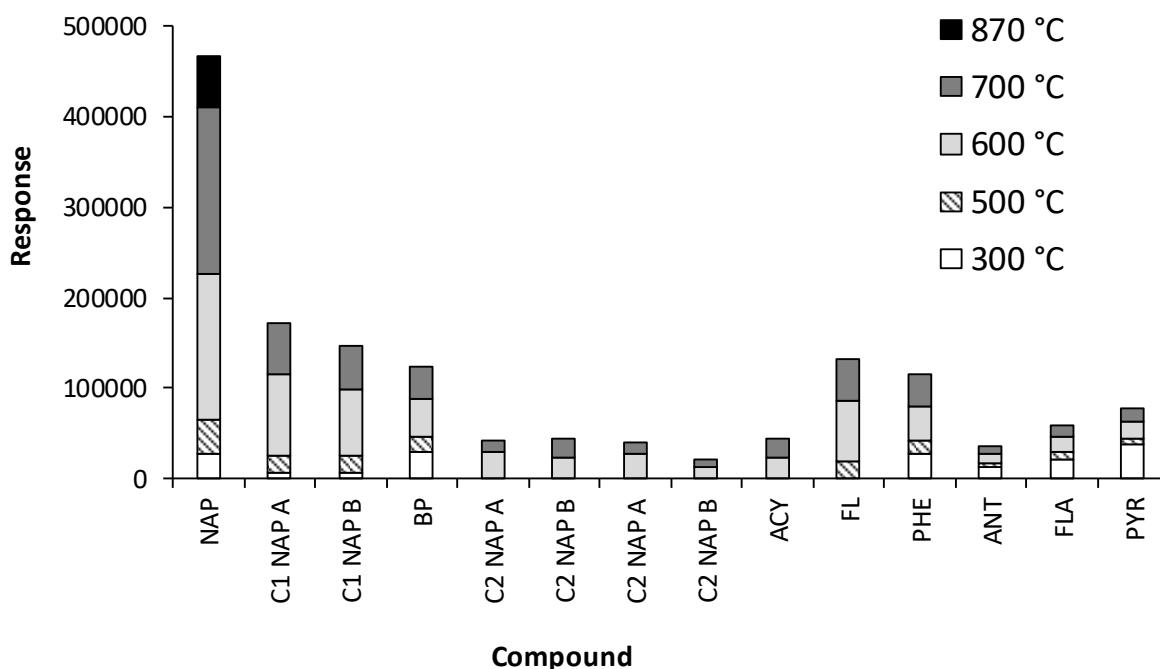


Figure 22. Representative distribution of PAHs observed during week 15. Abundances shown are determined total peak area of molecular ions for each PAH.

The observation of some PAHs exclusively in the Pyr fraction further suggests the breakdown of HMW species. Once again, only the use of the multi temperature TD-Pyr-GC-MS

setup allows for obtaining a comprehensive PM profile. Like *n*-alkylbenzenes, the most likely source of these LMW PAHs in this study is from biogenic sources, as underscored by their size profile ( $< C_{17}$ ) and abundance of NAP and alkyl substituted NAPs, which follows the presumed formation mechanism described above. Yet, unlike *n*-alkylbenzenes, the PAH profile in the Pyr fraction cannot be pinpointed to just TG pyrolysis, as follows from the occurrence of 3-4 ring PAHs. Furthermore, it is possible that some of the PAHs were emitted directly into atmosphere and then became tightly adsorbed to the filter or PM, such that their release occurred only at higher temperatures, i.e., in the Pyr fraction.

Along with the homological “fingerprint” of *n*-alkanes, alkenes, alkylbenzenes, and PAHs, all four BTEX compounds were found in the Pyr fractions. However, they were not included in the homology profile in Fig. 21 as these compounds dominated the Pyr fraction accounting for 40 – 66 % of the total Pyr profile (Appendix H, Table H3). Moreover, BTEX compounds have a wide range of possible sources, and therefore their origin could not be determined.

Lastly, phenol, along with its methylated and dimethylated derivatives, were detected within the Pyr fractions, with a preference for the 500 and 600 °C temperatures (Appendix G, Table G1-6). Phenols, along with methoxy phenols, are known to be formed from wood burning along with the pyrolysis of lignin.<sup>48-49, 101</sup> Similarly to alkanes and PAHs, some phenols, instead of being formed within the pyroprobe, may actually be present in the original PM as tightly adsorbed species as we see a small amount in the TD fraction. Then, only the use of Pyr temperatures allows for the full recovery of all these three groups of compounds from the decomposition of their theorized HMW parent compounds.

## CONCLUSIONS

In this thesis, we have developed a novel approach to the comprehensive characterization of atmospheric OC PM through the use of TD-Pyr-GC-MS in combination with TOA. The TD-Pyr-GC-MS method was optimized using standard mixtures of compounds generally found in PM (alkanes, FAs) as well as model compounds (TGs) that are theorized to exist in the atmospheric PM, but are harder to identify. Furthermore, collected PM samples were analyzed and the occurrence of these compounds was semi-quantified across TD-Pyr fractions assessed. More importantly, the identification and abundance of specific atmospheric tracers in TD-Pyr fractions were used to pinpoint the source of PM in the sampling area during a specific time period.

The model compounds analyzed by TD-Pyr-GC-MS in this thesis, namely TGs and FAs, aided in the understanding of the formation of many Pyr products observed during the PM filter analysis. Furthermore, the model compound Pyr homology profiles observed, i.e., alkenes, alkylbenzenes, and light PAHs, led to the discovery of competing mechanistic reactions: hydrodeoxygenation without a catalyst, which had been considered essential prior to this work, and decarboxylation. In addition to helping identify compounds in PM, these Pyr products and their mechanisms of formation can have vast implications for industries looking into using these compounds as feedstocks for fuels and energy.

Analysis of PM collected from Grand Forks, ND showed that the select classes of compounds occurred in specific TD or Pyr fractions. *n*-Alkanes, acids, and specific tracers

including levoglucosan and 6,10,14-trimethyl-2-pentadecanone dominated the TD fraction, whereas homology profiles of *n*-alkenes, *n*-alkylbenzenes, PAHs, and substituted phenols appeared in Pyr fractions. The compounds and tracers present in the TD fraction over the sampling weeks were apparent to be mostly of biogenic origin. The subsequent Pyr fractions, which are rarely used for atmospheric chemical composition studies, contributed as much as 30-70 % of the total abundance of OC compounds found by GC-MS. This suggested the breakdown of HMW compounds, which were also thought to be of mostly biogenic origin. Overall, this combined thermal technique showed that well known methods such as solvent extraction, AMS, and thermal desorption GC-MS may not give a complete profile of OC PM in the atmosphere unless the Pyr fraction is considered.

Overall, TD-Pyr-GC-MS is a novel approach, which is simple, comprehensive, and removes the need for solvent and time consuming steps that more commonly used solvent extraction GC-MS methods employ. It allows for a complete characterization of compounds, ranging from volatile to non-volatile, through extensive thermal profiles. When used in combination with TOA, excessive knowledge of PM, namely the carbonaceous fraction, can be determined.

## APPENDICES

## Appendix A

### *TD-Pyr-GC-MS Protocol and Heating profiles*

#### **Connecting the GC to the Pyroprobe**

1. Turn off the column pressure to the back inlet (split/splitless inlet) via the keypad on the front of the GC. Unscrew the big inlet nut to get access to the split/splitless liner, and ensure the liner is a split liner with no quartz wool. Replace the gold O-ring if Unscrew the septa nut from the inlet body and remove the green septa (Thermolite 11mm Low Bleed).

2. Take a new septa and puncture the transfer line needle through the middle (If a septa is already on the transfer line needle always replace it with a new one). Make sure to center the needle on the septa as best as possible, this helps to ensure the needle will be straight when place into the liner of the inlet. Take a kim-wipe and methanol and wipe the needle to ensure it is clean.

3. Now connect the transfer line to GC inlet. Make sure to **NOT OVERTIGHTEN** the septum nut as this will cause leaks to occur around the threading.

4. Turn both the EPC 3-way valve (directs the He carrier gas to the pyroprobe) located on the top of the GC and the 2-way valve for the He auxillary gas to the pyroprobe located behind the GC to the right direction (arrows facing the right way).

5. Turn the column pressure to the back inlet on again. Wait approximately 30-40 mins to allow any residual air in the GC system (from exposing the inlet while installing the pyroprobe transfer line) to pass through. The vacuum pressure should reach back to the original value within 5 mins, but it is best to wait longer to purge the system.

6. Check for air leaks on the MS by performing a manual tune. First go to “instrument” on top of Chemstation menu, then “edit tune parameters” for a manual tune. Go to “more parameters”



and then “tune parameters.” Monitor only in range 10-100  $m/z$ . The masses 69 (calibration solution), 18 ( $H_2O$ ), and 28  $m/z$  ( $N_2$ ) should be entered. The relative abundance of the  $H_2O$  peak (18  $m/z$ ) should be less than  $N_2$  (28  $m/z$ ), and both peaks should be less than 5% of the 69  $m/z$  PFTBA (large peak). Let stabilize for 1 min. After viewing, click “stop” and **hit the “MS off” button**. Go to file in the top left tool bar, print the results and add to the tunes and maintenance binder. After this, hit “cancel” button. If leak is observed contact operator. Do not start the work if  $N_2$  is higher than 5 %.

### **Creating Sequence and Turning GC to Ready**

1. After ensuring that the system is free of leaks, blank runs can be done to ensure correct baseline. In the Chemstation screen, build the sequence of samples to be analyzed in the same manner as when an autosampler sequence is built. Go to “sequence” at the top of the ChemStation screen, and then to “edit sequence.” Erase any previous sequences. Under method for each temperature step for a sample, right click on method and browse for the GC method. For “data file,” start at 1 and give the name that will show up in your Chemstation data file. For “data path” at the top of the screen, click browse and go to the present year and month in the central data file, and then “make new folder” (button at the bottom), name by date, initials and Py. **The first analysis of the day should be a blank run at 870 °C to ensure proper baseline (if proper baseline is not achieved then repeat this step).**

2. Once sequence is made, make sure to save the sequence under the D drive with the correct name and date. Also make a copy of the lines from the sequence into an excel sheet (for each month there is a separate excel sheet for the sequences run in that month).

3. After your sequence is created properly, click “position and run sequence” and click on the data file that you want to start with and click OK. The run file will then show up. Put in operator name and a brief description of the sample. If you are re-doing a sequence, hit the “overwrite button”. If process keywords icon shows up, make sure to click “Yes” or the instrument will not run. The GC will then go into the waiting mode for the pyroprobe.

### **Pyroprobe Setup and Analysis**

1. Switch to pyroprobe software (wand icon). Select “sequence” at the left. In the pyroprobe software/sequence ensure correct sequence of temperature steps is loaded (it should match the same temperatures you set up under the GC sequence). If several temperature steps need to be made, the sequence has to be programmed by inserting different methods (by temperature), by double clicking on the line to select the method. When done, click on the method you want to start with. A sequence consisting of several methods can be saved for later use. Any sequence should be saved as an Excel file and saved in a central file indicated as a sequence folder.

2. To edit a method, go to “tools” then “method editor”- a table opens. Go to “file” in the upper left corner, then “open method” and open the method you want. Parameters can be changed. Save this and go to “file” again and select “send method” so that the indicated method at the top now matches your selected method. After your temperature methods on the pyroprobe match the ones you set on the GC you are not set to run the pyroprobe. Click run sequence to start your samples.

## Blank and Sample Analysis

1. Before analysis for the day, make sure that the quartz wool inside the quartz tube is clean if using liquid or solid samples. If running PM quartz filters, ensure that the quartz tube is empty and clean. If you are unsure, take out another tube and replace the quartz wool.

2. The first analysis of the day should always be a blank run (870 or 890 °C) to ensure that the baseline is correct. Before running, flush the quartz tube 3 times with ~25 µL of DCM for a total of 75 µL added (outside of the instrument). Then click dry (under the pyroprobe icon) at 100 °C for 15 seconds. Follow this up with two to three consecutive cleans of 870 °C for 10 seconds. This should allow for the decomposition of some of the contamination on the inside and outside of the quartz tube. After cleaning three times, run the first blank 870 °C step and analyze the baseline. If the baseline does not look proper, repeat all of step 2 to ensure no prior contamination before analysis.

3. After proper baseline is ensured, samples can be run. If analyzing a liquid sample ensure the correct concentration before analysis and if a drying step is needed. Drying DCM is usually set at 50 °C for 60 seconds prior to analysis to remove the solvent peak. If you do not dry the liquid sample make sure to add a solvent delay to the original GC method. To analyze solid samples, carefully remove the quartz tube from the filament and weigh the tube on the microbalance. Add the solid to the quartz tube and reweigh the quartz tube. Ensure that the sample is from 10-50 µg for most samples. If running a quartz filter sample, make sure that the quartz tube has no wool inside. Use the cutting device to cut a ~ 2 x 15mm strip of the quartz filter and place it inside the quartz tube, carefully with tweezers.

## Running Test Mix

1. At least once a week, or for new operators, test mix should be run on the pyroprobe to ensure proper working conditions of the instrument. Run a triplicate (sometimes 4 runs are needed as the first looks bad usually) of the mixture.

2. Begin by added 5  $\mu$ L of the test mix to the quartz tube and dry the sample for 60 seconds at 50 °C. Run the test mix at 300 °C. After triplicate or quadruplicate analysis of the test mix, process the results in an excel file to ensure that the RSD values look proper and that each peak is apparent in the chromatograms (there are normally 17 peaks present). For new users, ensure that the operator has seen the test mix and that you can move on to running your samples.

## Tips and Hints

1. The pyroprobe should be inserted smoothly into the unit, **NEVER force it**. If it does not go easily it is because you are not inserting it straight.

2. When removing or adding the quartz tube to the filament, never apply pressure or force to the tubing. Always allow it to fall out on its own. If the tube is stuck, hit the side of the pyroprobe rod with tweezers to help remove the quartz tube. When adding a new quartz tube, never push on the top of the tube to get it to go into the filament, allow gravity to do its work (do not touch the metal filament or bang on the filament itself).

3. The cost of the pyroprobe rods is ~ \$400 or refurbishing \$250, so always make sure we have a spare one.

4. Waiting too long before drying and running a sample may cause loss of the sample or sample discrimination.

5. Introducing sample on just cleaned (too hot probe) may lead to irreproducibility of results (wait 5 min).

6. To fill the tube with quartz wool, place carefully quartz wool (5-7 mm at the center of the tube) into the quartz tube and press it from both the ends so that it won't go down when injecting the sample.

Table A1. Pyroprobe heating profiles for filament and interface showing initial and optimized conditions.

	Initial Conditions					Optimized Conditions				
	300 °C	500 °C	600 °C	700 °C	870 °C	300 °C	500 °C	600 °C	700 °C	870 °C
<b>Filament initial temp (°C)</b>	40	40	40	40	40	40	40	40	40	40
<b>Filament initial time (sec)</b>	0	0	0	0	0	0	0	0	0	0
<b>Filament heating rate (°C/s)</b>	10	10	10	10	10	30	30	30	30	30
<b>Filament final temp (°C)</b>	300	500	600	700	870	300	500	600	700	870
<b>Filament final time (sec)</b>	30	30	30	30	10	30	30	30	30	10
<b>Interface rest temp (°C)</b>	40	40	40	40	40	40	40	40	40	40
<b>Interface initial temp (°C)</b>	40	40	40	40	40	40	40	40	40	40
<b>Interface initial time (min)</b>	0	0	0	0	0	0	0	0	0	0
<b>Interface heating rate (°C/s)<sup>a</sup></b>	0 <sup>a</sup>	0	0	0	0	0	0	0	0	0
<b>Interface final temp (°C)</b>	300	300	300	300	300	300	300	300	300	300
<b>Interface final time (min)</b>	2.5	2.5	2.5	2.5	2.5	0.9	0.9	0.9	0.9	0.9

<sup>a</sup> Interface heating rate of 0 means the interface was heated ballistically

## Appendix B

*MS information for compounds used in optimization of TD-Pyr-GC-MS*

Table B1. Standard mixture of compounds for optimization of pyroprobe conditions

	<b>Compound</b>	<b>Ret. Time</b>	<b>Key Ions (m/z)</b>
SM2	Benzene	1.987	<b>78</b> , 77, 51
	Toluene	3.029	<b>91</b> , 92, 65
	Ethylbenzene	3.919	<b>91</b> , 92, 106
	<i>m</i> -Xylene	3.983	<b>91</b> , 106, 105
SM1	Nonane	4.250	<b>43</b> , 57, 71
	Butylbenzene	5.450	<b>91</b> , 92, 134
	1-Tridecene	6.840	<b>43</b> , 55, 68
	Heptadecane	8.890	<b>57</b> , 71, 85
	Dotriacontane	14.180	<b>57</b> , 71, 85

Bold lettering denotes quantification ion

## Appendix C

### *TD-Pyr-GC-MS EIC values after analysis of standard mixture 2*

Table C1. EIC abundances, STD, and RSD values for SM2 after TD-Pyr-GC-MS analysis.

	Avg	STD	RSD	Avg	STD	RSD	Avg	STD	RSD
Benzene	1.13E+07	3.07E+06	27.3	2.02E+07	9.12E+06	45.3	1.30E+07	8.00E+06	61.5
Toluene	2.76E+07	5.07E+06	18.3	3.80E+07	1.09E+07	28.7	2.75E+07	1.02E+07	37.2
Ethylbenzene	3.15E+07	4.24E+06	13.4	3.82E+07	8.11E+06	21.2	2.96E+07	7.70E+06	26.0
m-Xylene	5.12E+07	5.97E+06	11.7	6.10E+07	1.01E+07	16.6	5.13E+07	8.61E+06	16.8
Nonane	1.22E+07	1.43E+06	11.7	1.45E+07	2.22E+06	15.3	1.21E+07	1.71E+06	14.2
Butylbenzene	5.58E+07	6.58E+06	11.8	5.81E+07	6.55E+06	11.3	5.43E+07	5.95E+06	10.9
Tridecene	6.06E+06	9.22E+05	15.2	6.33E+06	8.19E+05	12.9	6.30E+06	5.83E+05	9.3
Heptadecane	3.13E+07	5.09E+06	16.3	3.27E+07	4.20E+06	12.9	3.20E+07	3.25E+06	10.2
Dotriacontane	1.85E+07	3.64E+06	19.6	1.82E+07	1.61E+06	8.8	2.10E+07	4.71E+05	2.2



## Appendix D

### MS identification of compounds based on NIST database

a)

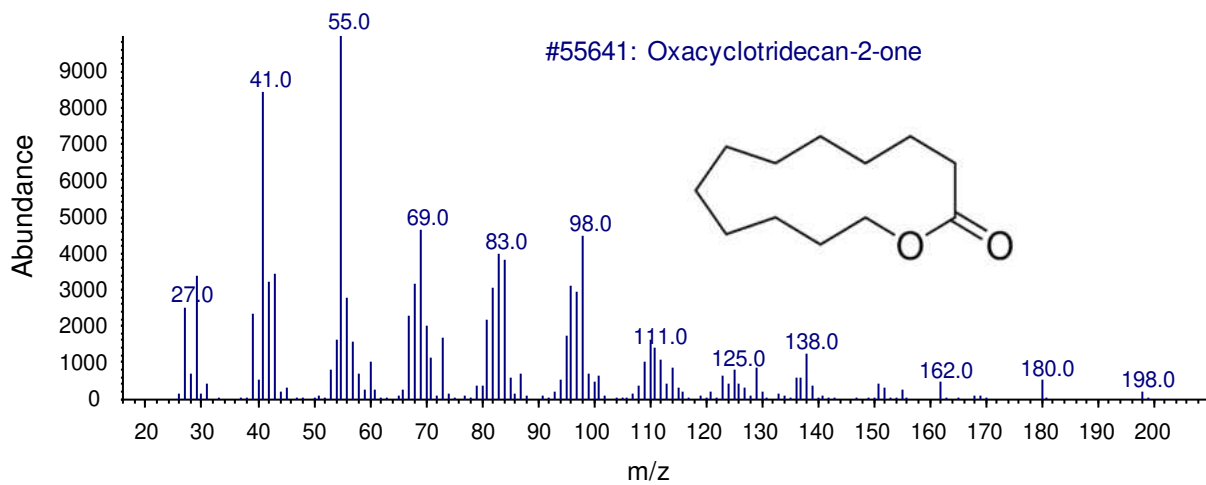
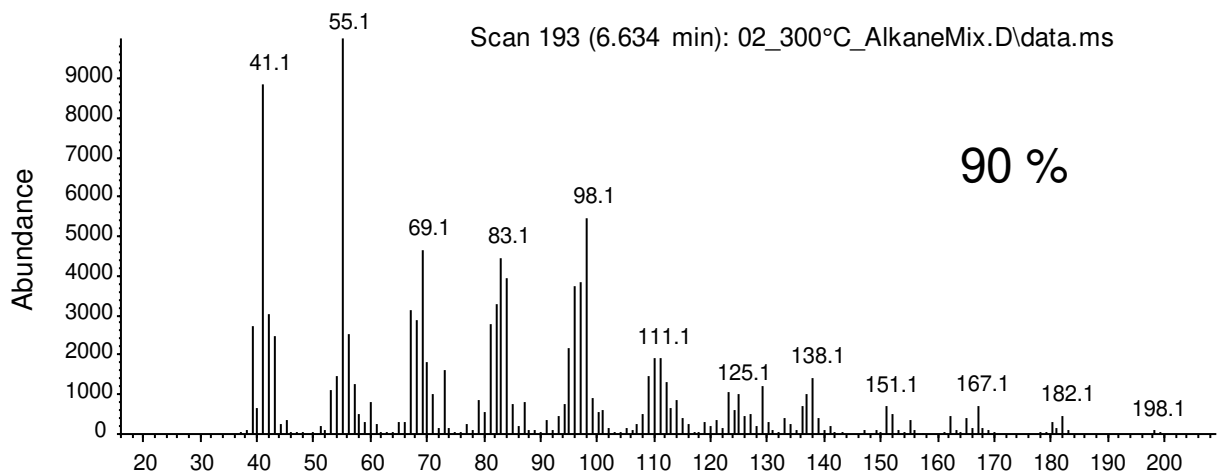


Figure D1. Mass spectra of select peaks of C<sub>21</sub>-C<sub>40</sub> alkane mix after TD-Pyr-GC-MS a) contaminant a b) contaminant b c) contaminant c.

Figure D1 cont.

b)

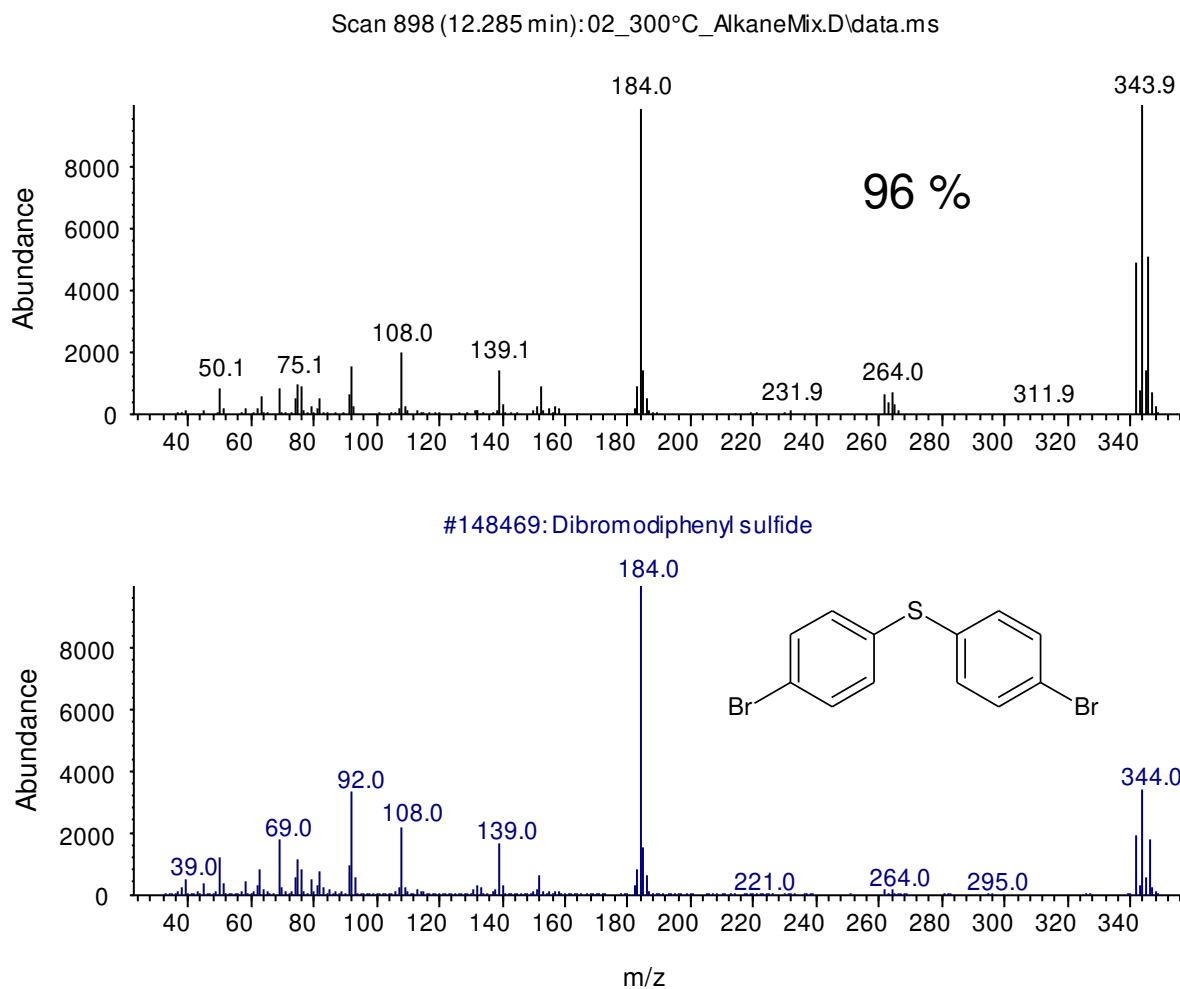


Figure D1. Mass spectra of select peaks of C<sub>21</sub>-C<sub>40</sub> alkane mix after TD-Pyr-GC-MS a) contaminant a b) contaminant b c) contaminant c.

Figure D1 cont.

c)

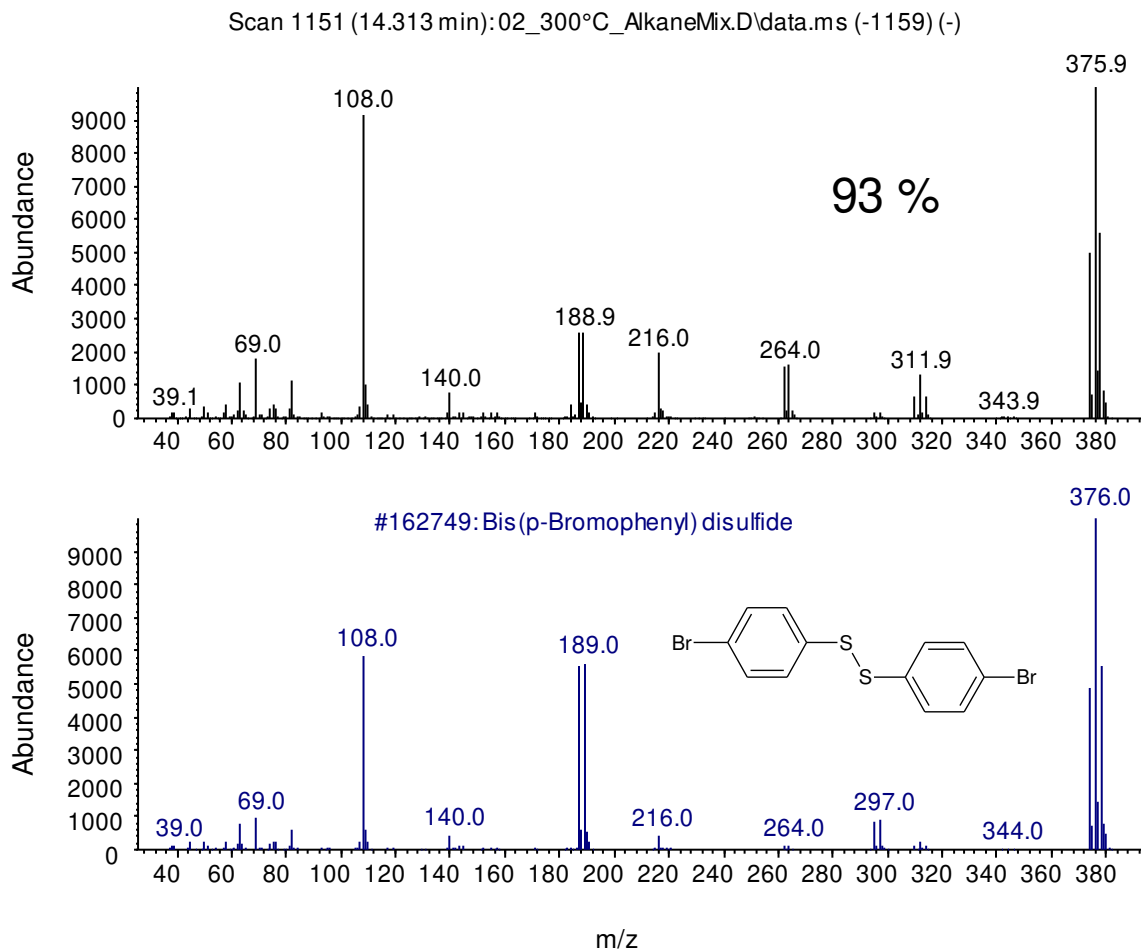


Figure D1. Mass spectra of select peaks of C<sub>21</sub>-C<sub>40</sub> alkane mix after TD-Pyr-GC-MS a) contaminant a b) contaminant b c) contaminant c.

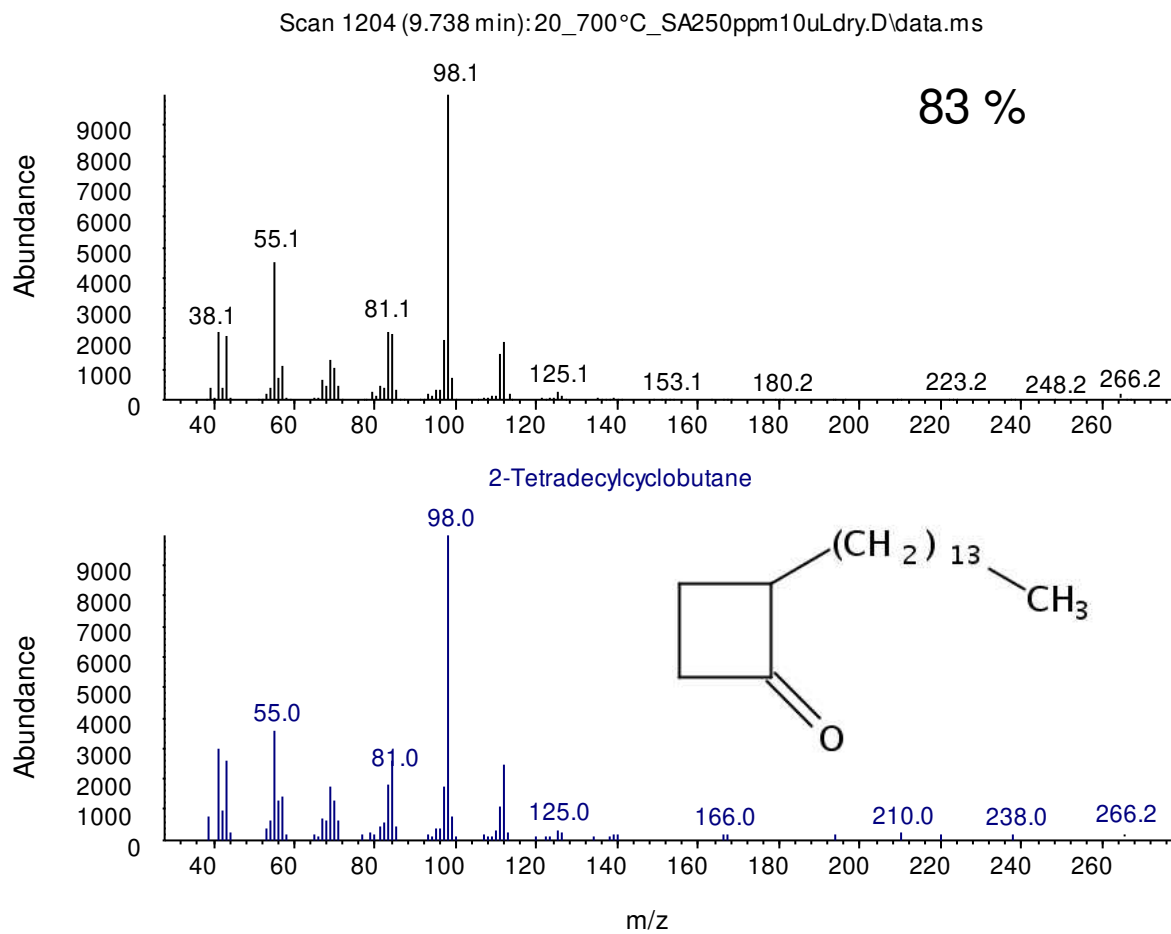


Figure D2. Mass spectra of 2-tetradecylcyclobutane peak comparison between sample and NIST library.  $\text{M}^+$  ion can be seen at 266  $m/z$ , which corresponds to the MW of tetradecylcyclobutane.

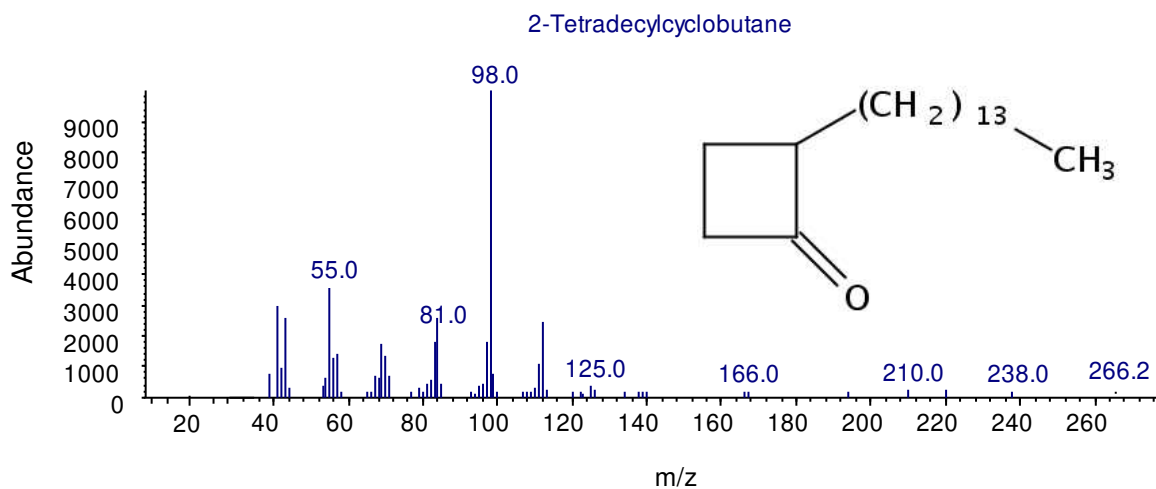
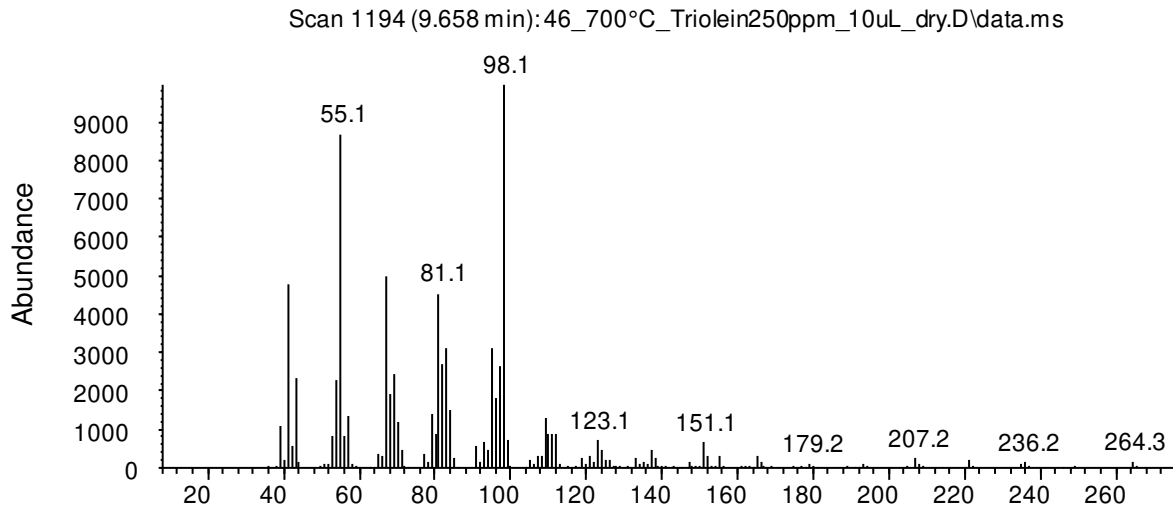


Figure D3. Mass spectra of tetradecenylcyclobutane peak comparison between sample and NIST library of 2-tetradecylcyclobutane. Above mass spectra shows loss of 2  $m/z$  from  $M^+$  fragment of tetradecylcyclobutane, verifying double bond within the molecule. The MW of tetradecenylcyclobutane is 264.

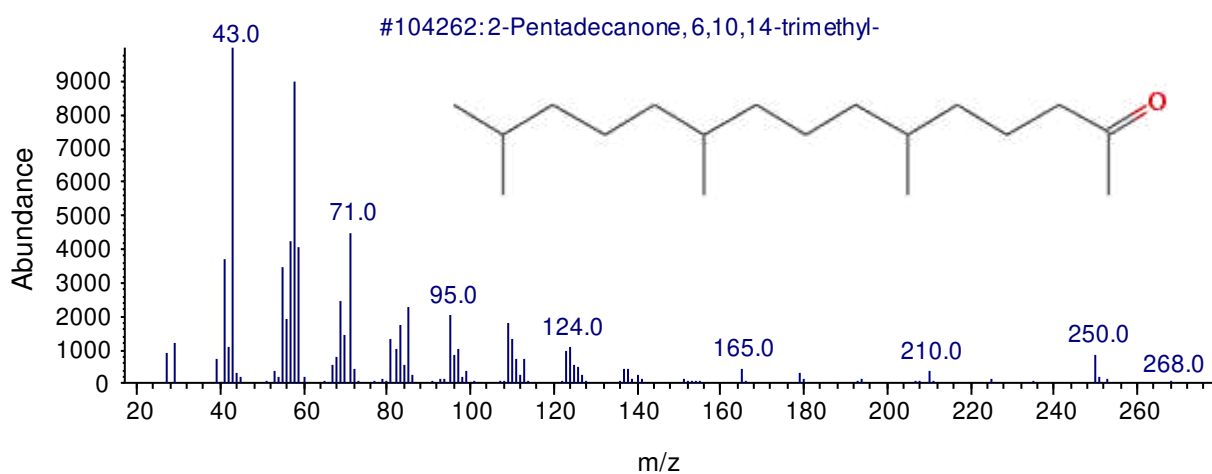
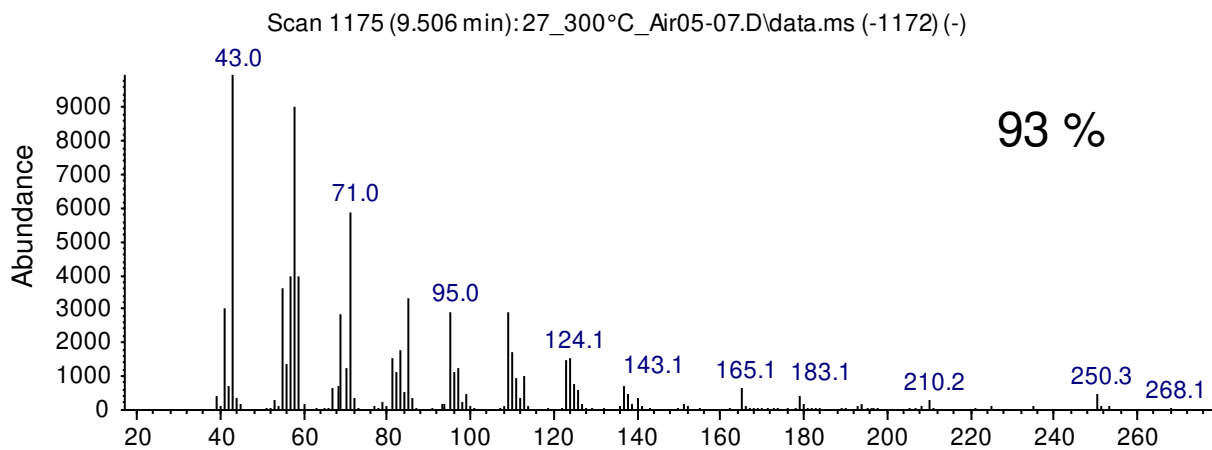


Figure D4. Mass spectra of 6,10,14-trimethyl-2-pentadecanone peak comparison between sample and NIST library.

Appendix E

Table E1. PM<sub>2.5</sub> and OC and EC concentrations with % of total PM<sub>2.5</sub> collected and measured during POLCAST campaign at Grand Forks, ND, 2012

	DOY			PM <sub>2.5</sub>	OC/EC conc. and % of PM <sub>2.5</sub>			
	Start	End	Week	conc.	Avg OC conc.	% of	Avg EC conc.	% of
				(µg/m <sup>3</sup> )	(µg/m <sup>3</sup> )	PM <sub>2.5</sub>	(µg/m <sup>3</sup> )	PM <sub>2.5</sub>
	173	180	1	3.86	1.74 ± 0.02	45	0.17 ± 0.01	4
	180	187	2	4.98	2.51 ± 0.04	50	0.27 ± 0.02	5
	187	194	3	4.23	2.48 ± 0.12	59	0.20 ± 0.01	5
	194	201	4	13.6	<b>7.70</b> ± 0.21	57	0.33 ± 0.01	2
	201	208	5	6.44	3.90 ± 0.03	61	0.26 ± 0.01	4
	208	215	6	7.37	3.08 ± 0.01	42	0.22 ± 0.04	3
	215	222	7	4.58	2.47 ± 0.14	54	0.23 ± 0.01	5
	222	229	8	4.51	2.21 ± 0.03	49	0.21 ± 0.01	5
	229	236	9	6.85	2.51 ± 0.15	37	0.35 ± 0.02	5
	236	243	10	7.28	2.88 ± 0.21	40	0.33 ± 0.04	4
	243	250	11	8.64	3.42 ± 0.03	40	0.30 ± 0.01	4
TD-Pyr-GC-MS	250	257	12	2.77	2.05 ± 0.04	<b>74</b>	0.22 ± 0.00	<b>8</b>
	257	264	13	5.81	1.69 ± 0.03	29	0.23 ± 0.01	4
	264	271	14	5.68	1.64 ± 0.08	29	0.25 ± 0.03	4
	271	278	15	<b>18.78</b>	5.05 ± 0.29	27	<b>0.55 ± 0.06</b>	3
	278	286	16	3.5	1.17 ± 0.04	33	0.19 ± 0.01	5
	286	293	17	6.9	3.05 ± 0.06	44	0.33 ± 0.02	5

## Appendix F

### *TD-Pyr-GC-MS Compounds*

Table F1. Compounds identified by TD-Pyr-GC-MS during POLCAST campaign, including retention times ( $t_R$ ) and MS ions

Compound	$t_R$ (min)	Quant. Ion ( $m/z$ )	Confirmation Ions ( $m/z$ )	Identification (S, R, H)
<b>Alkanes</b>				
C <sub>9</sub>	4.23	57	71, 85	S
C <sub>10</sub>	5.08	57	71, 85	H
C <sub>11</sub>	5.71	57	71, 85	H
C <sub>12</sub>	6.30	57	71, 85	H
C <sub>13</sub>	6.88	57	71, 85	H
C <sub>14</sub>	7.41	57	71, 85	H
C <sub>15</sub>	7.92	57	71, 85	H
C <sub>16</sub>	8.40	57	71, 85	H
C <sub>17</sub>	8.86	57	71, 85	S
C <sub>18</sub>	9.30	57	71, 85	H
C <sub>19</sub>	9.71	57	71, 85	H
C <sub>20</sub>	10.11	57	71, 85	H
C <sub>21</sub>	10.49	57	71, 85	H
C <sub>22</sub>	10.85	57	71, 85	H
C <sub>23</sub>	11.20	57	71, 85	H
C <sub>24</sub>	11.53	57	71, 85	H
C <sub>25</sub>	11.85	57	71, 85	H
C <sub>26</sub>	12.18	57	71, 85	H
C <sub>27</sub>	12.47	57	71, 85	H
C <sub>28</sub>	12.77	57	71, 85	H
C <sub>29</sub>	13.07	57	71, 85	H
C <sub>30</sub>	13.39	57	71, 85	H
C <sub>31</sub>	13.77	57	71, 85	H
C <sub>32</sub>	14.15	57	71, 85	S
C <sub>33</sub>	14.60	57	71, 85	H
C <sub>34</sub>	15.09	57	71, 85	H



Table F1 cont.

Compound	t <sub>R</sub> (min)	Quant. Ion ( <i>m/z</i> )	Confirmation Ions ( <i>m/z</i> )	Identification (S, R, H)
<b>Alkenes</b>				
C <sub>9</sub>	4.20	55	69, 83	S, H
C <sub>10</sub>	5.05	55	69, 83	S, H
C <sub>11</sub>	5.68	55	69, 83	S, H
C <sub>12</sub>	6.27	55	69, 83	S, H
C <sub>13</sub>	6.85	55	69, 83	S, H
C <sub>14</sub>	7.38	55	69, 83	S, H
C <sub>15</sub>	7.89	55	69, 83	S, H
C <sub>16</sub>	8.37	55	69, 83	S, H
C <sub>17</sub>	8.83	55	69, 83	S, H
C <sub>18</sub>	9.27	55	69, 83	S, H
C <sub>19</sub>	9.68	55	69, 83	S, H
C <sub>20</sub>	10.08	55	69, 83	S, H
C <sub>21</sub>	10.46	55	69, 83	S, H
C <sub>22</sub>	10.82	55	69, 83	S, H
C <sub>23</sub>	11.17	55	69, 83	S, H
C <sub>24</sub>	11.50	55	69, 83	S, H
C <sub>25</sub>	11.82	55	69, 83	S, H
C <sub>26</sub>	12.15	55	69, 83	S, H
C <sub>27</sub>	12.44	55	69, 83	S, H
C <sub>28</sub>	12.74	55	69, 83	S, H
C <sub>29</sub>	13.04	55	69, 83	S, H
C <sub>30</sub>	13.36	55	69, 83	S, H
C <sub>31</sub>	13.74	55	69, 83	S, H
C <sub>32</sub>	14.12	55	69, 83	S, H
C <sub>33</sub>	14.57	55	69, 83	S, H
C <sub>34</sub>	15.06	55	69, 83	S, H

Table F1 cont.

Compound	t <sub>R</sub> (min)	Quant. Ion ( <i>m/z</i> )	Confirmation Ions ( <i>m/z</i> )	Identification (S, R, H)
<b>Acids and Esters</b>				
C <sub>16</sub> FA	9.96	73	43, 129	S, H
C <sub>18</sub> FA	10.75	73	40, 129	S, H
C <sub>16</sub> FAME	9.83	74	87, 153	S, H
C <sub>17</sub> FAME	10.22	74	87, 153	S, H
C <sub>18</sub> FAME	10.60	74	87, 153	S, H
C <sub>19</sub> FAME	10.96	74	87, 153	S, H
C <sub>20</sub> FAME	11.31	74	87, 153	S, H
C <sub>21</sub> FAME	11.65	74	87, 153	S, H
C <sub>22</sub> FAME	11.97	74	87, 153	S, H
C <sub>23</sub> FAME	12.27	74	87, 153	S, H
C <sub>24</sub> FAME	12.59	74	87, 153	S, H
C <sub>25</sub> FAME	12.87	74	87, 153	S, H
C <sub>26</sub> FAME	13.19	74	87, 153	S, H
C <sub>27</sub> FAME	13.52	74	87, 153	S, H
C <sub>28</sub> FAME	13.82	74	87, 153	S, H
<b>PAHs</b>				
Naphthalene	6.34	128	127	S
1-Methylnaphthalene	6.981	142	141	R
2-Methylnaphthalene	7.077	142	141	R
Biphenyl	7.43	154	153	S
Dimethylnaphthalene	7.582	156	155	R
Dimethylnaphthalene 2	7.654	156	155	R
Dimethylnaphthalene 3	7.678	156	155	R
Dimethylnaphthalene 4	7.766	156	155	R
Acenaphthylene	7.846	152	151	S
Fluorene	8.504	166	165	S
Phenanthrene	9.442	178	176	S
Anthracene	9.49	178	176	S
Fluoranthene	10.612	202	200	S
Pyrene	10.828	202	200	S

Table F1 cont.

Compound	t <sub>R</sub> (min)	Quant. Ion ( <i>m/z</i> )	Confirmation Ions ( <i>m/z</i> )	Identification (S, R, H)
<b>BTEX</b>				
Benzene	2.845	78	77,51	S
Toluene	3.519	91	92, 65	S
Xylene	4.239	91	106	S
Ethyl-benzene	4.184	91	106	S
<b>Alkylbenzenes</b>				
C <sub>3</sub> benzene	4.833	91	92, 120	S, H
C <sub>3</sub> benzene	4.881	105	120, 91	S, H
C <sub>3</sub> benzene	4.921	105	120, 91	S, H
C <sub>3</sub> benzene	5.001	105	120, 91	S, H
C <sub>3</sub> benzene	5.097	105	120, 91	S, H
C <sub>3</sub> benzene	5.29	105	120, 91	H
C <sub>4</sub> benzene	5.442	105	120, 91	S
C <sub>5</sub> benzene	6.123	91	92, 148	S, H
C <sub>6</sub> benzene	6.708	91	92, 162	S, H
C <sub>7</sub> benzene	7.277	91	92, 176	S, H
C <sub>8</sub> benzene	7.822	91	92, 190	S, H
C <sub>9</sub> benzene	8.327	91	92, 204	S, H
C <sub>10</sub> benzene	8.808	91	92, 218	S, H
C <sub>11</sub> benzene	9.265	92	91, 232	S, H
C <sub>12</sub> benzene	9.698	92	91, 246	S, H
C <sub>13</sub> benzene	10.123	92	91, 260	S, H
C <sub>14</sub> benzene	10.524	92	91, 274	S, H
C <sub>15</sub> benzene	10.892	92	91, 288	S, H
C <sub>16</sub> benzene	11.261	92	91, 302	S, H
C <sub>17</sub> benzene	11.606	92	91, 316	S, H
C <sub>18</sub> benzene	11.942	92	91, 330	S, H
C <sub>19</sub> benzene	12.263	92	91, 344	S, H
C <sub>20</sub> benzene	12.576	92	91, 358	S, H
C <sub>21</sub> benzene	12.872	92	91, 372	S, H
C <sub>22</sub> benzene	13.201	92	91, 386	S, H
C <sub>23</sub> benzene	13.553	92	91, 400	S, H
C <sub>24</sub> benzene	13.866	92	91, 414	S, H
styrene	4.408	104	103, 78	

Table F1 cont.

Compound	tR (min)	Quant. Ion (m/z)	Confirmation Ions (m/z)	Identification (S, R, H, T)
<b>Phenols</b>				
Phenol	4.985	94	66,65	S
Methyl phenol	5.458	108	107, 77	R
Methyl phenol	5.594	108	107, 77	R
C <sub>2</sub> phenol	5.979	107	122, 77	R
C <sub>2</sub> phenol	6.051	107	122, 77	R
C <sub>2</sub> phenol	6.171	107	122, 77	R
C <sub>2</sub> phenol	6.227	107	122, 77	R
Butylated hydroxytoluene	8.047	205	145, 57	T
<b>Ketones/aldehydes</b>				
Nonanal	5.73	57	43, 70	T
6,10,14-Trimethyl-2-pentadecanone	9.5	58	71, 43	T
<b>Sugars</b>				
Levoglucosan	7.927	60	73, 98	S
Levoglucosenone	5.851	98	96, 126	T
<b>Phthalates</b>				
Dibutyl phthalate	9.642	149	205	S
Diisobutyl phthalate	10.027	149	223	S
Dioctyl phthalate	12.078	149	167, 279	S
Phthalic anhydride	7.085	148	104, 76	T
1-Isobenzofuranone	7.277	134	105, 77	T
<b>Nitrogen based</b>				
Diethyltoluamide	8.399	119	190, 91	T

## Appendix G

### *TD-Pyr-GC-MS Compounds*

Table G1. Compounds identified by TD-Pyr-GC-MS during POLCAST campaign week 12

<b>Week 12</b>								
<b>Alkanes</b>								
<b>Compound</b>	<b>300 °C</b>	<b>500 °C</b>	<b>600 °C</b>	<b>700 °C</b>	<b>870 °C</b>	<b>TD</b>	<b>Pyr</b>	<b>Total</b>
C <sub>9</sub>	0	0	0	0	0	0	0	0
C <sub>10</sub>	0	0	11148	0	0	0	11148	11148
C <sub>11</sub>	0	11293	13220	0	0	0	24513	24513
C <sub>12</sub>	0	13850	13049	3044	0	0	29943	29943
C <sub>13</sub>	0	11359	15030	3063	0	0	29451	29451
C <sub>14</sub>	0	13941	12787	3159	0	0	29886	29886
C <sub>15</sub>	0	18146	16082	4435	0	0	38662	38662
C <sub>16</sub>	0	13059	12295	1695	0	0	27049	27049
C <sub>17</sub>	0	14394	11911	1673	0	0	27978	27978
C <sub>18</sub>	0	13156	9139	0	0	0	22295	22295
C <sub>19</sub>	0	8249	9432	0	0	0	17681	17681
C <sub>20</sub>	0	9176	9961	0	0	0	19137	19137
C <sub>21</sub>	17357	12914	15575	0	0	17357	28489	45845
C <sub>22</sub>	26665	11226	8972	0	0	26665	20198	46864
C <sub>23</sub>	82957	22975	12549	0	0	82957	35523	118480
C <sub>24</sub>	71095	22653	10096	0	0	71095	32749	103845
C <sub>25</sub>	200465	19557	7561	0	0	200465	27118	227583
C <sub>26</sub>	111918	31242	11502	0	0	111918	42744	154662
C <sub>27</sub>	362417	17644	4007	0	0	362417	21651	384068
C <sub>28</sub>	94787	16775	5250	0	0	94787	22025	116813
C <sub>29</sub>	1050510	27442	2953	0	0	1050510	30395	1080905
C <sub>30</sub>	35267	8670	0	0	0	35267	8670	43937
C <sub>31</sub>	830154	16828	0	0	0	830154	16828	846982
C <sub>32</sub>	24850	0	0	0	0	24850	0	24850
C <sub>33</sub>	38033	0	0	0	0	38033	0	38033
C <sub>34</sub>	0	0	0	0	0	0	0	0
<b>Total</b>	2946475	334548	212518	17068	0	2946475	564134	3510609

Table G1 cont.

Week 12								
Alkenes								
Compound	300 °C	500 °C	600 °C	700 °C	870 °C	TD	Pyr	Total
C <sub>9</sub>	0	0	0	0	0	0	0	0
C <sub>10</sub>	0	0	0	0	0	0	0	0
C <sub>11</sub>	0	0	37043	13324	0	0	50367	50367
C <sub>12</sub>	0	28269	29166	11059	0	0	68493	68493
C <sub>13</sub>	0	24820	32148	12553	0	0	69521	69521
C <sub>14</sub>	0	26238	29762	9038	0	0	65038	65038
C <sub>15</sub>	0	26997	28125	7547	0	0	62669	62669
C <sub>16</sub>	0	25868	23837	4555	0	0	54261	54261
C <sub>17</sub>	0	19638	20882	4156	0	0	44676	44676
C <sub>18</sub>	0	18395	24286	3306	0	0	45987	45987
C <sub>19</sub>	0	16214	14088	0	0	0	30302	30302
C <sub>20</sub>	0	14641	8898	0	0	0	23538	23538
C <sub>21</sub>	0	15571	11068	0	0	0	26639	26639
C <sub>22</sub>	0	15377	9173	0	0	0	24550	24550
C <sub>23</sub>	0	21155	0	0	0	0	21155	21155
C <sub>24</sub>	0	0	0	0	0	0	0	0
<b>Total</b>	0	253183	268476	65539	0	0	587198	587198

Acids & Esters								
C <sub>16</sub> FA	122569	0	0	0	0	122569	0	122569
C <sub>18</sub> FA	25229	0	0	0	0	25229	0	25229
C <sub>16</sub> FAME	71323	0	0	0	0	71323	0	71323
C <sub>17</sub> FAME	0	0	0	0	0	0	0	0
C <sub>18</sub> FAME	44697	0	0	0	0	44697	0	44697
C <sub>19</sub> FAME	0	0	0	0	0	0	0	0
C <sub>20</sub> FAME	5405	0	0	0	0	5405	0	5405
C <sub>21</sub> FAME	0	0	0	0	0	0	0	0
C <sub>22</sub> FAME	14282	0	0	0	0	14282	0	14282
C <sub>23</sub> FAME	4147	0	0	0	0	4147	0	4147
C <sub>24</sub> FAME	15761	0	0	0	0	15761	0	15761
C <sub>25</sub> FAME	0	0	0	0	0	0	0	0
C <sub>26</sub> FAME	5848	0	0	0	0	5848	0	5848
C <sub>27</sub> FAME	0	0	0	0	0	0	0	0
C <sub>28</sub> FAME	0	0	0	0	0	0	0	0
<b>Total</b>	309261	0	0	0	0	309261	0	309261

Table G1 cont.

<b>Week 12</b>								
<b>PAHs</b>								
<b>Compound</b>	<b>300 °C</b>	<b>500 °C</b>	<b>600 °C</b>	<b>700 °C</b>	<b>870 °C</b>	<b>TD</b>	<b>Pyr</b>	<b>Total</b>
Naphthalene	21702	18793	55067	59922	0	21702	133782	155483
1-Methylnaphthalene	11190	7369	24764	17829	0	11190	49961	61151
2-Methylnaphthalene	7961	7264	21211	17914	0	7961	46390	54351
Biphenyl	15565	7297	9110	0	0	15565	16407	31972
Dimethylnaphthalene	0	0	0	0	0	0	0	0
Dimethylnaphthalene 2	0	0	0	0	0	0	0	0
Dimethylnaphthalene 3	0	0	0	0	0	0	0	0
Dimethylnaphthalene 4	0	0	0	0	0	0	0	0
Acenaphthylene	0	0	0	0	0	0	0	0
Fluorene	0	3635	16897	0	0	0	20532	20532
Phenanthrene	24107	5696	12741	0	0	24107	18437	42544
Anthracene	10501	2048	5393	0	0	10501	7441	17943
Fluoranthene	25163	1943	3206	0	0	25163	5149	30312
Pyrene	20984	1440	5651	0	0	20984	7090	28075
<b>Total</b>	137174	55485	154039	95665	0	137174	305189	442362
<b>BTEX</b>								
Benzene	0	43209	156272	197017	110395	0	506893	506893
Toluene	0	229941	424111	271709	81268	0	1007029	1007029
Xylene	0	79580	152432	80614	0	0	312625	312625
Ethylbenzene	0	23485	61566	25609	0	0	110660	110660
<b>Total</b>	0	376215	794381	574948	191663	0	1937207	1937207

Table G1 cont.

<b>Week 12</b>								
<b>Alkylbenzenes</b>								
<b>Compound</b>	<b>300 °C</b>	<b>500 °C</b>	<b>600 °C</b>	<b>700 °C</b>	<b>870 °C</b>	<b>TD</b>	<b>Pyr</b>	<b>Total</b>
C <sub>3</sub> benzene	0	0	12030	0	0	0	12030	12030
C <sub>3</sub> benzene	0	11528	40336	0	0	0	51864	51864
C <sub>3</sub> benzene	0	27457	23348	0	0	0	50805	50805
C <sub>3</sub> benzene	0	15727	28459	0	0	0	44187	44187
C <sub>3</sub> benzene	0	27992	40353	0	0	0	68344	68344
C <sub>3</sub> benzene	0	18305	23780	0	0	0	42084	42084
C <sub>4</sub> benzene	0	9840	13992	0	0	0	23832	23832
C <sub>5</sub> benzene	0	11665	15036	0	0	0	26701	26701
C <sub>6</sub> benzene	0	7963	9585	0	0	0	17549	17549
C <sub>7</sub> benzene	0	10547	9236	0	0	0	19782	19782
C <sub>8</sub> benzene	0	9197	7688	0	0	0	16885	16885
C <sub>9</sub> benzene	0	5762	5533	0	0	0	11295	11295
C <sub>10</sub> benzene	0	7575	5555	0	0	0	13131	13131
C <sub>11</sub> benzene	0	3921	3765	0	0	0	7685	7685
C <sub>12</sub> benzene	0	7638	5281	0	0	0	12919	12919
C <sub>13</sub> benzene	0	0	0	0	0	0	0	0
Styrene	0	80996	82672	0	0	0	163668	163668
<b>Total</b>	0	256112	326648	0	0	0	582760	582760
<b>Phenols</b>								
Phenol	0	78133	85933	0	0	0	164066	164066
Methyl phenol	20232	26656	40512	0	0	20232	67168	87400
Methyl phenol	35304	57002	67630	0	0	35304	124631	159936
C <sub>2</sub> phenol	0	0	10344	0	0	0	10344	10344
C <sub>2</sub> phenol	0	0	12380	0	0	0	12380	12380
C <sub>2</sub> phenol	0	0	10321	0	0	0	10321	10321
C <sub>2</sub> phenol	0	0	9018	0	0	0	9018	9018
Butylated hydroxytoluene	0	0	0	0	0	0	0	0
<b>Total</b>	55537	161790	236137	0	0	55537	397927	453463



Table G1 cont.

<b>Week 12</b>								
<b>Ketones/Aldehydes</b>								
<b>Compound</b>	<b>300 °C</b>	<b>500 °C</b>	<b>600 °C</b>	<b>700 °C</b>	<b>870 °C</b>	<b>TD</b>	<b>Pyr</b>	<b>Total</b>
Nonanal	69252	0	0	0	0	69252	0	69252
6,10,14-trimethyl-2-pentadecanone	800295	0	0	0	0	800295	0	800295
<b>Total</b>	869547	0	0	0	0	869547	0	869547
<b>Sugars</b>								
levoglucosan	45749	0	0	0	0	45749	0	45749
levoglucosenone	371649	0	0	0	0	371649	0	371649
<b>Total</b>	417398	0	0	0	0	417398	0	417398
<b>Phthalates</b>								
Dibutyl phthalate	200854	0	0	0	0	200854	0	200854
Diosobutyl phthalate	265935	0	0	0	0	265935	0	265935
Dioctyl phthalate	144571	0	0	0	0	144571	0	144571
phthalic anhydride	27061	8642	0	0	0	27061	8642	35703
1-isobenzofuranone	20943	0	0	0	0	20943	0	20943
<b>Total</b>	659364	8642	0	0	0	659364	8642	668006
<b>Nitrogen Based</b>								
Diethyltoluamide	35165	0	0	0	0	35165	0	35165

Table G2. Compounds identified by TD-Pyr-GC-MS during POLCAST campaign week 13

<b>Week 13</b>								
<b>Alkanes</b>								
<b>Compound</b>	<b>300 °C</b>	<b>500 °C</b>	<b>600 °C</b>	<b>700 °C</b>	<b>870 °C</b>	<b>TD</b>	<b>Pyr</b>	<b>Total</b>
C <sub>9</sub>	0	0	0	0	0	0	0	0
C <sub>10</sub>	0	0	0	0	0	0	0	0
C <sub>11</sub>	0	9502	10558	0	0	0	20060	20060
C <sub>12</sub>	0	13177	8670	0	0	0	21846	21846
C <sub>13</sub>	0	12031	10916	0	0	0	22947	22947
C <sub>14</sub>	0	13476	12367	0	0	0	25844	25844
C <sub>15</sub>	0	11258	14595	0	0	0	25853	25853
C <sub>16</sub>	0	9047	8068	0	0	0	17115	17115
C <sub>17</sub>	0	15019	6400	0	0	0	21419	21419
C <sub>18</sub>	0	8419	4861	0	0	0	13280	13280
C <sub>19</sub>	0	11070	7246	0	0	0	18316	18316
C <sub>20</sub>	0	8331	8247	0	0	0	16578	16578
C <sub>21</sub>	19462	9569	6124	0	0	19462	15693	35155
C <sub>22</sub>	31225	17775	6059	0	0	31225	23834	55059
C <sub>23</sub>	106732	16149	5328	0	0	106732	21477	128209
C <sub>24</sub>	83722	22744	5694	0	0	83722	28438	112160
C <sub>25</sub>	307702	15968	4190	0	0	307702	20157	327859
C <sub>26</sub>	135235	26662	5902	0	0	135235	32564	167799
C <sub>27</sub>	359342	20246	0	0	0	359342	20246	379588
C <sub>28</sub>	146877	13890	0	0	0	146877	13890	160767
C <sub>29</sub>	725672	20409	0	0	0	725672	20409	746081
C <sub>30</sub>	49197	5874	0	0	0	49197	5874	55071
C <sub>31</sub>	545471	11797	0	0	0	545471	11797	557268
C <sub>32</sub>	21547	0	0	0	0	21547	0	21547
C <sub>33</sub>	27592	0	0	0	0	27592	0	27592
C <sub>34</sub>	0	0	0	0	0	0	0	0
<b>Total</b>	<b>2559776</b>	<b>292412</b>	<b>125225</b>	<b>0</b>	<b>0</b>	<b>2559776</b>	<b>417637</b>	<b>2977413</b>

Table G2 cont.

<b>Week 13</b>								
<b>Alkenes</b>								
<b>Compound</b>	<b>300 °C</b>	<b>500 °C</b>	<b>600 °C</b>	<b>700 °C</b>	<b>870 °C</b>	<b>TD</b>	<b>Pyr</b>	<b>Total</b>
C <sub>9</sub>	0	0	0	0	0	0	0	0
C <sub>10</sub>	0	0	0	0	0	0	0	0
C <sub>11</sub>	0	0	32963	0	0	0	32963	32963
C <sub>12</sub>	0	25871	24285	0	0	0	50156	50156
C <sub>13</sub>	0	15944	27544	0	0	0	43487	43487
C <sub>14</sub>	0	16955	27405	0	0	0	44360	44360
C <sub>15</sub>	0	20799	21949	0	0	0	42747	42747
C <sub>16</sub>	0	19801	13279	0	0	0	33079	33079
C <sub>17</sub>	0	12777	11416	0	0	0	24192	24192
C <sub>18</sub>	0	11011	14019	0	0	0	25030	25030
C <sub>19</sub>	0	17423	10311	0	0	0	27734	27734
C <sub>20</sub>	0	10400	9529	0	0	0	19929	19929
C <sub>21</sub>	0	14796	0	0	0	0	14796	14796
C <sub>22</sub>	0	11568	0	0	0	0	11568	11568
C <sub>23</sub>	0	0	0	0	0	0	0	0
<b>Total</b>	0	177342	192699	0	0	0	370041	370041

<b>Acids &amp; Esters</b>								
C <sub>16</sub> FA	82260	0	0	0	0	82260	0	82260
C <sub>18</sub> FA	0	0	0	0	0	0	0	0
C <sub>16</sub> FAME	61385	0	0	0	0	61385	0	61385
C <sub>17</sub> FAME	5249	0	0	0	0	5249	0	5249
C <sub>18</sub> FAME	54835	0	0	0	0	54835	0	54835
C <sub>19</sub> FAME	0	0	0	0	0	0	0	0
C <sub>20</sub> FAME	7215	0	0	0	0	7215	0	7215
C <sub>21</sub> FAME	0	0	0	0	0	0	0	0
C <sub>22</sub> FAME	19186	0	0	0	0	19186	0	19186
C <sub>23</sub> FAME	4260	0	0	0	0	4260	0	4260
C <sub>24</sub> FAME	24678	0	0	0	0	24678	0	24678
C <sub>25</sub> FAME	0	0	0	0	0	0	0	0
C <sub>26</sub> FAME	8438	0	0	0	0	8438	0	8438
C <sub>27</sub> FAME	0	0	0	0	0	0	0	0
C <sub>28</sub> FAME	0	0	0	0	0	0	0	0
<b>Total</b>	267508	0	0	0	0	267508	0	267508

Table G2 cont.

<b>Week 13</b>								
<b>PAHs</b>								
<b>Compound</b>	<b>300 °C</b>	<b>500 °C</b>	<b>600 °C</b>	<b>700 °C</b>	<b>870 °C</b>	<b>TD</b>	<b>Pyr</b>	<b>Total</b>
Naphthalene	21617	20516	62648	67448	62314	21617	212927	234544
1-Methylnaphthalene	10808	10248	33234	23150	0	10808	66631	77440
2-Methylnaphthalene	8163	9918	25232	25436	0	8163	60586	68749
Biphenyl	14510	7297	17660	0	0	14510	24956	39466
Dimethylnaphthalene	0	3848	10152	0	0	0	14000	14000
Dimethylnaphthalene 2	0	5716	14719	0	0	0	20435	20435
Dimethylnaphthalene 3	0	5715	14513	0	0	0	20228	20228
Dimethylnaphthalene 4	0	2873	11010	0	0	0	13883	13883
Acenaphthylene	0	0	12081	0	0	0	12081	12081
Fluorene	0	6640	17647	0	0	0	24287	24287
Phenanthrene	30745	7525	11922	0	0	30745	19447	50192
Anthracene	9313	3078	7759	0	0	9313	10838	20151
Fluoranthene	24053	0	0	0	0	24053	0	24053
Pyrene	27873	0	0	0	0	27873	0	27873
<b>Total</b>	147081	83375	238577	116035	62314	147081	500301	647382
<b>BTEX</b>								
Benzene	0	74963	174584	234530	189298	0	673375	673375
Toluene	0	180577	471871	308108	129971	0	1090527	1090527
Xylene	0	109933	169116	107881	0	0	386930	386930
Ethylbenzene	0	32735	58347	27661	0	0	118742	118742
<b>Total</b>	0	398207	873918	678180	319269	0	2269574	2269574

Table G2 cont.

<b>Week 13</b>								
<b>Alkylbenzenes</b>								
<b>Compound</b>	<b>300 °C</b>	<b>500 °C</b>	<b>600 °C</b>	<b>700 °C</b>	<b>870 °C</b>	<b>TD</b>	<b>Pyr</b>	<b>Total</b>
C <sub>3</sub> benzene	0	0	18553	0	0	0	18553	18553
C <sub>3</sub> benzene	0	0	33045	0	0	0	33045	33045
C <sub>3</sub> benzene	0	0	34347	0	0	0	34347	34347
C <sub>3</sub> benzene	0	0	27570	0	0	0	27570	27570
C <sub>3</sub> benzene	0	31265	48448	0	0	0	79713	79713
C <sub>3</sub> benzene	0	19835	21236	0	0	0	41070	41070
C <sub>4</sub> benzene	0	13058	17801	0	0	0	30859	30859
C <sub>5</sub> benzene	0	14527	15296	0	0	0	29823	29823
C <sub>6</sub> benzene	0	9695	13298	0	0	0	22993	22993
C <sub>7</sub> benzene	0	0	9737	0	0	0	9737	9737
C <sub>8</sub> benzene	0	0	6578	0	0	0	6578	6578
C <sub>9</sub> benzene	0	0	4346	0	0	0	4346	4346
C <sub>10</sub> benzene	0	0	5926	0	0	0	5926	5926
Styrene	0	70330	91715	0	0	0	162045	162045
<b>Total</b>	0	158710	347895	0	0	0	506605	506605
<b>Phenols</b>								
Phenol	0	64715	87228	0	0	0	151943	151943
Methyl phenol	18858	30832	42024	0	0	18858	72856	91714
Methyl phenol	43488	59263	60841	0	0	43488	120105	163593
C <sub>2</sub> phenol	0	0	0	0	0	0	0	0
C <sub>2</sub> phenol	0	15010	16201	0	0	0	31210	31210
C <sub>2</sub> phenol	0	6633	0	0	0	0	6633	6633
C <sub>2</sub> phenol	0	7245	10504	0	0	0	17749	17749
Butylated hydroxytoluene	24841	0	0	0	0	24841	0	24841
<b>Total</b>	87187	183699	216797	0	0	87187	400495	487683

Table G2 cont.

<b>Week 13</b>								
<b>Ketones/Aldehydes</b>								
<b>Compound</b>	<b>300 °C</b>	<b>500 °C</b>	<b>600 °C</b>	<b>700 °C</b>	<b>870 °C</b>	<b>TD</b>	<b>Pyr</b>	<b>Total</b>
Nonanal	107722	0	0	0	0	107722	0	107722
6,10,14-trimethyl-2-pentadecanone	1247540	0	0	0	0	1247540	0	1247540
<b>Total</b>	1355262	0	0	0	0	1355262	0	1355262
<b>Sugars</b>								
levoglucosan	0	0	0	0	0	0	0	0
levoglucosenone	457991	17961	0	0	0	457991	17961	475952
<b>Total</b>	457991	17961	0	0	0	457991	17961	475952
<b>Phthalates</b>								
Dibutyl phthalate	355130	0	0	0	0	355130	0	355130
Diosobutyl phthalate	432363	0	0	0	0	432363	0	432363
Diocetyl phthalate	189486	0	0	0	0	189486	0	189486
phthalic anhydride	31000	15048	0	0	0	31000	15048	46049
1-isobenzofuranone	15721	0	0	0	0	15721	0	15721
<b>Total</b>	1023701	15048	0	0	0	1023701	15048	1038749
<b>Nitrogen Based</b>								
Diethyltoluamide	63960	0	0	0	0	63960	0	63960

Table G3. Compounds identified by TD-Pyr-GC-MS during POLCAST campaign week 14

<b>Week 14</b>								
<b>Alkanes</b>								
<b>Compound</b>	<b>300 °C</b>	<b>500 °C</b>	<b>600 °C</b>	<b>700 °C</b>	<b>870 °C</b>	<b>TD</b>	<b>Pyr</b>	<b>Total</b>
C <sub>9</sub>	0	0	0	0	0	0	0	0
C <sub>10</sub>	0	0	0	0	0	0	0	0
C <sub>11</sub>	0	0	8703	0	0	0	8703	8703
C <sub>12</sub>	0	10431	8067	0	0	0	18498	18498
C <sub>13</sub>	0	8206	7457	0	0	0	15662	15662
C <sub>14</sub>	0	13268	9088	0	0	0	22356	22356
C <sub>15</sub>	0	12346	8302	0	0	0	20648	20648
C <sub>16</sub>	0	6591	5374	0	0	0	11965	11965
C <sub>17</sub>	0	8629	5956	0	0	0	14585	14585
C <sub>18</sub>	0	4954	4855	0	0	0	9809	9809
C <sub>19</sub>	0	7022	5547	0	0	0	12569	12569
C <sub>20</sub>	0	7304	3039	0	0	0	10343	10343
C <sub>21</sub>	0	7344	0	0	0	0	7344	7344
C <sub>22</sub>	20167	4278	0	0	0	20167	4278	24445
C <sub>23</sub>	95979	9016	0	0	0	95979	9016	104995
C <sub>24</sub>	64145	7688	0	0	0	64145	7688	71833
C <sub>25</sub>	183917	7494	0	0	0	183917	7494	191411
C <sub>26</sub>	89118	10842	0	0	0	89118	10842	99960
C <sub>27</sub>	192868	6305	0	0	0	192868	6305	199173
C <sub>28</sub>	59774	0	0	0	0	59774	0	59774
C <sub>29</sub>	271865	0	0	0	0	271865	0	271865
C <sub>30</sub>	34210	0	0	0	0	34210	0	34210
C <sub>31</sub>	192442	0	0	0	0	192442	0	192442
C <sub>32</sub>	10157	0	0	0	0	10157	0	10157
C <sub>33</sub>	14856	0	0	0	0	14856	0	14856
C <sub>34</sub>	0	0	0	0	0	0	0	0
<b>Total</b>	1229498	131719	66386	0	0	1229498	198105	1427602

Table G3 cont.

<b>Week 14</b>								
<b>Alkenes</b>								
<b>Compound</b>	<b>300 °C</b>	<b>500 °C</b>	<b>600 °C</b>	<b>700 °C</b>	<b>870 °C</b>	<b>TD</b>	<b>Pyr</b>	<b>Total</b>
C <sub>9</sub>	0	0	0	0	0	0	0	0
C <sub>10</sub>	0	0	0	0	0	0	0	0
C <sub>11</sub>	0	0	25776	0	0	0	25776	25776
C <sub>12</sub>	0	17556	18675	0	0	0	36231	36231
C <sub>13</sub>	0	14085	20772	0	0	0	34858	34858
C <sub>14</sub>	0	19807	18646	0	0	0	38453	38453
C <sub>15</sub>	0	17093	17757	0	0	0	34850	34850
C <sub>16</sub>	0	15623	13969	0	0	0	29592	29592
C <sub>17</sub>	0	9872	10089	0	0	0	19961	19961
C <sub>18</sub>	0	9434	10148	0	0	0	19582	19582
C <sub>19</sub>	0	6186	0	0	0	0	6186	6186
C <sub>20</sub>	0	6974	0	0	0	0	6974	6974
C <sub>21</sub>	0	0	0	0	0	0	0	0
<b>Total</b>	0	116630	135833	0	0	0	252463	252463
<b>Acids &amp; Esters</b>								
C <sub>16</sub> FA	91354	0	0	0	0	91354	0	91354
C <sub>18</sub> FA	19202	0	0	0	0	19202	0	19202
C <sub>16</sub> FAME	59449	0	0	0	0	59449	0	59449
C <sub>17</sub> FAME	0	0	0	0	0	0	0	0
C <sub>18</sub> FAME	49509	0	0	0	0	49509	0	49509
C <sub>19</sub> FAME	0	0	0	0	0	0	0	0
C <sub>20</sub> FAME	3149	0	0	0	0	3149	0	3149
C <sub>21</sub> FAME	0	0	0	0	0	0	0	0
C <sub>22</sub> FAME	9557	0	0	0	0	9557	0	9557
C <sub>23</sub> FAME	3442	0	0	0	0	3442	0	3442
C <sub>24</sub> FAME	9325	0	0	0	0	9325	0	9325
C <sub>25</sub> FAME	0	0	0	0	0	0	0	0
C <sub>26</sub> FAME	4958	0	0	0	0	4958	0	4958
C <sub>27</sub> FAME	0	0	0	0	0	0	0	0
C <sub>28</sub> FAME	0	0	0	0	0	0	0	0
<b>Total</b>	249946	0	0	0	0	249946	0	249946



Table G3 cont.

<b>Week 14</b>								
<b>PAHs</b>								
<b>Compound</b>	<b>300 °C</b>	<b>500 °C</b>	<b>600 °C</b>	<b>700 °C</b>	<b>870 °C</b>	<b>TD</b>	<b>Pyr</b>	<b>Total</b>
Naphthalene	25667	20348	64079	41510	0	25667	125937	151604
1-Methylnaphthalene	9622	8076	29255	9927	0	9622	47258	56879
2-Methylnaphthalene	7886	7162	22309	17431	0	7886	46902	54788
Biphenyl	13321	7916	9864	0	0	13321	17781	31102
Dimethylnaphthalene	0	0	11608	0	0	0	11608	11608
Dimethylnaphthalene 2	0	0	12943	0	0	0	12943	12943
Dimethylnaphthalene 3	0	0	9704	0	0	0	9704	9704
Dimethylnaphthalene 4	0	0	11414	0	0	0	11414	11414
Acenaphthylene	0	0	0	0	0	0	0	0
Fluorene	0	0	15861	4745	0	0	20606	20606
Phenanthrene	33312	0	0	0	0	33312	0	33312
Anthracene	12593	0	0	0	0	12593	0	12593
Fluoranthene	25364	0	4122	0	0	25364	4122	29486
Pyrene	27249	0	4827	0	0	27249	4827	32076
<b>Total</b>	155012	43502	195986	73613	0	155012	313101	468113
<b>BTEX</b>								
Benzene	0	0	199301	196439	90188	0	485928	485928
Toluene	0	191854	247900	242210	61111	0	743075	743075
Xylene	0	62801	134149	68738	0	0	265688	265688
Ethylbenzene	0	27806	35155	21609	0	0	84571	84571
<b>Total</b>	0	282461	616505	528997	151299	0	1579262	1579262

Table G3 cont.

<b>Week 14</b>								
<b>Alkylbenzenes</b>								
<b>Compound</b>	<b>300 °C</b>	<b>500 °C</b>	<b>600 °C</b>	<b>700 °C</b>	<b>870 °C</b>	<b>TD</b>	<b>Pyr</b>	<b>Total</b>
C <sub>3</sub> benzene	0	0	14216	0	0	0	14216	14216
C <sub>3</sub> benzene	0	0	0	0	0	0	0	0
C <sub>3</sub> benzene	0	0	0	0	0	0	0	0
C <sub>3</sub> benzene	0	0	0	0	0	0	0	0
C <sub>3</sub> benzene	0	31876	44959	19338	0	0	96173	96173
C <sub>3</sub> benzene	0	14787	24793	0	0	0	39579	39579
C <sub>4</sub> benzene	0	0	0	0	0	0	0	0
C <sub>5</sub> benzene	0	11908	11935	0	0	0	23843	23843
C <sub>6</sub> benzene	0	10672	8308	0	0	0	18980	18980
C <sub>7</sub> benzene	0	9785	4002	0	0	0	13787	13787
C <sub>8</sub> benzene	0	7462	6271	0	0	0	13732	13732
C <sub>9</sub> benzene	0	5358	7378	0	0	0	12736	12736
C <sub>10</sub> benzene	0	10402	5936	0	0	0	16337	16337
C <sub>11</sub> benzene	0	4598	4206	0	0	0	8804	8804
C <sub>12</sub> benzene	0	5906	4199	0	0	0	10105	10105
Styrene	0	88771	83650	0	0	0	172421	172421
<b>Total</b>	0	201524	219851	19338	0	0	440713	440713
<b>Phenols</b>								
Phenol	0	68203	81486	0	0	0	149688	149688
Methyl phenol	20079	31633	43180	0	0	20079	74813	94892
Methyl phenol	40687	51103	38196	0	0	40687	89299	129986
C <sub>2</sub> phenol	0	0	0	0	0	0	0	0
C <sub>2</sub> phenol	0	0	0	0	0	0	0	0
C <sub>2</sub> phenol	0	0	0	0	0	0	0	0
C <sub>2</sub> phenol	0	0	0	0	0	0	0	0
Butylated hydroxytoluene	9346	0	0	0	0	9346	0	9346
<b>Total</b>	70112	150938	162862	0	0	70112	313800	383913

Table G3 cont.

<b>Week 14</b>								
<b>Ketones/Aldehydes</b>								
<b>Compound</b>	<b>300 °C</b>	<b>500 °C</b>	<b>600 °C</b>	<b>700 °C</b>	<b>870 °C</b>	<b>TD</b>	<b>Pyr</b>	<b>Total</b>
Nonanal	136040	0	0	0	0	136040	0	136040
6,10,14-trimethyl-2-pentadecanone	344244	0	0	0	0	344244	0	344244
<b>Total</b>	480284	0	0	0	0	480284	0	480284
<b>Sugars</b>								
levoglucosan	0	0	0	0	0	0	0	0
levoglucosenone	235922	0	0	0	0	235922	0	235922
<b>Total</b>	235922	0	0	0	0	235922	0	235922
<b>Phthalates</b>								
Dibutyl phthalate	223440	0	0	0	0	223440	0	223440
Diosobutyl phthalate	270629	0	0	0	0	270629	0	270629
Diocetyl phthalate	93774	0	0	0	0	93774	0	93774
phthalic anhydride	19863	9343	0	0	0	19863	9343	29206
1-isobenzofuranone	13318	0	0	0	0	13318	0	13318
<b>Total</b>	621025	9343	0	0	0	621025	9343	630367
<b>Nitrogen Based</b>								
Diethyltoluamide	32910	0	0	0	0	32910	0	32910

Table G4. Compounds identified by TD-Pyr-GC-MS during POLCAST campaign week 15

<b>Week 15</b>								
<b>Alkanes</b>								
<b>Compound</b>	<b>300 °C</b>	<b>500 °C</b>	<b>600 °C</b>	<b>700 °C</b>	<b>870 °C</b>	<b>TD</b>	<b>Pyr</b>	<b>Total</b>
C <sub>9</sub>	0	0	0	0	0	0	0	0
C <sub>10</sub>	0	0	36913	11078	0	0	47991	47991
C <sub>11</sub>	0	17409	27683	10169	0	0	55262	55262
C <sub>12</sub>	0	18928	34786	10628	0	0	64342	64342
C <sub>13</sub>	0	17230	36760	10796	0	0	64786	64786
C <sub>14</sub>	0	24386	34601	10294	0	0	69281	69281
C <sub>15</sub>	0	27584	36524	7326	0	0	71435	71435
C <sub>16</sub>	0	18923	31080	7064	0	0	57066	57066
C <sub>17</sub>	0	26987	29594	7892	0	0	64473	64473
C <sub>18</sub>	0	19027	29685	6295	0	0	55006	55006
C <sub>19</sub>	0	27648	28467	5915	0	0	62030	62030
C <sub>20</sub>	41523	20352	27036	4880	0	41523	52267	93790
C <sub>21</sub>	44738	26225	20851	3941	0	44738	51017	95755
C <sub>22</sub>	74645	23458	20809	4946	0	74645	49213	123857
C <sub>23</sub>	208177	48938	25062	3088	0	208177	77088	285265
C <sub>24</sub>	178137	52581	31337	3717	0	178137	87636	265773
C <sub>25</sub>	455019	45162	26710	4355	0	455019	76226	531245
C <sub>26</sub>	236882	67081	28967	4425	0	236882	100473	337355
C <sub>27</sub>	586826	31927	14155	0	0	586826	46082	632908
C <sub>28</sub>	166451	31116	11758	0	0	166451	42873	209324
C <sub>29</sub>	883152	33615	8616	0	0	883152	42232	925384
C <sub>30</sub>	64448	13867	4296	0	0	64448	18163	82611
C <sub>31</sub>	641635	20710	4220	0	0	641635	24930	666565
C <sub>32</sub>	47615	4966	0	0	0	47615	4966	52581
C <sub>33</sub>	63879	6685	0	0	0	63879	6685	70564
C <sub>34</sub>	11934	0	0	0	0	11934	0	11934
<b>Total</b>	<b>3705061</b>	<b>624805</b>	<b>549910</b>	<b>116808</b>	<b>0</b>	<b>3705061</b>	<b>1291523</b>	<b>4996584</b>

Table G4 cont.

<b>Week 15</b>								
<b>Alkenes</b>								
<b>Compound</b>	<b>300 °C</b>	<b>500 °C</b>	<b>600 °C</b>	<b>700 °C</b>	<b>870 °C</b>	<b>TD</b>	<b>Pyr</b>	<b>Total</b>
C <sub>9</sub>	0	0	46024	0	0	0	46024	46024
C <sub>10</sub>	0	0	84105	0	0	0	84105	84105
C <sub>11</sub>	0	0	51905	20821	0	0	72726	72726
C <sub>12</sub>	0	34369	52413	17119	0	0	103902	103902
C <sub>13</sub>	0	35710	54239	18833	0	0	108782	108782
C <sub>14</sub>	0	35608	49155	14383	0	0	99146	99146
C <sub>15</sub>	0	31204	42645	13174	0	0	87023	87023
C <sub>16</sub>	0	32661	39557	8831	0	0	81048	81048
C <sub>17</sub>	0	28409	32747	9022	0	0	70178	70178
C <sub>18</sub>	0	31471	30895	5967	0	0	68333	68333
C <sub>19</sub>	0	22028	25274	6975	0	0	54277	54277
C <sub>20</sub>	0	28567	20963	5958	0	0	55487	55487
C <sub>21</sub>	0	31569	18464	0	0	0	50033	50033
C <sub>22</sub>	0	29549	19015	0	0	0	48564	48564
C <sub>23</sub>	0	17010	0	0	0	0	17010	17010
<b>Total</b>	0	358155	567401	121082	0	0	1046638	1046638
<b>Acids &amp; Esters</b>								
C <sub>16</sub> FA	141565	0	0	0	0	141565	0	141565
C <sub>18</sub> FA	28378	0	0	0	0	28378	0	28378
C <sub>16</sub> FAME	96385	12177	0	0	0	96385	12177	108562
C <sub>17</sub> FAME	7972	0	0	0	0	7972	0	7972
C <sub>18</sub> FAME	51487	5747	0	0	0	51487	5747	57235
C <sub>19</sub> FAME	5230	0	0	0	0	5230	0	5230
C <sub>20</sub> FAME	21732	0	0	0	0	21732	0	21732
C <sub>21</sub> FAME	10283	0	0	0	0	10283	0	10283
C <sub>22</sub> FAME	90695	4733	0	0	0	90695	4733	95428
C <sub>23</sub> FAME	28871	0	0	0	0	28871	0	28871
C <sub>24</sub> FAME	129458	5556	0	0	0	129458	5556	135014
C <sub>25</sub> FAME	12850	0	0	0	0	12850	0	12850
C <sub>26</sub> FAME	68738	0	0	0	0	68738	0	68738
C <sub>27</sub> FAME	0	0	0	0	0	0	0	0
C <sub>28</sub> FAME	22704	0	0	0	0	22704	0	22704
<b>Total</b>	716350	28213	0	0	0	716350	28213	744563

Table G4 cont.

<b>Week 15</b>								
<b>PAHs</b>								
<b>Compound</b>	<b>300 °C</b>	<b>500 °C</b>	<b>600 °C</b>	<b>700 °C</b>	<b>870 °C</b>	<b>TD</b>	<b>Pyr</b>	<b>Total</b>
Naphthalene	26471	39586	160407	183658	57565	26471	441216	467687
1-Methylnaphthalene	7022	18524	89527	57437	0	7022	165487	172509
2-Methylnaphthalene	6270	20126	72474	47433	0	6270	140033	146302
Biphenyl	28805	17936	41599	34753	0	28805	94288	123093
Dimethylnaphthalene	0	0	29869	13113	0	0	42982	42982
Dimethylnaphthalene 2	0	0	22739	21816	0	0	44555	44555
Dimethylnaphthalene 3	0	0	27087	13700	0	0	40788	40788
Dimethylnaphthalene 4	0	0	12906	9348	0	0	22254	22254
Acenaphthylene	0	0	23669	20961	0	0	44630	44630
Fluorene	0	18975	67289	45366	0	0	131630	131630
Phenanthrene	27223	14849	38307	34703	0	27223	87860	115083
Anthracene	12675	4180	11133	8171	0	12675	23483	36157
Fluoranthene	20522	8141	18304	12383	0	20522	38828	59350
Pyrene	37161	7194	18137	16216	0	37161	41547	78709
<b>Total</b>	166148	149511	633448	519059	57565	166148	1359582	1525729
<b>BTEX</b>								
Benzene	0	124175	534134	506875	263340	0	1428524	1428524
Toluene	111117	545561	1126360	722857	209931	111117	2604709	2715826
Xylene	0	186520	391180	221348	46086	0	845134	845134
Ethylbenzene	0	52882	92977	48194	12274	0	206326	206326
<b>Total</b>	111117	909138	2144651	1499274	531631	111117	5084693	5195810

Table G4 cont.

<b>Week 15</b>								
<b>Alkylbenzenes</b>								
<b>Compound</b>	<b>300 °C</b>	<b>500 °C</b>	<b>600 °C</b>	<b>700 °C</b>	<b>870 °C</b>	<b>TD</b>	<b>Pyr</b>	<b>Total</b>
C <sub>3</sub> benzene	0	28117	49309	21648	0	0	99074	99074
C <sub>3</sub> benzene	0	54978	91309	23674	0	0	169960	169960
C <sub>3</sub> benzene	0	41702	77079	24448	0	0	143229	143229
C <sub>3</sub> benzene	0	29442	65746	18476	0	0	113664	113664
C <sub>3</sub> benzene	0	51375	108163	41319	0	0	200857	200857
C <sub>3</sub> benzene	0	37497	44627	23710	0	0	105834	105834
C <sub>4</sub> benzene	0	15093	29510	13845	0	0	58448	58448
C <sub>5</sub> benzene	0	15871	24245	11957	0	0	52073	52073
C <sub>6</sub> benzene	0	19688	22199	9890	0	0	51777	51777
C <sub>7</sub> benzene	0	25892	18061	7053	0	0	51006	51006
C <sub>8</sub> benzene	0	17048	16184	7521	0	0	40753	40753
C <sub>9</sub> benzene	0	13647	12381	6486	0	0	32513	32513
C <sub>10</sub> benzene	0	10548	11980	0	0	0	22528	22528
C <sub>11</sub> benzene	0	8861	8102	0	0	0	16963	16963
C <sub>12</sub> benzene	0	10742	11623	0	0	0	22365	22365
C <sub>13</sub> benzene	0	8686	6613	0	0	0	15299	15299
C <sub>14</sub> benzene	0	9029	6532	0	0	0	15561	15561
C <sub>15</sub> benzene	0	11297	4984	0	0	0	16280	16280
C <sub>16</sub> benzene	0	11565	0	0	0	0	11565	11565
C <sub>17</sub> benzene	0	7272	0	0	0	0	7272	7272
Styrene	0	155494	193369	70790	0	0	419653	419653
<b>Total</b>	0	598802	802016	280815	0	0	1681633	1681633
<b>Phenols</b>								
Phenol	128403	407540	436173	200720	0	128403	1044433	1172836
Methyl phenol	25188	108106	138641	30027	0	25188	276774	301962
Methyl phenol	52524	194779	216031	41425	0	52524	452235	504759
C <sub>2</sub> phenol	0	22649	30504	0	0	0	53153	53153
C <sub>2</sub> phenol	0	49311	64164	0	0	0	113475	113475
C <sub>2</sub> phenol	0	41325	50174	0	0	0	91499	91499
C <sub>2</sub> phenol	0	12784	21617	0	0	0	34401	34401
Butylated hydroxytoluene	18520	0	0	0	0	18520	0	18520
<b>Total</b>	224636	836494	957303	272172	0	224636	2065969	2290605

Table G4 cont.

<b>Week 15</b>								
<b>Ketones/Aldehydes</b>								
<b>Compound</b>	<b>300 °C</b>	<b>500 °C</b>	<b>600 °C</b>	<b>700 °C</b>	<b>870 °C</b>	<b>TD</b>	<b>Pyr</b>	<b>Total</b>
Nonanal	81714	0	0	0	0	81714	0	81714
6,10,14-trimethyl-2-pentadecanone	278936	0	0	0	0	278936	0	278936
<b>Total</b>	360650	0	0	0	0	360650	0	360650
<b>Sugars</b>								
levoglucosan	186212	0	0	0	0	186212	0	186212
levoglucosenone	230937	0	0	0	0	230937	0	230937
<b>Total</b>	417149	0	0	0	0	417149	0	417149
<b>Phthalates</b>								
Dibutyl phthalate	111899	0	0	0	0	111899	0	111899
Diosobutyl phthalate	200080	0	0	0	0	200080	0	200080
Diocetyl phthalate	194072	0	0	0	0	194072	0	194072
phthalic anhydride	40216	20805	0	0	0	40216	20805	61021
1-isobenzofuranone	35231	18866	0	0	0	35231	18866	54097
<b>Total</b>	581498	39671	0	0	0	581498	39671	621169
<b>Nitrogen Based</b>								
Diethyltoluamide	0	0	0	0	0	0	0	0



Table G5. Compounds identified by TD-Pyr-GC-MS during POLCAST campaign week 16

<b>Week 16</b>								
<b>Alkanes</b>								
<b>Compound</b>	<b>300 °C</b>	<b>500 °C</b>	<b>600 °C</b>	<b>700 °C</b>	<b>870 °C</b>	<b>TD</b>	<b>Pyr</b>	<b>Total</b>
C <sub>9</sub>	0	0	0	0	0	0	0	0
C <sub>10</sub>	0	0	0	0	0	0	0	0
C <sub>11</sub>	0	0	0	0	0	0	0	0
C <sub>12</sub>	0	0	0	0	0	0	0	0
C <sub>13</sub>	0	0	0	0	0	0	0	0
C <sub>14</sub>	0	0	0	0	0	0	0	0
C <sub>15</sub>	0	4003	0	0	0	0	4003	4003
C <sub>16</sub>	0	3726	0	0	0	0	3726	3726
C <sub>17</sub>	0	4932	0	0	0	0	4932	4932
C <sub>18</sub>	0	2623	0	0	0	0	2623	2623
C <sub>19</sub>	0	1996	0	0	0	0	1996	1996
C <sub>20</sub>	31081	0	0	0	0	31081	0	31081
C <sub>21</sub>	28043	0	0	0	0	28043	0	28043
C <sub>22</sub>	56322	0	0	0	0	56322	0	56322
C <sub>23</sub>	116840	0	0	0	0	116840	0	116840
C <sub>24</sub>	120761	0	0	0	0	120761	0	120761
C <sub>25</sub>	165939	0	0	0	0	165939	0	165939
C <sub>26</sub>	142002	0	0	0	0	142002	0	142002
C <sub>27</sub>	148128	0	0	0	0	148128	0	148128
C <sub>28</sub>	72723	0	0	0	0	72723	0	72723
C <sub>29</sub>	151784	0	0	0	0	151784	0	151784
C <sub>30</sub>	28779	0	0	0	0	28779	0	28779
C <sub>31</sub>	70633	0	0	0	0	70633	0	70633
C <sub>32</sub>	0	0	0	0	0	0	0	0
C <sub>33</sub>	0	0	0	0	0	0	0	0
C <sub>34</sub>	0	0	0	0	0	0	0	0
<b>Total</b>	1133035	17280	0	0	0	1133035	17280	1150315

Table G5 cont.

<b>Week 16</b>								
<b>Alkenes</b>								
<b>Compound</b>	<b>300 °C</b>	<b>500 °C</b>	<b>600 °C</b>	<b>700 °C</b>	<b>870 °C</b>	<b>TD</b>	<b>Pyr</b>	<b>Total</b>
C <sub>9</sub>	0	0	0	0	0	0	0	0
C <sub>10</sub>	0	0	0	0	0	0	0	0
C <sub>11</sub>	0	0	0	0	0	0	0	0
C <sub>12</sub>	0	15895	11619	0	0	0	27514	27514
C <sub>13</sub>	0	26105	8537	0	0	0	34642	34642
C <sub>14</sub>	0	10676	8234	0	0	0	18910	18910
C <sub>15</sub>	0	8349	6629	0	0	0	14978	14978
C <sub>16</sub>	0	7716	4724	0	0	0	12440	12440
C <sub>17</sub>	0	5494	0	0	0	0	5494	5494
C <sub>18</sub>	0	4520	0	0	0	0	4520	4520
C <sub>19</sub>	0	0	0	0	0	0	0	0
<b>Total</b>	0	78755	39743	0	0	0	118498	118498
<b>Acids &amp; Esters</b>								
C <sub>16</sub> FA	61268	0	0	0	0	61268	0	61268
C <sub>18</sub> FA	0	0	0	0	0	0	0	0
C <sub>16</sub> FAME	32786	0	0	0	0	32786	0	32786
C <sub>17</sub> FAME	0	0	0	0	0	0	0	0
C <sub>18</sub> FAME	32037	0	0	0	0	32037	0	32037
C <sub>19</sub> FAME	0	0	0	0	0	0	0	0
C <sub>20</sub> FAME	5267	0	0	0	0	5267	0	5267
C <sub>21</sub> FAME	0	0	0	0	0	0	0	0
C <sub>22</sub> FAME	15257	0	0	0	0	15257	0	15257
C <sub>23</sub> FAME	3148	0	0	0	0	3148	0	3148
C <sub>24</sub> FAME	11672	0	0	0	0	11672	0	11672
C <sub>25</sub> FAME	0	0	0	0	0	0	0	0
C <sub>26</sub> FAME	5128	0	0	0	0	5128	0	5128
C <sub>27</sub> FAME	0	0	0	0	0	0	0	0
C <sub>28</sub> FAME	0	0	0	0	0	0	0	0
<b>Total</b>	166563	0	0	0	0	166563	0	166563

Table G5 cont.

<b>Week 16</b>								
<b>PAHs</b>								
<b>Compound</b>	<b>300 °C</b>	<b>500 °C</b>	<b>600 °C</b>	<b>700 °C</b>	<b>870 °C</b>	<b>TD</b>	<b>Pyr</b>	<b>Total</b>
Naphthalene	17771	12154	29335	0	0	17771	41489	59260
1-Methylnaphthalene	7150	4855	13181	0	0	7150	18037	25187
2-Methylnaphthalene	6312	5300	12179	0	0	6312	17479	23790
Biphenyl	8830	5467	0	0	0	8830	5467	14297
Dimethylnaphthalene	0	0	0	0	0	0	0	0
Dimethylnaphthalene 2	0	0	0	0	0	0	0	0
Dimethylnaphthalene 3	0	0	0	0	0	0	0	0
Dimethylnaphthalene 4	0	0	0	0	0	0	0	0
Acenaphthylene	0	0	0	0	0	0	0	0
Fluorene	0	2364	7148	0	0	0	9511	9511
Phenanthrene	16721	0	0	0	0	16721	0	16721
Anthracene	8715	0	0	0	0	8715	0	8715
Fluoranthene	23244	0	0	0	0	23244	0	23244
Pyrene	27844	0	0	0	0	27844	0	27844
<b>Total</b>	116586	30140	61842	0	0	116586	91982	208568
<b>BTEX</b>								
Benzene	0	49226	102958	72726	84888	0	309797	309797
Toluene	0	101105	205406	112309	57543	0	476363	476363
Xylene	0	48262	67853	0	0	0	116115	116115
Ethylbenzene	0	18821	16858	0	0	0	35679	35679
<b>Total</b>	0	217413	393075	185035	142431	0	937954	937954

Table G5 cont.

<b>Week 16</b>								
<b>Alkylbenzenes</b>								
<b>Compound</b>	<b>300 °C</b>	<b>500 °C</b>	<b>600 °C</b>	<b>700 °C</b>	<b>870 °C</b>	<b>TD</b>	<b>Pyr</b>	<b>Total</b>
C <sub>3</sub> benzene	0	0	0	0	0	0	0	0
C <sub>3</sub> benzene	0	0	0	0	0	0	0	0
C <sub>3</sub> benzene	0	0	0	0	0	0	0	0
C <sub>3</sub> benzene	0	0	0	0	0	0	0	0
C <sub>3</sub> benzene	0	0	27436	0	0	0	27436	27436
C <sub>3</sub> benzene	0	0	0	0	0	0	0	0
<b>Total</b>	0	598802	802016	280815	0	0	1681633	1681633
<b>Phenols</b>								
Phenol	0	41970	0	0	0	0	41970	41970
Methyl phenol	23232	9877	0	0	0	23232	9877	33109
Methyl phenol	39077	22808	0	0	0	39077	22808	61885
C <sub>2</sub> phenol	0	0	0	0	0	0	0	0
C <sub>2</sub> phenol	0	0	0	0	0	0	0	0
C <sub>2</sub> phenol	0	0	0	0	0	0	0	0
C <sub>2</sub> phenol	0	0	0	0	0	0	0	0
Butylated hydroxytoluene	0	0	0	0	0	0	0	0
<b>Total</b>	62309	74655	0	0	0	62309	74655	136964
<b>Ketones/Aldehydes</b>								
Nonanal	45654	0	0	0	0	45654	0	45654
6,10,14-trimethyl-2-pentadecanone	159219	0	0	0	0	159219	0	159219
<b>Total</b>	204873	0	0	0	0	204873	0	204873
<b>Sugars</b>								
levoglucosan	0	0	0	0	0	0	0	0
levoglucosenone	729830	35443	0	0	0	729830	35443	765273
<b>Total</b>	729830	35443	0	0	0	729830	35443	765273

Table G5 cont.

<b>Week 16</b>								
<b>Phthalates</b>								
<b>Compound</b>	<b>300 °C</b>	<b>500 °C</b>	<b>600 °C</b>	<b>700 °C</b>	<b>870 °C</b>	<b>TD</b>	<b>Pyr</b>	<b>Total</b>
Dibutyl phthalate	103762	0	0	0	0	103762	0	103762
Diosobutyl phthalate	149805	0	0	0	0	149805	0	149805
Dioctyl phthalate	91854	0	0	0	0	91854	0	91854
phthalic anhydride	27554	0	0	0	0	27554	0	27554
1-isobenzofuranone	0	0	0	0	0	0	0	0
<b>Total</b>	<b>372975</b>	<b>0</b>	<b>0</b>	<b>0</b>	<b>0</b>	<b>372975</b>	<b>0</b>	<b>372975</b>
<b>Nitrogen Based</b>								
Diethyltoluamide	0	0	0	0	0	0	0	0

Table G6. Compounds identified by TD-Pyr-GC-MS during POLCAST campaign week 17

<b>Week 17</b>								
<b>Alkanes</b>								
<b>Compound</b>	<b>300 °C</b>	<b>500 °C</b>	<b>600 °C</b>	<b>700 °C</b>	<b>870 °C</b>	<b>TD</b>	<b>Pyr</b>	<b>Total</b>
C <sub>9</sub>	0	0	0	0	0	0	0	0
C <sub>10</sub>	0	0	0	0	0	0	0	0
C <sub>11</sub>	0	0	14630	0	0	0	14630	14630
C <sub>12</sub>	0	10159	11128	0	0	0	21288	21288
C <sub>13</sub>	0	16386	13764	4169	0	0	34319	34319
C <sub>14</sub>	0	14698	15963	3853	0	0	34514	34514
C <sub>15</sub>	0	17313	14818	4993	0	0	37123	37123
C <sub>16</sub>	0	14054	11613	1823	0	0	27491	27491
C <sub>17</sub>	0	15061	12078	2924	0	0	30062	30062
C <sub>18</sub>	0	12816	12137	2947	0	0	27900	27900
C <sub>19</sub>	0	10023	11622	1557	0	0	23202	23202
C <sub>20</sub>	0	16579	13918	0	0	0	30498	30498
C <sub>21</sub>	14344	15841	14058	0	0	14344	29899	44243
C <sub>22</sub>	46883	16930	9474	0	0	46883	26405	73288
C <sub>23</sub>	90119	13390	16568	0	0	90119	29958	120077
C <sub>24</sub>	132476	25127	11586	0	0	132476	36712	169188
C <sub>25</sub>	290013	19149	8177	0	0	290013	27326	317339
C <sub>26</sub>	207990	28203	11485	0	0	207990	39687	247677
C <sub>27</sub>	412925	16719	5067	0	0	412925	21786	434711
C <sub>28</sub>	147014	14054	5441	0	0	147014	19494	166508
C <sub>29</sub>	787030	17013	0	0	0	787030	17013	804043
C <sub>30</sub>	76770	9356	0	0	0	76770	9356	86126
C <sub>31</sub>	515923	8116	0	0	0	515923	8116	524039
C <sub>32</sub>	23583	0	0	0	0	23583	0	23583
C <sub>33</sub>	52225	0	0	0	0	52225	0	52225
C <sub>34</sub>	0	0	0	0	0	0	0	0
<b>Total</b>	2797295	310985	213528	22264	0	2797295	546778	3344073

Table G6 cont.

<b>Week 17</b>								
<b>Alkenes</b>								
<b>Compound</b>	<b>300 °C</b>	<b>500 °C</b>	<b>600 °C</b>	<b>700 °C</b>	<b>870 °C</b>	<b>TD</b>	<b>Pyr</b>	<b>Total</b>
C <sub>9</sub>	0	0	0	0	0	0	0	0
C <sub>10</sub>	0	0	0	0	0	0	0	0
C <sub>11</sub>	0	0	45694	17968	0	0	63663	63663
C <sub>12</sub>	0	25595	45271	11462	0	0	82328	82328
C <sub>13</sub>	0	29068	31485	12172	0	0	72725	72725
C <sub>14</sub>	0	32099	35425	7867	0	0	75391	75391
C <sub>15</sub>	0	29659	32681	9241	0	0	71581	71581
C <sub>16</sub>	0	31536	24343	6097	0	0	61976	61976
C <sub>17</sub>	0	21748	21572	3602	0	0	46922	46922
C <sub>18</sub>	0	18909	21234	0	0	0	40143	40143
C <sub>19</sub>	0	19397	17125	0	0	0	36522	36522
C <sub>20</sub>	0	16808	15231	0	0	0	32039	32039
C <sub>21</sub>	0	20765	19043	0	0	0	39808	39808
<b>Total</b>	0	245584	309104	68409	0	0	623097	623097
<b>Acids &amp; Esters</b>								
C <sub>16</sub> FA	144919	0	0	0	0	144919	0	144919
C <sub>18</sub> FA	19761	0	0	0	0	19761	0	19761
C <sub>16</sub> FAME	46564	0	0	0	0	46564	0	46564
C <sub>17</sub> FAME	0	0	0	0	0	0	0	0
C <sub>18</sub> FAME	18237	0	0	0	0	18237	0	18237
C <sub>19</sub> FAME	0	0	0	0	0	0	0	0
C <sub>20</sub> FAME	21558	0	0	0	0	21558	0	21558
C <sub>21</sub> FAME	7719	0	0	0	0	7719	0	7719
C <sub>22</sub> FAME	66775	0	0	0	0	66775	0	66775
C <sub>23</sub> FAME	34737	0	0	0	0	34737	0	34737
C <sub>24</sub> FAME	82996	0	0	0	0	82996	0	82996
C <sub>25</sub> FAME	6090	0	0	0	0	6090	0	6090
C <sub>26</sub> FAME	25044	0	0	0	0	25044	0	25044
C <sub>27</sub> FAME	0	0	0	0	0	0	0	0
C <sub>28</sub> FAME	10448	0	0	0	0	10448	0	10448
<b>Total</b>	484847	0	0	0	0	484847	0	484847

Table G6 cont.

<b>Week 17</b>								
<b>PAHs</b>								
<b>Compound</b>	<b>300 °C</b>	<b>500 °C</b>	<b>600 °C</b>	<b>700 °C</b>	<b>870 °C</b>	<b>TD</b>	<b>Pyr</b>	<b>Total</b>
Naphthalene	27826	26913	63889	81868	30977	27826	203647	231472
1-Methylnaphthalene	12394	11859	43972	36300	0	12394	92131	104525
2-Methylnaphthalene	6197	12667	36509	27325	0	6197	76501	82697
Biphenyl	11207	10207	16074	13281	0	11207	39562	50769
Dimethylnaphthalene	0	8487	20917	7321	0	0	36725	36725
Dimethylnaphthalene 2	0	6686	12801	9022	0	0	28509	28509
Dimethylnaphthalene 3	0	7382	17999	10413	0	0	35794	35794
Dimethylnaphthalene 4	0	8283	15384	5309	0	0	28977	28977
Acenaphthylene	0	0	14262	10714	0	0	24975	24975
Fluorene	0	12358	36829	23239	0	0	72426	72426
Phenanthrene	26581	12610	18262	18266	0	26581	49138	75719
Anthracene	10915	4562	10019	9029	0	10915	23610	34525
Fluoranthene	29093	0	8148	5363	0	29093	13511	42604
Pyrene	27441	0	8213	5093	0	27441	13305	40746
<b>Total</b>	151653	122013	323277	262544	30977	151653	738810	890463
<b>BTEX</b>								
Benzene	0	112097	182250	234935	158030	0	687312	687312
Toluene	0	285121	659161	375472	102187	0	1421941	1421941
Xylene	0	113605	218482	121033	0	0	453120	453120
Ethylbenzene	0	36493	69935	23479	0	0	129907	129907
<b>Total</b>	0	547316	1129828	754919	260217	0	2692280	2692280



Table G6 cont.

<b>Week 17</b>								
<b>Alkylbenzenes</b>								
<b>Compound</b>	<b>300 °C</b>	<b>500 °C</b>	<b>600 °C</b>	<b>700 °C</b>	<b>870 °C</b>	<b>TD</b>	<b>Pyr</b>	<b>Total</b>
C <sub>3</sub> benzene	0	10860	22256	0	0	0	33116	33116
C <sub>3</sub> benzene	0	35156	36505	0	0	0	71661	71661
C <sub>3</sub> benzene	0	27702	35311	0	0	0	63013	63013
C <sub>3</sub> benzene	0	16709	34124	15010	0	0	65843	65843
C <sub>3</sub> benzene	0	28609	53618	25771	0	0	107997	107997
C <sub>3</sub> benzene	0	19579	27906	11360	0	0	58845	58845
C <sub>4</sub> benzene	0	15985	26970	0	0	0	42955	42955
C <sub>5</sub> benzene	0	13882	33424	0	0	0	47306	47306
C <sub>6</sub> benzene	0	14986	15842	0	0	0	30828	30828
C <sub>7</sub> benzene	0	6662	12961	0	0	0	19623	19623
C <sub>8</sub> benzene	0	9205	9767	0	0	0	18972	18972
C <sub>9</sub> benzene	0	11286	7647	0	0	0	18933	18933
C <sub>10</sub> benzene	0	13525	9338	0	0	0	22863	22863
C <sub>11</sub> benzene	0	5262	4134	0	0	0	9396	9396
C <sub>12</sub> benzene	0	8824	5734	0	0	0	14558	14558
C <sub>13</sub> benzene	0	5873	3739	0	0	0	9612	9612
C <sub>14</sub> benzene	0	5000	0	0	0	0	5000	5000
C <sub>15</sub> benzene	0	4853	0	0	0	0	4853	4853
Styrene	0	87864	107362	48230	0	0	243457	243457
<b>Total</b>	0	341824	446637	100371	0	0	888832	888832
<b>Phenols</b>								
Phenol	0	243564	242008	136395	0	0	621967	621967
Methyl phenol	20053	60707	81308	28980	0	20053	170994	191047
Methyl phenol	48735	108601	123367	41414	0	48735	273382	322117
C <sub>2</sub> phenol	0	11855	13074	0	0	0	24929	24929
C <sub>2</sub> phenol	0	29214	31358	0	0	0	60572	60572
C <sub>2</sub> phenol	0	22832	29189	0	0	0	52022	52022
C <sub>2</sub> phenol	0	7347	12886	0	0	0	20233	20233
Butylated hydroxytoluene	591007	0	0	0	0	591007	0	591007
<b>Total</b>	659794	484120	533191	206789	0	659794	1224100	1883894

Table G6 cont.

<b>Week 17</b>								
<b>Ketones/Aldehydes</b>								
<b>Compound</b>	<b>300 °C</b>	<b>500 °C</b>	<b>600 °C</b>	<b>700 °C</b>	<b>870 °C</b>	<b>TD</b>	<b>Pyr</b>	<b>Total</b>
Nonanal	70361	0	0	0	0	70361	0	70361
6,10,14-trimethyl-2-pentadecanone	41531	0	0	0	0	41531	0	41531
<b>Total</b>	111893	0	0	0	0	111893	0	111893
<b>Sugars</b>								
levoglucosan	676491	0	0	0	0	676491	0	676491
levoglucosenone	241323	23516	0	0	0	241323	23516	264839
<b>Total</b>	917814	23516	0	0	0	917814	23516	941330
<b>Phthalates</b>								
Dibutyl phthalate	31398	0	0	0	0	31398	0	31398
Diosobutyl phthalate	29402	0	0	0	0	29402	0	29402
Diocetyl phthalate	173916	0	0	0	0	173916	0	173916
phthalic anhydride	70500	13862	0	0	0	70500	13862	84362
1-isobenzofuranone	28896	0	0	0	0	28896	0	28896
<b>Total</b>	334113	13862	0	0	0	334113	13862	347975
<b>Nitrogen Based</b>								
Diethyltoluamide	0	0	0	0	0	0	0	0

## Appendix H

### *TD-Pyr-GC-MS Normalized Data*

Table H1. TD-Pyr-GC-MS data normalized to its own week

Compound	Week 12			Week 13			Week 14		
	TD	Pyr	Total	TD	Pyr	Total	TD	Pyr	Total
n-Alkanes Odd	26.3	3.0	29.4	20.0	2.1	22.1	15.4	1.7	17.1
n-Alkanes Even	3.7	2.7	6.4	4.5	1.9	6.4	4.5	1.5	6.0
n-Alkenes	0.0	6.0	6.0	0.0	3.5	3.5	0.0	4.1	4.1
Acids & esters	3.2	0.0	3.2	2.6	0.0	2.6	4.0	0.0	4.0
PAHs	1.4	3.1	4.5	1.4	4.8	6.2	2.5	5.1	7.6
BTEX	0.0	19.7	19.7	0.0	21.7	21.7	0.0	25.5	25.5
Alkylbenzenes	0.0	5.9	5.9	0.0	4.8	4.8	0.0	7.1	7.1
Phenol	0.6	4.1	4.6	0.8	3.8	4.7	1.1	5.1	6.2
Ketone/aldehyde	8.9	0.0	8.9	13.0	0.0	13.0	7.8	0.0	7.8
Sugars	4.3	0.0	4.3	4.4	0.2	4.6	3.8	0.0	3.8
Phthalates	6.7	0.1	6.8	9.8	0.1	9.9	10.0	0.2	10.2
Nitrogen Based	0.4	0.0	0.4	0.6	0.0	0.6	0.5	0.0	0.5
<b>Total</b>	55.3	44.7	100.0	57.0	43.0	100.0	49.7	50.3	100.0

Compound	Week 15			Week 16			Week 17		
	TD	Pyr	Total	TD	Pyr	Total	TD	Pyr	Total
n-Alkanes Odd	15.3	3.4	18.7	16.2	0.3	16.5	17.7	2.2	20.0
n-Alkanes Even	4.4	3.4	7.8	10.7	0.2	10.9	5.2	2.2	7.4
n-Alkenes	0.0	5.5	5.5	0.0	2.8	2.8	0.0	5.1	5.1
Acids & esters	3.8	0.1	3.9	4.0	0.0	4.0	4.0	0.0	4.0
PAHs	0.9	7.2	8.1	2.8	2.2	5.0	1.2	6.1	7.3
BTEX	0.6	26.9	27.5	0.0	22.3	22.3	0.0	22.1	22.1
Alkylbenzenes	0.0	8.9	8.9	0.0	3.3	3.3	0.0	7.3	7.3
Phenol	1.2	10.9	12.1	1.5	1.8	3.3	5.4	10.0	15.4
Ketone/aldehyde	1.9	0.0	1.9	4.9	0.0	4.9	0.9	0.0	0.9
Sugars	2.2	0.0	2.2	17.4	0.8	18.2	7.5	0.2	7.7
Phthalates	3.1	0.2	3.3	8.9	0.0	8.9	2.7	0.1	2.9
Nitrogen Based	0.0	0.0	0.0	0.0	0.0	0.0	0.0	0.0	0.0
<b>Total</b>	33.3	66.7	100.0	66.3	33.7	100.0	44.7	55.3	100.0

Table H2. TD-Pyr-GC-MS data normalized to sample week 15 (most abundant week)

Compound	Week 12			Week 13			Week 14		
	TD	Pyr	Total	TD	Pyr	Total	TD	Pyr	Total
n-Alkanes Odd	13.7	1.6	15.3	11.1	1.2	12.2	5.0	0.5	5.6
n-Alkanes Even	1.9	1.4	3.3	2.5	1.1	3.5	1.5	0.5	2.0
n-Alkenes	0.0	3.1	3.1	0.0	2.0	2.0	0.0	1.3	1.3
Acids & Esters	1.6	0.0	1.6	1.4	0.0	1.4	1.3	0.0	1.3
PAHs	0.7	1.6	2.3	0.8	2.6	3.4	0.8	1.7	2.5
BTEX	0.0	10.3	10.3	0.0	12.0	12.0	0.0	8.4	8.4
Alkylbenzenes	0.0	3.1	3.1	0.0	2.7	2.7	0.0	2.3	2.3
Phenols	0.3	2.1	2.4	0.5	2.1	2.6	0.4	1.7	2.0
Ketone/aldehyde	4.6	0.0	4.6	7.2	0.0	7.2	2.5	0.0	2.5
Sugars	2.2	0.0	2.2	2.4	0.1	2.5	1.2	0.0	1.2
Phthalates	3.5	0.0	3.5	5.4	0.1	5.5	3.3	0.0	3.3
Nitrogen Based	0.2	0.0	0.2	0.3	0.0	0.3	0.2	0.0	0.2
<b>Total</b>	<b>28.8</b>	<b>23.2</b>	<b>52.0</b>	<b>31.6</b>	<b>23.8</b>	<b>55.4</b>	<b>16.3</b>	<b>16.5</b>	<b>32.7</b>

Compound	Week 15			Week 16			Week 17		
	TD	Pyr	Total	TD	Pyr	Total	TD	Pyr	Total
n-Alkanes Odd	15.3	3.4	18.7	3.6	0.1	3.7	11.5	1.4	12.9
n-Alkanes Even	4.4	3.4	7.8	2.4	0.0	2.4	3.4	1.4	4.8
n-Alkenes	0.0	5.5	5.5	0.0	0.6	0.6	0.0	3.3	3.3
Acids & Esters	3.8	0.1	3.9	0.9	0.0	0.9	2.6	0.0	2.6
PAHs	0.9	7.2	8.1	0.6	0.5	1.1	0.8	3.9	4.7
BTEX	0.6	26.9	27.5	0.0	5.0	5.0	0.0	14.3	14.3
Alkylbenzenes	0.0	8.9	8.9	0.0	0.7	0.7	0.0	4.7	4.7
Phenols	1.2	10.9	12.1	0.3	0.4	0.7	3.5	6.5	10.0
Ketone/aldehyde	1.9	0.0	1.9	1.1	0.0	1.1	0.6	0.0	0.6
Sugars	2.2	0.0	2.2	3.9	0.2	4.1	4.9	0.1	5.0
Phthalates	3.1	0.2	3.3	2.0	0.0	2.0	1.8	0.1	1.8
Nitrogen Based	0.0	0.0	0.0	0.0	0.0	0.0	0.0	0.0	0.0
<b>Total</b>	<b>33.3</b>	<b>66.7</b>	<b>100.0</b>	<b>14.8</b>	<b>7.5</b>	<b>22.3</b>	<b>28.9</b>	<b>35.8</b>	<b>64.7</b>

Table H3. TD-Pyr-GC-MS data normalized to TD and Pyr fractions

Compound	Week 12			Week 13			Week 14		
	TD	Pyr	Total	TD	Pyr	Total	TD	Pyr	Total
n-Alkanes Odd	47.5	6.8	29.4	35.1	4.9	22.1	31.0	3.3	17.1
n-Alkanes Even	6.7	6.1	6.4	7.8	4.4	6.4	9.0	3.1	6.0
n-Alkenes	0.0	13.4	6.0	0.0	8.2	3.5	0.0	8.1	4.1
Acids & Esters	5.7	0.0	3.2	4.5	0.0	2.6	8.1	0.0	4.0
PAHs	2.5	7.0	4.5	2.5	11.1	6.2	5.0	10.1	7.6
BTEX	0.0	44.2	19.7	0.0	50.5	21.7	0.0	50.8	25.5
Alkylbenzenes	0.0	13.3	5.9	0.0	11.3	4.8	0.0	14.2	7.1
Phenols	1.0	9.1	4.6	1.5	8.9	4.7	2.3	10.1	6.2
Ketone/aldehyde	16.0	0.0	8.9	22.7	0.0	13.0	15.6	0.0	7.8
Sugars	7.7	0.0	4.3	7.7	0.4	4.6	7.7	0.0	3.8
Phthalates	12.1	0.2	6.8	17.2	0.3	9.9	20.2	0.3	10.2
Nitrogen Based	0.6	0.0	0.4	1.1	0.0	0.6	1.1	0.0	0.5
<b>Total</b>	100.0	100.0	100.0	100.0	100.0	100.0	100.0	100.0	100.0

Compound	Week 12			Week 13			Week 14		
	TD	Pyr	Total	TD	Pyr	Total	TD	Pyr	Total
n-Alkanes Odd	45.9	5.1	18.7	24.5	0.8	16.5	39.6	4.1	20.0
n-Alkanes Even	13.1	5.2	7.8	16.2	0.4	10.9	11.6	4.0	7.4
n-Alkenes	0.0	8.3	5.5	0.0	8.4	2.8	0.0	9.2	5.1
Acids & Esters	11.4	0.2	3.9	6.0	0.0	4.0	8.9	0.0	4.0
PAHs	2.6	10.8	8.1	4.2	6.5	5.0	2.8	10.9	7.3
BTEX	1.8	40.4	27.5	0.0	66.2	22.3	0.0	39.9	22.1
Alkylbenzenes	0.0	13.3	8.9	0.0	9.9	3.3	0.0	13.2	7.3
Phenols	3.6	16.4	12.1	2.2	5.3	3.3	12.1	18.1	15.4
Ketone/aldehyde	5.7	0.0	1.9	7.4	0.0	4.9	2.1	0.0	0.9
Sugars	6.6	0.0	2.2	26.2	2.5	18.2	16.8	0.3	7.7
Phthalates	9.3	0.3	3.3	13.4	0.0	8.9	6.1	0.2	2.9
Nitrogen Based	0.0	0.0	0.0	0.0	0.0	0.0	0.0	0.0	0.0
<b>Total</b>	100.0	100.0	100.0	100.0	100.0	100.0	100.0	100.0	100.0

## REFERENCES

1. Kushta, J.; Kallos, G.; Astitha, M.; Solomos, S.; Spyrou, C.; Mitsakou, C.; Lelieveld, J. Impact of natural aerosols on atmospheric radiation and consequent feedbacks with the meteorological and photochemical state of the atmosphere. *J. Geophys. Res. Atmos* **2013**, *119*, 1463-1491.
2. Kim, K.-H.; Kabir, E.; Kabir, S. A review on the human health impact of airborne particulate matter. *Environ. Int.* **2015**, *74*, 136-143.
3. Li, C.; Martin, R. V.; van Donkelaar, A.; Boys, B. L.; Hammer, M. S.; Xu, J.-W.; Marais, E. A.; Reff, A.; Strum, M.; Ridley, D. A., et al. Trends in Chemical Composition of Global and Regional Population-Weighted Fine Particulate Matter Estimated for 25 Years. *Environ. Sci. Technol.* **2017**, *51* (19), 11185-11195.
4. US EPA. Particulate Matter (PM) Pollution. Particulate Matter (PM) Basics. <https://www.epa.gov/pm-pollution> (accessed March 3 2017).
5. World Health Organization. Ambient (outdoor) air quality and health. <http://www.who.int/mediacentre/factsheets/fs313/en/> (accessed March 3 ).
6. Snider, G.; L. Weagle, C.; K. Murdymootoo, K.; Ring, A.; Ritchie, Y.; Walsh, A.; Akoshile, C.; Xuan Anh, N.; Brook, J.; Qonitan, F., et al. Variation in Global Chemical Composition of PM<sub>2.5</sub>: Emerging Results from SPARTAN. *Atmos. Chem. Phys.* **2016**, *16*, 9629-9653.
7. Chen, L. C.; Lippmann, M. Effects of metals within ambient air particulate matter (PM) on human health. *Inhal Toxicol* **2009**, *21* (1), 1-31.

8. Cabada, J. C.; Pandis, S. N.; Robinson, A. L. Sources of Atmospheric Carbonaceous Particulate Matter in Pittsburgh, Pennsylvania. *Journal of the Air & Waste Management Association* **2002**, *52* (6), 732-741.
9. Turpin, B. J.; Lim, H.-J. Species Contributions to PM<sub>2.5</sub> Mass Concentrations: Revisiting Common Assumptions for Estimating Organic Mass. *Aerosol Sci. Technol.* **2001**, *35* (1), 602-610.
10. Dewangan, S.; Pervez, S.; Chakrabarty, R.; Watson, J. G.; Chow, J. C.; Pervez, Y.; Tiwari, S.; Rai, J. Study of carbonaceous fractions associated with indoor PM<sub>2.5</sub>/PM<sub>10</sub> during Asian cultural and ritual burning practices. *Build. Environ.* **2016**, *106*, 229-236.
11. Giri, B.; Patel, K. S.; Jaiswal, N. K.; Sharma, S.; Ambade, B.; Wang, W.; Simonich, S. L. M.; Simoneit, B. R. T. Composition and sources of organic tracers in aerosol particles of industrial central India. *Atmos. Res.* **2013**, *120-121*, 312-324.
12. Rogge, W. F.; Hildemann, L. M.; Mazurek, M. A.; Cass, G. R.; Simoneit, B. R. T. Sources of fine organic aerosol. 4. Particulate abrasion products from leaf surfaces of urban plants. *Environ. Sci. Technol.* **1993**, *27* (13), 2700-2711.
13. Schauer, J. J.; Rogge, W. F.; Hildemann, L. M.; Mazurek, M. A.; Cass, G. R. Source apportionment of airborne particulate matter using organic compounds as tracers. *Atmos. Environ.* **1996**, *30* (22), 3837-3855.
14. Rogge, W. F.; Mazurek, M. A.; Hildemann, L. M.; Cass, G. R.; Simoneit, B. R. T. Quantification of urban organic aerosols at a molecular level: Identification, abundance and seasonal variation. *Atmos. Environ. A-Gen.* **1993**, *27* (8), 1309-1330.
15. Ding, L. C.; Ke, F.; Wang, D. K. W.; Dann, T.; Austin, C. C. A new direct thermal desorption-GC/MS method: Organic speciation of ambient particulate matter collected in Golden, BC. *Atmos. Environ.* **2009**, *43* (32), 4894-4902.

16. Rogge, W. F.; Hildemann, L. M.; Mazurek, M. A.; Cass, G. R.; Simoneit, B. R. T. Sources of fine organic aerosol. 2. Noncatalyst and catalyst-equipped automobiles and heavy-duty diesel trucks. *Environ. Sci. Technol.* **1993**, *27* (4), 636-651.
17. Schauer, J. J.; Kleeman, M. J.; Cass, G. R.; Simoneit, B. R. T. Measurement of emissions from air pollution sources. 2. C1 through C30 organic compounds from medium duty diesel trucks. *Environ. Sci. Technol.* **1999**, *33* (10), 1578-1587.
18. Rogge, W. F.; Hildemann, L. M.; Mazurek, M. A.; Cass, G. R.; Simoneit, B. R. T. Sources of Fine Organic Aerosol. 8. Boilers Burning No. 2 Distillate Fuel Oil. *Environ. Sci. Technol.* **1997**, *31* (10), 2731-2737.
19. Rogge, W. F.; Hildemann, L. M.; Mazurek, M. A.; Cass, G. R.; Simoneit, B. R. T. Sources of fine organic aerosol. 1. Charbroilers and meat cooking operations. *Environ. Sci. Technol.* **1991**, *25* (6), 1112-1125.
20. Schauer, J. J.; Kleeman, M. J.; Cass, G. R.; Simoneit, B. R. T. Measurement of Emissions from Air Pollution Sources. 1. C1 through C29 Organic Compounds from Meat Charbroiling. *Environ. Sci. Technol.* **1999**, *33* (10), 1566-1577.
21. Rogge, W. F.; Hildemann, L. M.; Mazurek, M. A.; Cass, G. R.; Simoneit, B. R. T. Sources of Fine Organic Aerosol. 7. Hot Asphalt Roofing Tar Pot Fumes. *Environ. Sci. Technol.* **1997**, *31* (10), 2726-2730.
22. Alves, C. Characterisation of solvent extractable organic constituents in atmospheric particulate matter: An overview. *An. Acad. Bras. Cienc.* **2008**, *80* (1), 21-82.
23. Oros, D. R.; Simoneit, B. R. T. Identification of Molecular Tracers in Organic Aerosols from Temperate Climate Vegetation Subjected to Biomass Burning. *Aerosol Sci. Technol.* **1999**, *31* (6), 433-445.



24. Bin Abas, M. R.; Simoneit, B. R. T.; Elias, V.; Cabral, J. A.; Cardoso, J. N. Composition of higher molecular weight organic matter in smoke aerosol from biomass combustion in Amazonia. *Chemosphere* **1995**, *30* (5), 995-1015.
25. Alves, C.; Vicente, A.; Pio, C.; Kiss, G.; Hoffer, A.; Decesari, S.; Prevôt, A. S. H.; Minguillón, M. C.; Querol, X.; Hillamo, R., et al. Organic compounds in aerosols from selected European sites – Biogenic versus anthropogenic sources. *Atmos. Environ.* **2012**, *59*, 243-255.
26. Rogge, W. F.; Hildemann, L. M.; Mazurek, M. A.; Cass, G. R.; Simoneit, B. R. T. Sources of fine organic aerosol. 3. Road dust, tire debris, and organometallic brake lining dust: roads as sources and sinks. *Environ. Sci. Technol.* **1993**, *27* (9), 1892-1904.
27. Kubátová, A.; Vermeylen, R.; Claeys, M.; Cafmeyer, J.; Maenhaut, W.; Roberts, G.; Artaxo, P. Carbonaceous aerosol characterization in the Amazon basin, Brazil: novel dicarboxylic acids and related compounds. *Atmos. Environ.* **2000**, *34* (29), 5037-5051.
28. Rogge, W. F.; Hildemann, L. M.; Mazurek, M. A.; Cass, G. R.; Simoneit, B. R. T. Sources of fine organic aerosol. 9. pine, oak, and synthetic log combustion in residential fireplaces. *Environ. Sci. Technol.* **1998**, *32* (1), 13-22.
29. Simoneit, B. R. T. Characterization of Organic Constituents in Aerosols in Relation to Their origin and Transport: A Review. *Int. J. Environ. Anal. Chem.* **1986**, *23* (3), 207-237.
30. Kawamura, K.; Gagosian, R. B. Implications of  $\omega$ -oxocarboxylic acids in the remote marine atmosphere for photo-oxidation of unsaturated fatty acids. *Nature* **1987**, *325*, 330.
31. Ho, K. F.; Lee, S. C.; Ho, S. S. H.; Kawamura, K.; Tachibana, E.; Cheng, Y.; Zhu, T. Dicarboxylic acids, ketocarboxylic acids,  $\alpha$ -dicarbonyls, fatty acids, and benzoic acid in urban aerosols collected during the 2006 Campaign of Air Quality Research in Beijing (CAREBeijing-2006). *J. Geophys. Res. Atmos* **2010**, *115* (D19).

32. Kawamura, K.; Steinberg, S.; Kaplan, I. R. Homologous series of C1–C10 monocarboxylic acids and C1–C6 carbonyls in Los Angeles air and motor vehicle exhausts. *Atmos. Environ.* **2000**, *34* (24), 4175-4191.
33. Radke, M.; Willsch, H. Generation of alkylbenzenes and benzo[b]thiophenes by artificial thermal maturation of sulfur-rich coal. *Fuel* **1993**, *72* (8), 1103-1108.
34. Schnelle-Kreis, J.; Sklorz, M.; Orasche, J.; Stölzel, M.; Peters, A.; Zimmermann, R. Semi Volatile Organic Compounds in Ambient PM2.5. Seasonal Trends and Daily Resolved Source Contributions. *Environ. Sci. Technol.* **2007**, *41* (11), 3821-3828.
35. Simoneit, B. R. T. Application of Molecular Marker Analysis to Vehicular Exhaust for Source Reconciliations. *Int. J. Environ. Anal. Chem.* **1985**, *22* (3-4), 203-232.
36. Standley, L. J.; Simoneit, B. R. T. Characterization of extractable plant wax, resin, and thermally matured components in smoke particles from prescribed burns. *Environ. Sci. Technol.* **1987**, *21* (2), 163-169.
37. Elias, V. O.; Simoneit, B. R. T.; Pereira, A. S.; Cabral, J. A.; Cardoso, J. N. Detection of High Molecular Weight Organic Tracers in Vegetation Smoke Samples by High-Temperature Gas Chromatography–Mass Spectrometry. *Environ. Sci. Technol.* **1999**, *33* (14), 2369-2376.
38. O. Elias, V.; Simoneit, B.; S. Pereira, A.; Cardoso, J. Mass spectra of triterpenyl alkanates, novel natural products. *J. Mass Spectrom.* **1997**, *32*, 1356-1361.
39. K., S. J.; B., G. R. Particle size distribution of lipids in aerosols off the coast of Peru. *J. Geophys. Res. Atmos* **1985**, *90* (D5), 7889-7898.
40. Oros, D. R.; Simoneit, B. R. T. Identification and emission factors of molecular tracers in organic aerosols from biomass burning Part 1. Temperate climate conifers. *Appl. Geochem.* **2001**, *16* (13), 1513-1544.

41. Elias, V. O.; Simoneit, B. R. T.; Pereira, A. S.; Cardoso, J. N. High Temperature Gas Chromatography with a Glass Capillary Column for the Analysis of High Molecular Weight Tracers in Smoke Samples from Biomass Burning. *J. High Resolut. Chromatogr.* **1998**, *21* (2), 87-93.
42. Simoneit, B. Biomass burning — a review of organic tracers for smoke from incomplete combustion. *Appl. Geochem.* **2002**, *17* (3), 129-162.
43. Simoneit, B. A review of biomarker compounds as source indicators and tracers for air pollution. *Environ. Sci. Pollut. Res. Int.* **1999**, *6* (3), 159-69.
44. Zdráhal, Z.; Oliveira, J.; Vermeylen, R.; Claeys, M.; Maenhaut, W. Improved Method for Quantifying Levoglucosan and Related Monosaccharide Anhydrides in Atmospheric Aerosols and Application to Samples from Urban and Tropical Locations. *Environ. Sci. Technol.* **2002**, *36* (4), 747-753.
45. Radzi bin Abas, M.; Oros, D. R.; Simoneit, B. R. T. Biomass burning as the main source of organic aerosol particulate matter in Malaysia during haze episodes. *Chemosphere* **2004**, *55* (8), 1089-1095.
46. Vlada, P.; Reinhilde, V.; Gyorgy, V.; Willy, M.; Magda, C. Development of a gas chromatographic/ion trap mass spectrometric method for the determination of levoglucosan and saccharidic compounds in atmospheric aerosols. Application to urban aerosols. *J. Mass Spectrom.* **2002**, *37* (12), 1249-1257.
47. Puxbaum, H.; Caseiro, A.; Sánchez-Ochoa, A.; Kasper-Giebl, A.; Claeys, M.; Gelencsér, A.; Legrand, M.; Preunkert, S.; Pio, C. Levoglucosan levels at background sites in Europe for assessing the impact of biomass combustion on the European aerosol background. *J. Geophys. Res. Atmos* **2007**, *112* (D23).

48. Hawthorne, S. B.; Miller, D. J.; Barkley, R. M.; Krieger, M. S. Identification of methoxylated phenols as candidate tracers for atmospheric wood smoke pollution. *Environ. Sci. Technol.* **1988**, *22* (10), 1191-1196.
49. Simoneit, B. R. T.; Rogge, W. F.; Mazurek, M. A.; Standley, L. J.; Hildemann, L. M.; Cass, G. R. Lignin pyrolysis products, lignans, and resin acids as specific tracers of plant classes in emissions from biomass combustion. *Environ. Sci. Technol.* **1993**, *27* (12), 2533-2541.
50. Alves, C. A.; Vicente, A. M. P.; Gomes, J.; Nunes, T.; Duarte, M.; Bandowe, B. A. M. Polycyclic aromatic hydrocarbons (PAHs) and their derivatives (oxygenated-PAHs, nitrated-PAHs and azaarenes) in size-fractionated particles emitted in an urban road tunnel. *Atmos. Res.* **2016**, *180*, 128-137.
51. Dat, N.-D.; Chang, M. B. Review on characteristics of PAHs in atmosphere, anthropogenic sources and control technologies. *Sci. Total Environ.* **2017**, *609*, 682-693.
52. Zhang, H.; Hu, D.; Chen, J.; Ye, X.; Wang, S. X.; Hao, J. M.; Wang, L.; Zhang, R.; An, Z. Particle Size Distribution and Polycyclic Aromatic Hydrocarbons Emissions from Agricultural Crop Residue Burning. *Environ. Sci. Technol.* **2011**, *45* (13), 5477-5482.
53. Li, J.; Li, X.; Li, M.; Lu, S.; Yan, J.; Xie, W.; Liu, C.; Qi, Z. Influence of Air Pollution Control Devices on the Polycyclic Aromatic Hydrocarbon Distribution in Flue Gas from an Ultralow-Emission Coal-Fired Power Plant. *Energy Fuels* **2016**, *30* (11), 9572-9579.
54. Rogge, W. F.; Hildemann, L. M.; Mazurek, M. A.; Cass, G. R.; Simoneit, B. R. T. Sources of fine organic aerosol. 5. Natural gas home appliances. *Environ. Sci. Technol.* **1993**, *27* (13), 2736-2744.
55. Thuren, A.; Larsson, P. Phthalate esters in the Swedish atmosphere. *Environ. Sci. Technol.* **1990**, *24* (4), 554-559.

56. Kubátová, A.; Vermeylen, R.; Claeys, M.; Cafmeyer, J.; Maenhaut, W. Organic compounds in urban aerosols from Gent, Belgium: Characterization, sources, and seasonal differences. *J. Geophys. Res. Atmos* **2002**, *107* (D21), ICC 5-1-ICC 5-12.
57. Wang, G.; Kawamura, K.; Lee, S.; Ho, K.; Cao, J. Molecular, Seasonal, and Spatial Distributions of Organic Aerosols from Fourteen Chinese Cities. *Environ. Sci. Technol.* **2006**, *40* (15), 4619-4625.
58. Kourtchev, I.; Ruuskanen, T. M.; Keronen, P.; Sogacheva, L.; Dal Maso, M.; Reissell, A.; Chi, X.; Vermeylen, R.; Kulmala, M.; Maenhaut, W., et al. Determination of isoprene and  $\alpha$ - $\beta$ -pinene oxidation products in boreal forest aerosols from Hyytiälä, Finland: diel variations and possible link with particle formation events. *Plant Biology* **2008**, *10* (1), 138-149.
59. Calogirou, A.; Larsen, B. R.; Kotzias, D. Gas-phase terpene oxidation products: a review. *Atmos. Environ.* **1999**, *33* (9), 1423-1439.
60. Yasmineen, F.; Szmigielski, R.; Vermeylen, R.; Gómez-González, Y.; Surratt, J. D.; Chan, A. W. H.; Seinfeld, J. H.; Maenhaut, W.; Claeys, M. Mass spectrometric characterization of isomeric terpenoic acids from the oxidation of  $\alpha$ -pinene,  $\beta$ -pinene, d-limonene, and  $\Delta^3$ -carene in fine forest aerosol. *J. Mass Spectrom.* **2011**, *46* (4), 425-442.
61. Liao, J.; Froyd, K. D.; Murphy, D. M.; Keutsch, F. N.; Yu, G.; Wennberg, P. O.; St. Clair, J. M.; Crounse, J. D.; Wisthaler, A.; Mikoviny, T., et al. Airborne measurements of organosulfates over the continental U.S. *J. Geophys. Res. Atmos* **2015**, *120* (7), 2990-3005.
62. Chan, M. N.; Surratt, J. D.; Claeys, M.; Edgerton, E. S.; Tanner, R. L.; Shaw, S. L.; Zheng, M.; Knipping, E. M.; Eddingsaas, N. C.; Wennberg, P. O., et al. Characterization and Quantification of Isoprene-Derived Epoxydiols in Ambient Aerosol in the Southeastern United States. *Environ. Sci. Technol.* **2010**, *44* (12), 4590-4596.

63. Surratt, J. D.; Chan, A. W. H.; Eddingsaas, N. C.; Chan, M.; Loza, C. L.; Kwan, A. J.; Hersey, S. P.; Flagan, R. C.; Wennberg, P. O.; Seinfeld, J. H. Reactive intermediates revealed in secondary organic aerosol formation from isoprene. *Proc. Natl. Acad. Sci.* **2010**, *107* (15), 6640-6645.
64. Surratt, J. D.; Gómez-González, Y.; Chan, A. W. H.; Vermeulen, R.; Shahgholi, M.; Kleindienst, T. E.; Edney, E. O.; Offenberg, J. H.; Lewandowski, M.; Jaoui, M., et al. Organosulfate Formation in Biogenic Secondary Organic Aerosol. *J. Phys. Chem. A* **2008**, *112* (36), 8345-8378.
65. Briggs, N. L.; Long, C. M. Critical review of black carbon and elemental carbon source apportionment in Europe and the United States. *Atmos. Environ.* **2016**, *144*, 409-427.
66. Bond, T. C.; Doherty, S. J.; Fahey, D. W.; Forster, P. M.; Berntsen, T.; DeAngelo, B. J.; Flanner, M. G.; Ghan, S.; Kärcher, B.; Koch, D., et al. Bounding the role of black carbon in the climate system: A scientific assessment. *J. Geophys. Res. Atmos* **2013**, *118* (11), 5380-5552.
67. Chow, J. C.; Watson, J. G.; Crow, D.; Lowenthal, D. H.; Merrifield, T. Comparison of IMPROVE and NIOSH Carbon Measurements. *Aerosol Sci. Technol.* **2001**, *34* (1), 23-34.
68. Wu, C.; Huang, X. H. H.; Ng, W. M.; Griffith, S. M.; Yu, J. Z. Inter-comparison of NIOSH and IMPROVE protocols for OC and EC determination: implications for inter-protocol data conversion. *Atmos. Meas. Tech.* **2016**, *9* (9), 4547-4560.
69. Karanasiou, A.; Diapouli, E.; Viana, M.; Alastuey, A.; Querol, X.; C, R.; Eleftheriadis, K. On the quantification of atmospheric carbonate carbon by thermal/optical analysis protocol. *Atmos. Meas. Tech.* **2010**, *4*, 2409-2419.

70. Ammerlaan, B. A. J.; Jedynska, A. D.; Henzing, J. S.; Holzinger, R. On a possible bias in elemental carbon measurements with the Sunset thermal/optical carbon analyser caused by unstable laser signal. *Atmos. Environ.* **2015**, *122*, 571-576.
71. Baurès, E.; Blanchard, O.; Mercier, F.; Surget, E.; le Cann, P.; Rivier, A.; Gangneux, J.-P.; Florentin, A. Indoor air quality in two French hospitals: Measurement of chemical and microbiological contaminants. *Sci. Total Environ.* **2018**, *642*, 168-179.
72. Mazurek, M. A.; Simoneit, B. R. T.; Cass, G. R.; Gray, H. A. Quantitative high-resolution gas chromatography and high-resolution gas chromatography/mass spectrometry analyses of carbonaceous fine aerosol particles. *Int. J. Environ. Anal. Chem.* **1987**, *29* (1-2), 119-39.
73. Hildemann, L. M.; Mazurek, M. A.; Cass, G. R.; Simoneit, B. R. T. Quantitative characterization of urban sources of organic aerosol by high-resolution gas chromatography. *Environ. Sci. Technol.* **1991**, *25* (7), 1311-25.
74. Hettiyadura, A. P. S.; Xu, L.; Jayarathne, T.; Skog, K.; Guo, H.; Weber, R. J.; Nenes, A.; Keutsch, F. N.; Ng, N. L.; Stone, E. A. Source apportionment of organic carbon in Centreville, AL using organosulfates in organic tracer-based positive matrix factorization. *Atmos. Environ.* **2018**, *186*, 74-88.
75. Cropper, P. M.; Overson, D. K.; Cary, R. A.; Eatough, D. J.; Chow, J. C.; Hansen, J. C. Development of the GC-MS organic aerosol monitor (GC-MS OAM) for in-field detection of particulate organic compounds. *Atmos. Environ.* **2017**, *169*, 258-266.
76. Orasche, J.; Schnelle-Kreis, J.; Abbaszade, G.; Zimmermann, R. Technical Note: In-situ derivatization thermal desorption GC-TOFMS for direct analysis of particle-bound non-polar and polar organic species. *Atmos. Chem. Phys.* **2011**, *11* (17), 17.

77. Graham, L. A.; Tong, A.; Poole, G.; Ding, L.; Ke, F.; Wang, D.; Caravaggio, G.; Charland, J. P.; MacDonald, P.; Hall, A., et al. A comparison of direct thermal desorption with solvent extraction for gas chromatography-mass spectrometry analysis of semivolatile organic compounds in diesel particulate matter. *Int. J. Environ. Anal. Chem.* **2010**, *90* (7), 511-534.
78. Lambe, A. T.; Chacon-Madrid, H. J.; Nguyen, N. T.; Weitkamp, E. A.; Kreisberg, N. M.; Hering, S. V.; Goldstein, A. H.; Donahue, N. M.; Robinson, A. L. Organic Aerosol Speciation: Intercomparison of Thermal Desorption Aerosol GC/MS (TAG) and Filter-Based Techniques. *Aerosol Sci. Technol.* **2010**, *44* (2), 141-151.
79. Chow, J. C.; Yu, J. Z.; Watson, J. G.; Hang Ho, S. S.; Bohannon, T. L.; Hays, M. D.; Fung, K. K. The application of thermal methods for determining chemical composition of carbonaceous aerosols: A review. *J. Environ. Sci. Health A* **2007**, *42* (11), 1521-1541.
80. Falkovich, A. H.; Rudich, Y. Analysis of Semivolatile Organic Compounds in Atmospheric Aerosols by Direct Sample Introduction Thermal Desorption GC/MS. *Environ. Sci. Technol.* **2001**, *35* (11), 2326-2333.
81. Xu, L.; Suresh, S.; Guo, H.; Weber, R. J.; Ng, N. L. Aerosol characterization over the southeastern United States using high-resolution aerosol mass spectrometry: spatial and seasonal variation of aerosol composition and sources with a focus on organic nitrates. *Atmos. Chem. Phys.* **2015**, *15* (13), 7307-7336.
82. Zhang, X.; Xu, J.; Kang, S.; Liu, Y.; Zhang, Q. Chemical characterization of long-range transport biomass burning emissions to the Himalayas: insights from high-resolution aerosol mass spectrometry. *Atmos. Chem. Phys. Discuss.* **2017**, 1-28.
83. Dzepina, K.; Mazzoleni, C.; Fialho, P.; China, S.; Zhang, B.; Owen, R. C.; Helmig, D.; Hueber, J.; Kumar, S.; Perlinger, J. A., et al. Molecular characterization of free tropospheric



aerosol collected at the Pico Mountain Observatory: a case study with a long-range transported biomass burning plume. *Atmos. Chem. Phys.* **2015**, *15* (9), 5047-5068.

84. Nozière, B.; Kalberer, M.; Claeys, M.; Allan, J.; D'Anna, B.; Decesari, S.; Finessi, E.; Glasius, M.; Grgić, I.; Hamilton, J. F., et al. The Molecular Identification of Organic Compounds in the Atmosphere: State of the Art and Challenges. *Chem. Rev.* **2015**, *115* (10), 3919-3983.

85. Xu, W.; Sun, Y.; Wang, Q.; Du, W.; Zhao, J.; Ge, X.; Han, T.; Zhang, Y.; Zhou, W.; Li, J., et al. Seasonal Characterization of Organic Nitrogen in Atmospheric Aerosols Using High Resolution Aerosol Mass Spectrometry in Beijing, China. *ACS Earth Space Chem.* **2017**, *1* (10), 673-682.

86. Labban, R.; Veranth, J. M.; Watson, J. G.; Chow, J. C. Feasibility of soil dust source apportionment by the pyrolysis-gas chromatography/mass spectrometry method. *J. Air Waste Manag. Assoc.* **2006**, *56* (9), 1230-1242.

87. Streibel, T.; Weh, J.; Mitschke, S.; Zimmermann, R. Thermal desorption/pyrolysis coupled with photoionization time-of-flight mass spectrometry for the analysis of molecular organic compounds and oligomeric and polymeric fractions in urban particulate matter. *Anal. Chem.* **2006**, *78* (15), 5354-5361.

88. Beranek, J.; Kozliak, E.; Kubatova, A. Evaluation of sequential solvent and thermal extraction followed by analytical pyrolysis for chemical characterization of carbonaceous particulate matter. *J. Chromatogr., A* **2013**, *1279*, 27-35.

89. Zhao, J.; Peng, P. a.; Song, J.; Ma, S.; Sheng, G.; Fu, J. Characterization of organic matter in total suspended particles by thermodesorption and pyrolysis-gas chromatography-mass spectrometry. *J. Environ. Sci.* **2009**, *21* (12), 1658-1666.

90. Lappi, H.; Alén, R. Pyrolysis of vegetable oil soaps—Palm, olive, rapeseed and castor oils. *J. Anal. Appl. Pyr.* **2011**, *91* (1), 154-158.
91. Lappi, H.; Alén, R. Production of vegetable oil-based biofuels—Thermochemical behavior of fatty acid sodium salts during pyrolysis. *J. Anal. Appl. Pyr.* **2009**, *86* (2), 274-280.
92. Wang, S.; Wang, D.; Tang, Y.; Sun, Y.; Jiang, D.; Su, T. Study of pyrolysis behavior of hydrogen-rich bark coal by TGA and Py-GC/MS. *J. Anal. Appl. Pyr.* **2017**, *128*, 136-142.
93. Nali, M.; Corana, F.; Montanari, L.; Pellegrini, L. A pyrolysis-gas chromatography/mass spectrometry study on coals. *J. Anal. Appl. Pyr.* **1994**, *29* (1), 15-23.
94. Lievens, C.; Ci, D.; Bai, Y.; Ma, L.; Zhang, R.; Chen, J. Y.; Gai, Q.; Long, Y.; Guo, X. A study of slow pyrolysis of one low rank coal via pyrolysis–GC/MS. *Fuel Proc. Technol.* **2013**, *116*, 85-93.
95. Kubátová, A.; Luo, Y.; Št'ávoová, J.; Sadrameli, S. M.; Aulich, T.; Kozliak, E.; Seames, W. New path in the thermal cracking of triacylglycerols (canola and soybean oil). *Fuel* **2011**, *90* (8), 2598-2608.
96. Nip, M.; De Leeuw, J. W.; Crelling, J. C. Chemical structure of bituminous coal and its constituting maceral fractions as revealed by flash pyrolysis. *Energy Fuels* **1992**, *6* (2), 125-136.
97. Kubátová, A.; Št'ávoová, J.; Seames, W. S.; Luo, Y.; Sadrameli, S. M.; Linnen, M. J.; Baglayeva, G. V.; Smoliakova, I. P.; Kozliak, E. I. Triacylglyceride Thermal Cracking: Pathways to Cyclic Hydrocarbons. *Energy Fuels* **2012**, *26* (1), 672-685.
98. Lu, Q.; Yang, X.-c.; Dong, C.-q.; Zhang, Z.-f.; Zhang, X.-m.; Zhu, X.-f. Influence of pyrolysis temperature and time on the cellulose fast pyrolysis products: Analytical Py-GC/MS study. *J. Anal. Appl. Pyr.* **2011**, *92* (2), 430-438.

99. Pastorova, I.; Botto, R. E.; Arisz, P. W.; Boon, J. J. Cellulose char structure: a combined analytical Py-GC-MS, FTIR, and NMR study. *Carbohydr. Res.* **1994**, *262* (1), 27-47.
100. Wang, S.; Guo, X.; Liang, T.; Zhou, Y.; Luo, Z. Mechanism research on cellulose pyrolysis by Py-GC/MS and subsequent density functional theory studies. *Bioresour. Technol.* **2012**, *104*, 722-728.
101. Voeller, K.; Bílek, H.; Kreft, J.; Dostálková, A.; Kozliak, E.; Kubátová, A. Thermal Carbon Analysis Enabling Comprehensive Characterization of Lignin and Its Degradation Products. *ACS Sustain. Chem. Eng.* **2017**, *5* (11), 10334-10341.
102. Dong, J.; Li, F.; Xie, K. Study on the source of polycyclic aromatic hydrocarbons (PAHs) during coal pyrolysis by PY-GC-MS. *J. Hazard. Mater.* **2012**, *243*, 80-85.
103. Kubátová, A.; Geetla, A.; Casey, J.; Linnen, M. J.; Seames, W. S.; Smoliakova, I. P.; Kozliak, E. I. Cleavage of Carboxylic Acid Moieties in Triacylglycerides During Non-Catalytic Pyrolysis. *J. Am. Oil Chem. Soc.* **2015**, *92* (5), 755-767.
104. Delene, D. Suitability of North Dakota For Conducting Effective Hygroscopic Seeding. *Journal of Weather Modification* **2016**, *48*, 43-67.
105. Kubátová, A.; Lahren, T. J.; Beránek, J.; Smoliakova, I. P.; Braun, A.; Huggins, F. E. Extractable Organic Carbon and its Differentiation by Polarity in Diesel Exhaust, Wood Smoke, and Urban Particulate Matter. *Aerosol Sci. Technol.* **2009**, *43* (7), 714-729.
106. Barbezan, A. B.; Martins, R.; Bueno, J. B.; Villavicencio, A. L. C. H. Ames Test to Detect Mutagenicity of 2-Alkylcyclobutanones: A Review. *J. Food Sci.* **2017**, *82* (7), 1518-1522.
107. Maher, K. D.; Kirkwood, K. M.; Gray, M. R.; Bressler, D. C. Pyrolytic Decarboxylation and Cracking of Stearic Acid. *Ind. Eng. Chem. Res.* **2008**, *47* (15), 5328-5336.

108. Ayodele, O. B.; Abbas, H. F.; Daud, W. M. A. W. Hydrodeoxygenation of Stearic Acid into Normal and Iso-Octadecane Biofuel with Zeolite Supported Palladium-Oxalate Catalyst. *Energy Fuels* **2014**, *28* (9), 5872-5881.
109. US EPA. Query AirData. <https://aqs.epa.gov/api> (accessed January 12).
110. Simmons, G. M.; Gentry, M. Kinetic formation of CO, CO<sub>2</sub>, H<sub>2</sub>, and light hydrocarbon gases from cellulose pyrolysis. *J. Anal. Appl. Pyr.* **1986**, *10* (2), 129-138.
111. Li, S.; Lyons-Hart, J.; Banyasz, J.; Shafer, K. Real-time evolved gas analysis by FTIR method: an experimental study of cellulose pyrolysis. *Fuel* **2001**, *80* (12), 1809-1817.
112. Simoneit, B. R. T. Organic matter of the troposphere — V: Application of molecular marker analysis to biogenic emissions into the troposphere for source reconciliations. *J. Atm. Chem.* **1989**, *8* (3), 251-275.
113. Simoneit, B. R. T.; Cardoso, J. N.; Robinson, N. An assessment of terrestrial higher molecular weight lipid compounds in aerosol particulate matter over the south atlantic from about 30–70°S. *Chemosphere* **1991**, *23* (4), 447-465.
114. Gupta, S.; Gadi, R.; Mandal, T. K.; Sharma, S. K. Seasonal variations and source profile of n-alkanes in particulate matter (PM<sub>10</sub>) at a heavy traffic site, Delhi. *Environ Monit Assess* **2017**, *189* (1), 43.
115. Brandenberger, S.; Mohr, M.; Grob, K.; Neukom, H. P. Contribution of unburned lubricating oil and diesel fuel to particulate emission from passenger cars. *Atmos. Environ.* **2005**, *39* (37), 6985-6994.
116. Kasumba, J.; Holmén, B. A. Nonpolar Organic Compound Emission Rates for Light-Duty Diesel Engine Soybean and Waste Vegetable Oil Biodiesel Fuel Combustion. *Energy Fuels* **2016**, *30* (11), 9783-9792.

117. Kasumba, J.; Holmén, B. A. Heterogeneous ozonation reactions of PAHs and fatty acid methyl esters in biodiesel particulate matter. *Atmos. Environ.* **2018**, *175*, 15-24.
118. Brown, S. G.; Herckes, P.; Ashbaugh, L.; Hannigan, M. P.; Kreidenweis, S. M.; Collett Jr, J. L. Characterization of organic aerosol in Big Bend National Park, Texas. *Atmos. Environ.* **2002**, *36* (38), 5807-5818.
119. Kesselmeier, J.; Staudt, M. Biogenic Volatile Organic Compounds (VOC): An Overview on Emission, Physiology and Ecology. *J. Atm. Chem.* **1999**, *33* (1), 23-88.
120. Fraser, M. P.; Lakshaman, K. Using levoglucosan as a molecular marker for the long-range transport of biomass combustion aerosols. *Environ. Sci. Technol.* **2000**, *34* (21), 4560-4564.
121. Nolte, C. G.; Schauer, J. I.; Cass, G. R.; Simoneit, B. R. Highly polar organic compounds present in wood smoke and in the ambient atmosphere. *Environ. Sci. Technol.* **2001**, *35* (10), 1912-1919.
122. Giannoni, M.; Martellini, T.; Del Bubba, M.; Gambaro, A.; Zangrando, R.; Chiari, M.; Lepri, L.; Cincinelli, A. The use of levoglucosan for tracing biomass burning in PM<sub>2.5</sub> samples in Tuscany (Italy). *Environ. Pollut.* **2012**, *167*, 7-15.
123. Salma, I.; Németh, Z.; Weidinger, T.; Maenhaut, W.; Claeys, M.; Molnár, M.; Major, I.; Ajtai, T.; Utry, N.; Bozóki, Z. Source apportionment of carbonaceous chemical species to fossil fuel combustion, biomass burning and biogenic emissions by a coupled radiocarbon–levoglucosan marker method. *Atmos. Chem. Phys.* **2017**, *17* (22), 13767-13781.
124. Greatrex, B. W.; Meisner, J.; Glover, S. A.; Raverty, W. Support for a Dioxyallyl Cation in the Mechanism Leading to (–)-Levoglucosenone. *J. Org. Chem.* **2017**, *82* (23), 12294-12299.

125. Ye, X.-n.; Lu, Q.; Wang, X.; Guo, H.-q.; Cui, M.-s.; Dong, C.-q.; Yang, Y.-p. Catalytic Fast Pyrolysis of Cellulose and Biomass to Selectively Produce Levoglucosenone Using Activated Carbon Catalyst. *ACS Sustain. Chem. Eng.* **2017**, *5* (11), 10815-10825.
126. Polidori, A.; Turpin, B.; Meng, Q. Y.; Lee, J. H.; Weisel, C.; Morandi, M.; Colome, S.; Stock, T.; Winer, A.; Zhang, J., et al. Fine organic particulate matter dominates indoor-generated PM<sub>2.5</sub> in RIOPA homes. *J Expo Sci Environ Epidemiol* **2006**, *16* (4), 321-31.
127. Ellickson, K. M.; McMahon, C. M.; Herbrandson, C.; Krause, M. J.; Schmitt, C. M.; Lippert, C. J.; Pratt, G. C. Analysis of polycyclic aromatic hydrocarbons (PAHs) in air using passive sampling calibrated with active measurements. *Environ. Pollut.* **2017**, *231*, 487-496.
128. Ravindra, K.; Sokhi, R.; Vangrieken, R. Atmospheric polycyclic aromatic hydrocarbons: Source attribution, emission factors and regulation. *Atmos. Environ.* **2008**, *42* (13), 2895-2921.
129. Tobiszewski, M.; Namiesnik, J. PAH diagnostic ratios for the identification of pollution emission sources. *Environ. Pollut.* **2012**, *162*, 110-9.
130. Kubátová, A.; Šťávoňová, J.; Seames, W. S.; Luo, Y.; Sadrameli, S. M.; Linnen, M. J.; Baglayeva, G. V.; Smoliakova, I. P.; Kozliak, E. I. Triacylglyceride thermal cracking: Pathways to cyclic hydrocarbons. *Energy and Fuels* **2012**, *26* (1), 672-685.
131. Shen, G.; Wang, W.; Yang, Y.; Ding, J.; Xue, M.; Min, Y.; Zhu, C.; Shen, H.; Li, W.; Wang, B., et al. Emissions of PAHs from Indoor Crop Residue Burning in a Typical Rural Stove: Emission Factors, Size Distributions, and Gas-Particle Partitioning. *Environ. Sci. Technol.* **2011**, *45* (4), 1206-1212.